AN ABSTRACT OF THE THESIS OF

Yongseok Seo for the degree of Doctor of Philosophy in Electrical and Computer Engineering presented on July 15, 1997. Title : The Embedded Passives in a Multilayer Medium.

Redacted for privacy

Abstract approved: _____

Vijai K. Tripathi

Recent advances in high density low cost RF and microwave three dimensional integration technologies using LTCC(Low Temperature Cofired Ceramics), laminate and other multilayer hybrid and integrated circuits have increased interest in the design of embedded passive components such as inductors, capacitors and filters. The purpose of this study is to develop the design methodology of multilayer components such as coupled line filters in a multilevel inhomogeneous medium. Although multilayer assembly including simple components have been used in the past for digital and low frequency systems, RF and microwave circuits have been fabricated mostly in single level configurations. The use of multilayer three dimensional components and circuits makes microwave circuits more compact and the design more flexible.

This thesis describes the basic principles and computational procedure for the design of multilayer components such as, planar single and two-level spirals for applications as an inductive elements for RF and MICs, and coupled line band-pass filter circuits consisting of multiple sections. It is shown that both the quality factor and the inductance values can be enhanced by using multilevel spirals. Design

methodology for general multisection filter consisting of asymmetric and multiple coupled lines is formulated and presented. It is shown that given the filter specifications, e.g., bandwidth, selectivity, input and output impedances, single, two and multilevel coupled line filters can be physically realized.

The design procedure for narrow band filters is formulated in the conventional manner by using the equivalent circuit with admittance inverters and the component values of the low-pass prototype for Butterworth, Chebyshev and other response functions. Examples of Butterworth and Chebyshev multisection filters are included to demonstrate the design procedure.

The physical multilevel filter is then optimized by using the *SPICE* model for coupled multiconductor lines on commercial *CAD* tool like *LIBRA*. The optimized multilevel structure design has been validated by *MOMENTUM* commercial electromagnetic simulator tool. The design methodology is validated by comparing the theoretical results with measurement data for a strip line filter fabricated on FR-4.

Embedded Passives in a Multilayer Medium

by

Yongseok Seo

A THESIS

submitted to

Oregon State University

in partial fulfillment of
the requirements for the
degree of

Doctor of Philosophy

Completed July 15, 1997
Commencement June 1998

Doctor of Philosophy thesis of Yongseok Seo presented on July 15, 1997

APPROVED:

Redacted for privacy

Major Professor, representing Electrical and Computer Engineering

Redacted for privacy

Head of Department of Electrical and Computer Engineering

Redacted for privacy

Dean of Graduate School

I understand that my thesis will become part of the permanent collection of Oregon State University libraries. My signature below authorizes release of my thesis to any reader upon request.

Redacted for privacy

Yongseok Seo, Author

ACKNOWLEDGEMENT

First, thanks to my Lord, Jesus Christ for his love, encouragement, and guidance. And I am very grateful to my mother, my wife, and my three daughters for their unconditional support, prayers, and patience.

My special thanks goes to Dr. Vijai K. Tripathi who was my major advisor. His guidance and advice have been extremely valuable during my academic years at Oregon State University as a foreign student. Heart filled thanks to Richard Lutz and Alok Tripathi for their kind help to develop this thesis. I would like to thank my committee members Dr. Lee, Dr. Lu and Dr. Mohler and Dr. Warnes from Mechanical Engineering.

This thesis is dedicated to my mother, wife Kyehwa, and lovely three girls - Jimin, Jiwon, and Jihyo.

TABLE OF CONTENTS

LIST OF FIGURES

LIST OF TABLES

EMBEDDED PASSIVES IN A MULTILAYER MEDIUM

1. INTRODUCTION

Coupled linear and nonlinear distributed circuits have been a subject of continued interest due to their applications in many branches of engineering ranging from multiphase power distribution systems to opto-electronic circuits. Recent advances in high speed and high density integrated circuits, MMIC's and OEIC's has resulted in a renewed interest on the theory and applications of general lossy, uniform, nonuniform as well as active linear and nonlinear coupled structures. Such systems are used for a host of applications that include passive components like filters and couplers and active components like tunable circuits, switches and amplifiers at microwave through optical frequencies [1]- [20]. In addition, with the advances in high performance communication and computer circuits and systems, the signal integrity and noise analysis of interconnects associated with the IC's and the packaging can only be conducted by modeling these as coupled distributed parameter system.

Recent advances in high density low cost RF and microwave three dimensional integration technologies using LTCC(Low Temperature Cofired Ceramics), laminate and multilayer integrated circuits have also increased interest in the design of embedded passive components such as inductors, capacitors and filters as shown in Figure 1.1. That is why the analysis and modeling of coupled transmission systems including multiconductor transmission lines has been a topic of considerable interest in recent years. Advances in planar and layered interconnect and propagation structures and components in microwave, high speed digital and mixed signal

circuits has resulted in increased interest in efficient, accurate analysis and design of these circuits and systems [11–13].

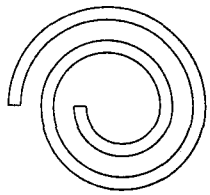

(a) Circular spiral Inductor

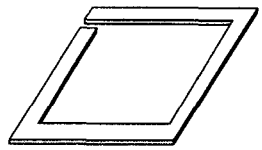

(b) Single level rectangular sprial Inductor

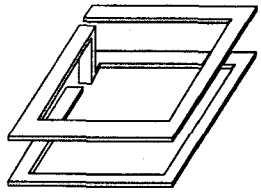

(c) Two level rectangular spiral Inductor

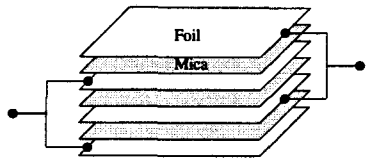

(d) Multilayer capacitor

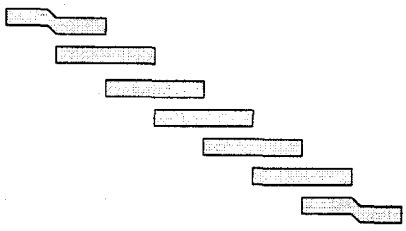

(e) Unfolded symmetric coupled line Band-Pass Filter

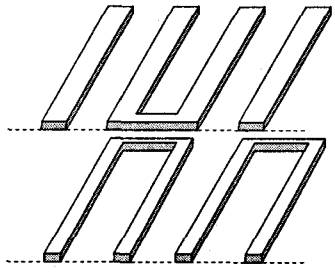

(f) 2-level asymmetric coupled line Band-Pass Filter

Figure 1.1. Inductors, capacitors, and filters

The theory of asymmetric uniform coupled transmission lines in an inhomogeneous medium has received considerable attention due to its potential applications in filters, couplers, impedance transformers and other microwave networks. Asymmetric and/or inhomogeneous line structures provide greater flexibility through introducing degree of freedom in terms of impedance transformation.

The theory of coupled lines in a homogeneous medium has been formulated by expressing their four-port parameters in terms of the properties of even and odd excitation modes as defined by Cristal(1966) and Ekinge(1971). The even voltage-mode, odd current-mode pair, as defined by Ekinge for homogeneous lines, has been considered by Allen(1975) and Speciale(1975) for the case of asymmetric coupled lines in an inhomogeneous medium. Speciale indicated that these two modes are the normal modes of the coupled lines only if a congruence condition between the line parameters is satisfied. Tripathi(1975) has formulated the exact analysis for the general case of uniform asymmetric coupled lines in an inhomogeneous medium in terms of the properties of the two uncoupled, normal modes and derived the four-port Y and Z-matrices.

The analysis procedure for linear uniform structures can be in terms of the coupled modes of the system where the system variables are the mode amplitudes representing the power flow along the lines, e.g., the distributed scattering parameters of the lines or in terms of the basic system variable like the voltages and currents or the electric and magnetic fields. Whereas the analysis of the coupled systems in terms of the coupled modes of the systems allows us to consider the coupling between two modes at a time and leads to a better physical understanding of the coupling mechanisms, the formulation in terms of the system variables, where the coupled transmission line equations are solved directly, is more aminable to circuit analysis and design. It leads directly to the multiport network functions and is compatible with the simulation and the design of the circuits. In the following section the normal mode analysis procedure, where the problem is formulated in terms of system variables, is exemplified in terms of the coupled transmission line equations which can be used to represent not only structures consisting of metallic strips but also other coupled propagation systems with active as well as passive

distributed structures. This includes many diverse coupled systems such as coupled schottky lines, coupled strip slot structures and coupled dielectric waveguides at optical frequencies. For linear systems these coupled equations are,

$$\frac{\partial v]}{\partial z} = -[Z]i]$$
$$\frac{\partial i]}{\partial z} = -[Y]v]$$

where vectors $v]$ and $i]$ represent voltages and currents on different lines and

$$[Z] = [R] + j\omega[L], \qquad [Y] = [G] + j\omega[C]$$

[R], [L], [G], [C] are the per unit length line constant matrices whose elements are in general frequency dependent.

The uniform system in frequency domain is characterized by the eigenvalues which for the lossless case define a set of orthogonal modes with the corresponding field distributions. For coupled transmission line quasi-TEM case this field distribution represents the relationship between the voltages and currents on the lines. At higher frequencies, the voltages are not uniquely defined and we may need to represent the distribution in terms of frequency dependent equivalent line variables. For other hybrid systems and dielectric waveguides a functional utility definition of impedance and eigenvectors in terms of electric and magnetic fields may be used to help facilitate the design of the multiport circuits.

The case of multiconductor lines in a homogeneous medium where all the mode velocities are equal leading to an arbitrary choice of the eigenvectors has been treated in detail and used in the analysis and design of various multiports including filters, couplers, antennas and other multiports [1,3]. For the general case of the coupled systems with distinct eigenvalues, the multiports can be analyzed directly in terms of the immittance matrix of the multiports or the equivalent circuit which can

be used as subcircuit model in commercially available time and frequency domain circuit simulators. The characteristic parameters of the coupled systems are the propagation constants for the normal modes, characteristic impedances associated with these modes and the eigenvector matrices characterizing the voltage, current or the field distribution associated with the normal modes. For the quasi-TEM case of coupled strips, these normal mode parameters are found in terms of the equivalent self and mutual line constants [R], [L], [G] and [C] of the multiconductor systems. In general for hybrid modes or for other coupled systems such as fin lines and dielectric waveguides the normal mode parameters can be found directly from the dynamic full wave analysis of the coupled system.

It is seen that, unlike the single line case where the characteristic impedance is defined in an unique unambiguous manner, three useful basic definitions for characteristic impedances have been used in the past for coupled line structures. These are:

Line Mode Impedance Matrix Z_{lm}: The elements of this matrix represent the ratio of the voltage of line l to the current on the same line for a given mode m traveling in $+z$ direction. The lines must be terminated in these impedances in order to match the lines when this mode is excited. These impedance matrices can be readily used to evaluate the multiport immittance and other network functions as demonstrated in [6,7] and for lower order systems and [5,9,11] for the general case. These matrix elements are also compatible with full wave dynamic analysis of multiconductor system and are calculated from the eigenvalues, current eigenvectors and the total power associated with all the normal modes of the system as shown in [12]. It should be noted that this matrix is unique for a given system, is in general not symmetrical and can have positive as well as negative elements.

Decoupled Modal Impedances Z_O: This is a diagonal matrix and represents the characteristic impedances of the normal modes for the decoupled transmission line system. These are used in the equivalent circuit representation of the multiconductor system such as the *SPICE* model used in [10,11]. These impedances of the decoupled lines are not unique and depend on how the voltage and current eigenvector matrices M_V and M_I are normalized.

Characteristic Termination Impedance Matrix Z_{OT}: It is the open circuit impedance of an N port network that perfectly terminates all the lines for all the modes, i.e., any arbitrary excitation on the multiconductor system is matched by this impedance matrix. This is perhaps the definition which is most similar to the one used for a single transmission line. This matrix is obviously symmetrical, dominant and represents a unique realizable passive network. The above matrices are interrelated. For example

$$[Y_{OT}] = [M_I][Y_O][M_I]^T.$$

The normal mode propagation constants, line mode impedances and current eigenvectors lead to the equivalent coupled transmission line representation of the structure and hence the associated network function. The decoupled modal impedances Z_O, together with propagation constants and eigenvectors, are used to derive the equivalent circuit model(e.g. *SPICE* model) of the coupled line structure [10,11].

For time domain simulation the basic techniques include the use of the augmented frequency domain network functions, techniques based on Fourier and Laplace transforms, numerical integration based on the method of characteristics as well as the use of the equivalent circuit models [9,14]. It should be noted that for the special cases of axial symmetry or tridiagonal [C] and [L] matrices, the eigenvalues,

eigenvectors and impedance matrices can be expressed in a closed form. This results in an efficient computation of the frequency and time domain response of coupled distributed systems. In addition, for coupled two line structures, it is possible to realize systems with purely co- or contra-directional coupling. For example, coupling is purely co-directional for transmission lines in a homogeneous medium and purely contra-directional for systems with coupling coefficient = 0 for wave traveling in opposite direction. In the first case the two eigenvalues are equal whereas in the second case the two mode impedances must be equal. In general for most systems both types of coupling is present, that is, all forward and backward waves are coupled to each other. The normal mode approach can be extended with required modification to coupled nonlinear structures for the analysis of distributed amplifiers, logic elements,tunable circuits and many other active elements [18].

In order to demonstrate the applications of the coupled distributed structures, some representative examples are given in here. These include the application of the multiple coupled line theory in the analysis and design of components like a spiral inductor, coupled microstrip filter DC-block, multi-section coupled line filters, other structures such as interconnects can also be treated. Other applications of such linear systems include the analysis and design of interdigitated structures for application in MMIC's and photodetectors [16], various other four, six and other multiport directional couplers and power dividers.

In this dissertation, The design procedure for embedded passives such as multilevel coupled line filters and spiral inductors in a layered medium is presented with physical examples at RF frequencies. The design techniques for asymmetric coupled line filters offers the design flexibility in a layered structure, in addition they can naturally be used for impedance matching over a desired band of frequencies.

In Chapter 2, planar single and two-level spirals are analyzed for applications as inductive elements for RF and microwave integrated circuits by using coupled line theory. CAD compatible techniques to evaluate frequency dependent inductance, self resonance frequency, quality factor and equivalent circuits for various configurations are presented including the case of a compact two level spiral with broad side and edge coupled strips.

In Chapter 3, the theory of asymmetric uniform coupled transmission lines in an inhomogeneous medium and a homogeneous medium are reviewed in terms of the properties of the two uncoupled, normal modes. This is followed by Chapter 4 where the design procedure for general symmetric as well as asymmetric transformer/filters with a desired impedance transformation for single section DC block, and multi-section(3-section, 4-section) structures in a homogeneous medium are presented.

Chapter 5 presents a methodology for a designing asymmetric coupled line band-pass filter circuits. It is shown that these can be physically realized in microstrip and strip line. A filter with 3-sections was fabricated and measured to validate the design methodology. For physical realization the normal mode parameters, and the relationships between characteristic impedances and capacitances in an inhomogeneous medium and a homogeneous medium, respectively and the procedure using a quasi-static program were illustrated. For validation of the design methodology and the fabricated 3-section band-pass filter a *SPICE* model simulation [52–54] on *LIBRA* and a full-wave *EM* simulator, *MOMENTUM* were used.

In Chapter 6, a methodology for designing asymmetric coupled line filter circuits in multilevel configuration is presented. A sensitivity analysis for a 3-section coupled line two level band-pass filter is presented. Methods for arriving at filter

dimensions is described for the embedded(homogeneous dielectric) configurations. The method developed here is verified by comparison with results obtained from a full-wave electromagnetic simulation.

Then conclusions and suggestion for future work are given in chapter 7.

2. SPIRAL INDUCTORS IN RFIC'S AND MMIC'S

Planar single and two-level spirals are analyzed for applications as an inductive elements for RF and microwave integrated circuits. CAD compatible techniques to evaluate frequency dependent inductance, self resonance frequency, quality factor and equivalent circuits for various configurations are presented including the case of a compact two level spiral with broad side and edge coupled strips [21–23].

2.1. INTRODUCTION

A considerable amount of work has been done in recent years on the modeling and design of planar rectangular and circular-spiral inductors in MMIC's [24–26] and other hybrid layered structures. Lumped element, distributed circuit as well as electromagnetic models have been used to analyze and design these structures. In this paper, the distributed modeling technique is extended to formulate the analysis and design procedures for a class of two level spiral inductors e.g., Figure 2.1 that lead to the realization of compact inductors with high inductances for RF and microwave Si as well as GaAs based integrated circuits.

2.2. SPIRAL INDUCTORS

The distributed rigorous models, in general, consist of broad side- and edge-coupled multiconductor lines that are interconnected by bends, coupled bends [27] and vias to form a two port. That is, the two port admittance matrix characterizing the spiral is obtained in terms of the admittance matrix of the n coupled line $2n$ port and the admittance or ABCD matrices characterizing the coupled bends and vias. Figure 2.2 shows the schematic corresponding to the spiral structure of Figure 2.1.

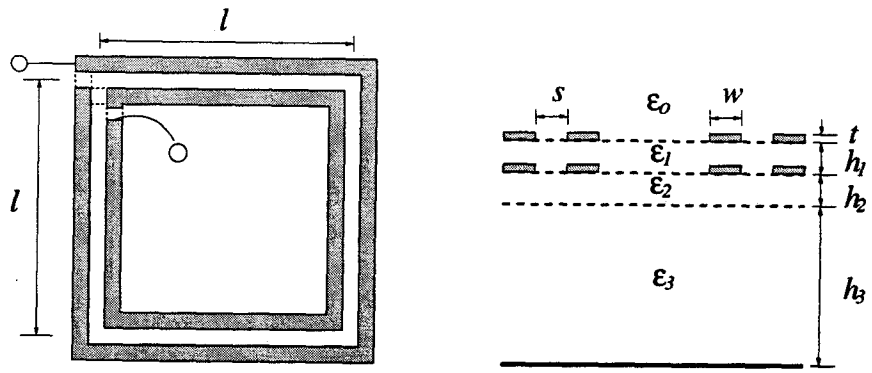

(a) Top view (b) Cross sectional view

Figure 2.1. A two level rectangular spiral

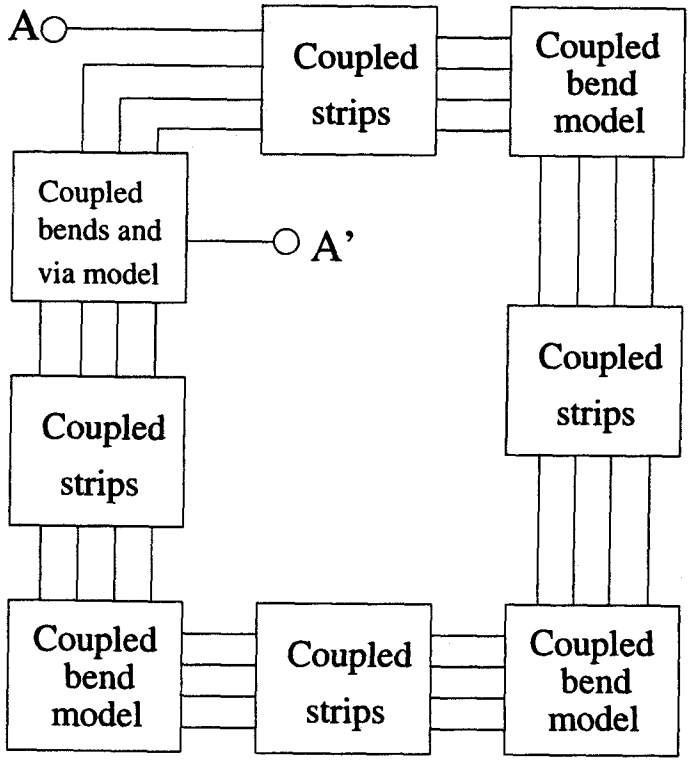

Figure 2.2. Block diagram for the analysis of a two level four turn spiral

The matrix reduction is readily accomplished with the help of general circuit parameters of the multiport. For an n- line $2n$ port, the immittance matrix can be found in terms of the quasi-TEM multiconductor line constants [R], [L], [G], and [C] per unit length at lower frequencies or by the full-wave solution for the complex eigenvalues and eigenfunctions of the coupled system. For example the admittance matrix is given as [11],

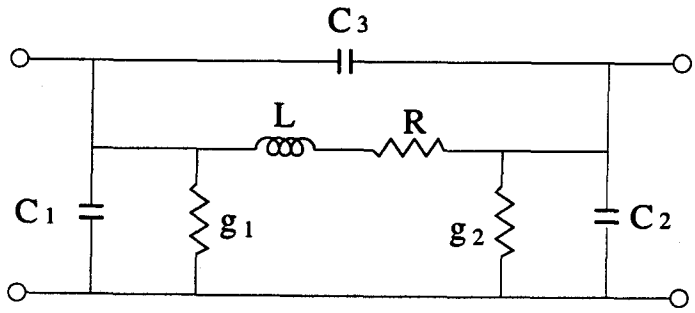

Figure 2.3. Spiral equivalent circuit

$$[Y] = \begin{bmatrix} [Y_A] & [Y_B] \\ [Y_B] & [Y_A] \end{bmatrix} \tag{2.1}$$

where

$$[Y_A] = [M_V]^T [Coth(\gamma_k l)]_{diag} [Y_k]_{diag} [M_V]^{-1}$$

$$[Y_B] = [M_V]^T [Csch(\gamma_k l)]_{diag} [Y_k]_{diag} [M_V]^{-1}$$

with the decoupled modal characteristic admittance matrix,

$$[Y_k] = [M_V]^{-1} [C] [M_V]$$

$[M_V]$ is the voltage eigenvector matrix of the coupled system, γ_k is the propagation constant and [C] is the equivalent per unit length capacitance matrix of the n line structure.

An equivalent circuit representing the low frequency inductance, self resonance and conductor as well as substrate losses can be derived in a form shown in Figure 2.3 by using the two port parameters.

Here the element values are assumed to be constant over a narrow bend of frequencies resulting in a useful CAD model for a number of applications including RFIC's for wireless applications. In terms of the admittance of the two port the low frequency inductance of the spiral is

$$[L] = \frac{1}{\omega} Im[Z], \tag{2.2}$$

where

$$Z = \frac{Y_{11} + Y_{2n2n} + 2Y_{12n}}{Y_{11}Y_{2n2n} - Y_{12n}^2}$$

and the unloded quality factor is,

$$Q = \frac{Im[Z]}{Re[Z]}.$$

The Q can also be expressed as,

$$Q = \frac{1}{\frac{1}{Q_d} + \frac{1}{Q_c} + \frac{1}{Q_R}} \tag{2.3}$$

where Q_d, and Q_c and Q_R correspond to the quality factors associated with dielectric, conductor and radiation losses for the spiral.

An alternate modeling technique compatible with CAD is based on the equivalent circuit where elements can be extracted efficiently by using reliable empirical results and quasi-TEM techniques. For multilayer structure, these parameters are low frequency inductance L, the interwinding capacitances, self capacitance to ground and the dieletric, conductor, and radiation losses.

The quality factor based on dielectric losses exclusively, Q_d, can be computed as

$$Q_d = \frac{\omega\sqrt{\mu_o\epsilon_o\epsilon_{eff}}}{\alpha} \tag{2.4}$$

where α is the attenuation constant and ϵ_{eff} is the effective dielectric constant.

Ohmic losses are calculated using the skin effect frequency dependent resistance formulae given in [13], and the radiation losses are computed by using the following expression derived for low frequency radiation resistance of spirals above a ground plane

$$R_r = \frac{2}{\eta}\left|\frac{\omega\mu_o}{\lambda}\right|^2 \cdot \sum_{n=1}^{N} S_n \left[\frac{1}{3} + \frac{cos(2kh)}{(2kh)^2} - \frac{sin(2kh)}{(2kh)^3}\right] \tag{2.5}$$

where η is the wave impedance, S_n is the average cross sectional area for each of the N turns, and k is the wavenumber.

2.3. NUMERICAL RESULTS

Performances of single level spirals deposited on oxide or nitride dielectric layers, air bridge, and two level spirals are compared in this paper in terms of the quality factor Q and realizable inductance values per unit chip area occupied by the spirals.

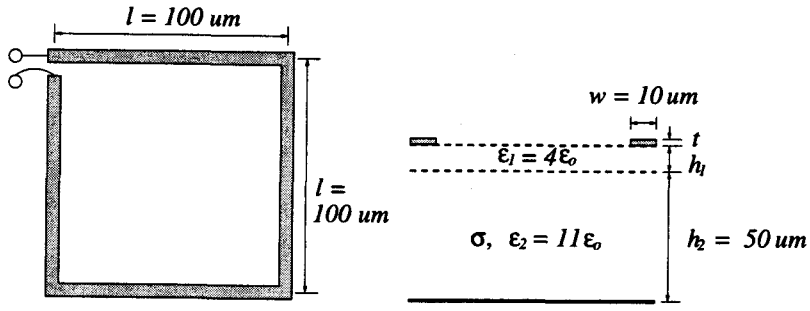

(a) Top view (b) Cross sectional view

Figure 2.4. Top view and cross sectional view of one level one turn rectangular spiral.

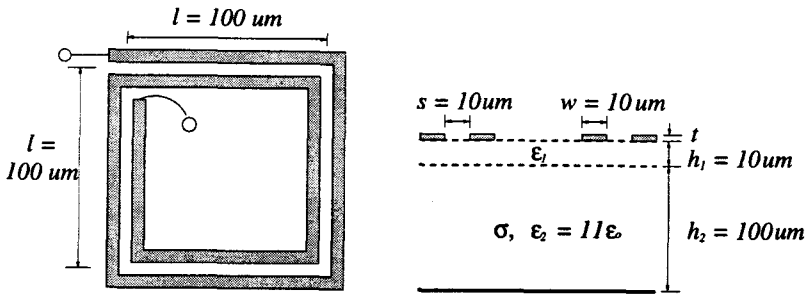

(a) Top view (b) Cross sectional view

Figure 2.5. Top view and cross sectional view of one level two turn rectangular spiral.

The multiconductor [R], [L], [G], [C] matrices bend and via models required for the computation of spiral properties can be computed by using a number of quasi-static and fullwave programs. The following results are based on the quasi-static computation techniques reported in [11,27,28]. Figure 2.6(a) shows the effect of substrate conductivity on the quality factor of a single turn spiral in Figure 2.4. As expected, Q_d decreases with increase in conductivity and decrease in the thickness of the oxide layer. Effective inductance is also dependent on the thickness of the oxide layer at higher frequencies as shown in Figure 2.6(b). The effective inductance of a two turn planar spiral in Figure 2.5 is shown in Figure 2.7(a) for air bridge line as well as lines deposited on an oxide layer. In addition to a higher resonance frequency, the air bridge spiral also has a higher quality factor as shown in Figure 2.7(b). The effective inductance increases with the number of turns associated with the spirals. Figure 2.11 demonstrates the inductance value as a function of the number of spiral turns for two level structures shown in Figure 2.8, Figure 2.9, and Figure 2.10.

For these calculations $h_1 = h_2 = 5\mu m, h_3 = 50\mu m$, $\epsilon_1 = \epsilon_2 = 4\epsilon_0$, and $\epsilon_3 = 11\epsilon_0$, $w = s = 5\mu m$ and the outer circumference for all the spirals is 400 μm.

As expected the effective inductance increases with the number of turns whereas the self resonance frequency decreases.

In conclusion planar and two level rectangular spiral are analyzed for applications as an inductive element in RF and microwave circuits. The technique is a general one and can be used to study other multiconductor multilevel circuit elements such as circular spiral inductors and rectangular transformer.

2.4. SUMMARY

Planar single and two-level spirals were analyzed for applications as an inductive elements for RF and microwave integrated circuits. CAD compatible techniques to evaluate frequency dependent inductance, self resonance frequency, quality factor and equivalent circuits for various configurations were presented including the case of a compact two level spiral with broad side and edge coupled strips.

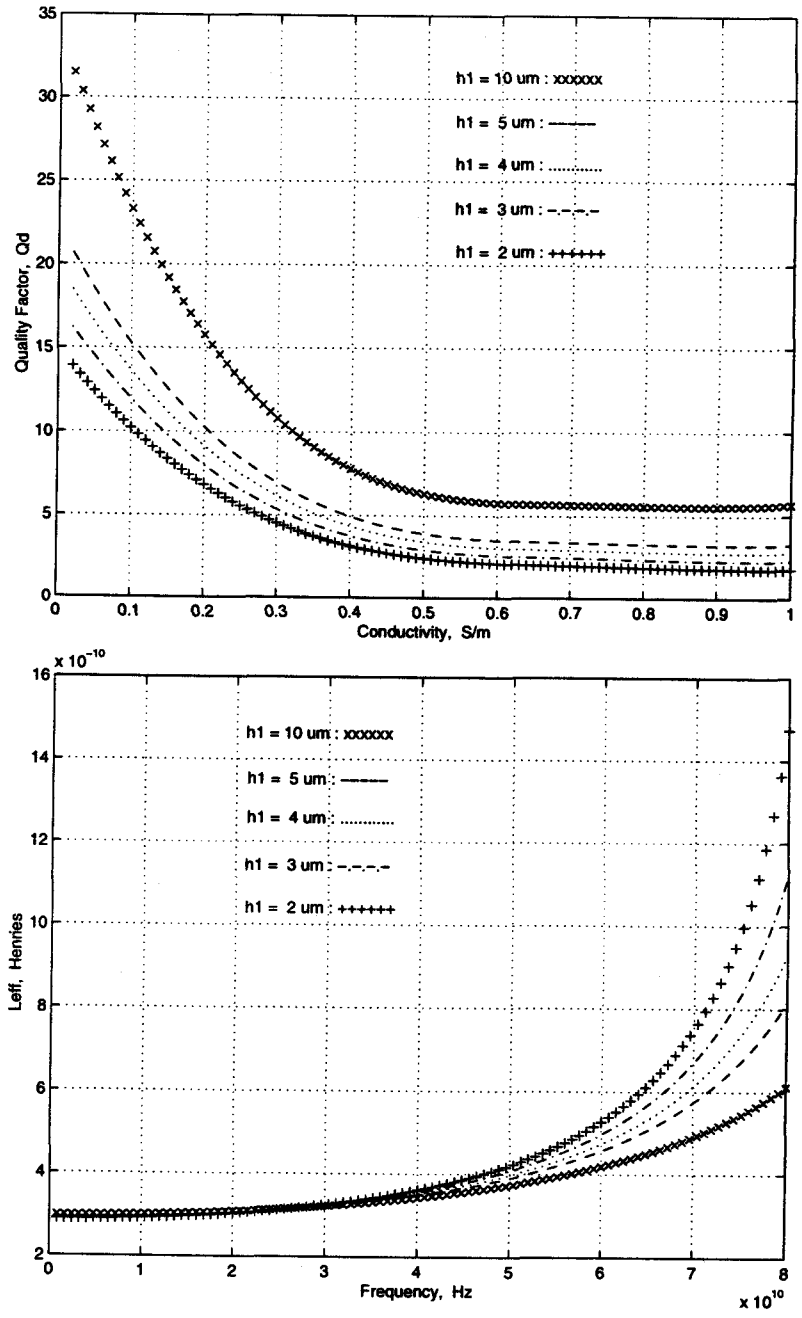

Figure 2.6. (a) Quality factor(Dielectric substrate loss only) as a function of substrate conductivity. One turn spiral with circumference 400 μm, nominal $L_{dc} = 0.3$ nH. (b) Effective inductance as a function of frequency and oxide layer thickness for one turn spiral.

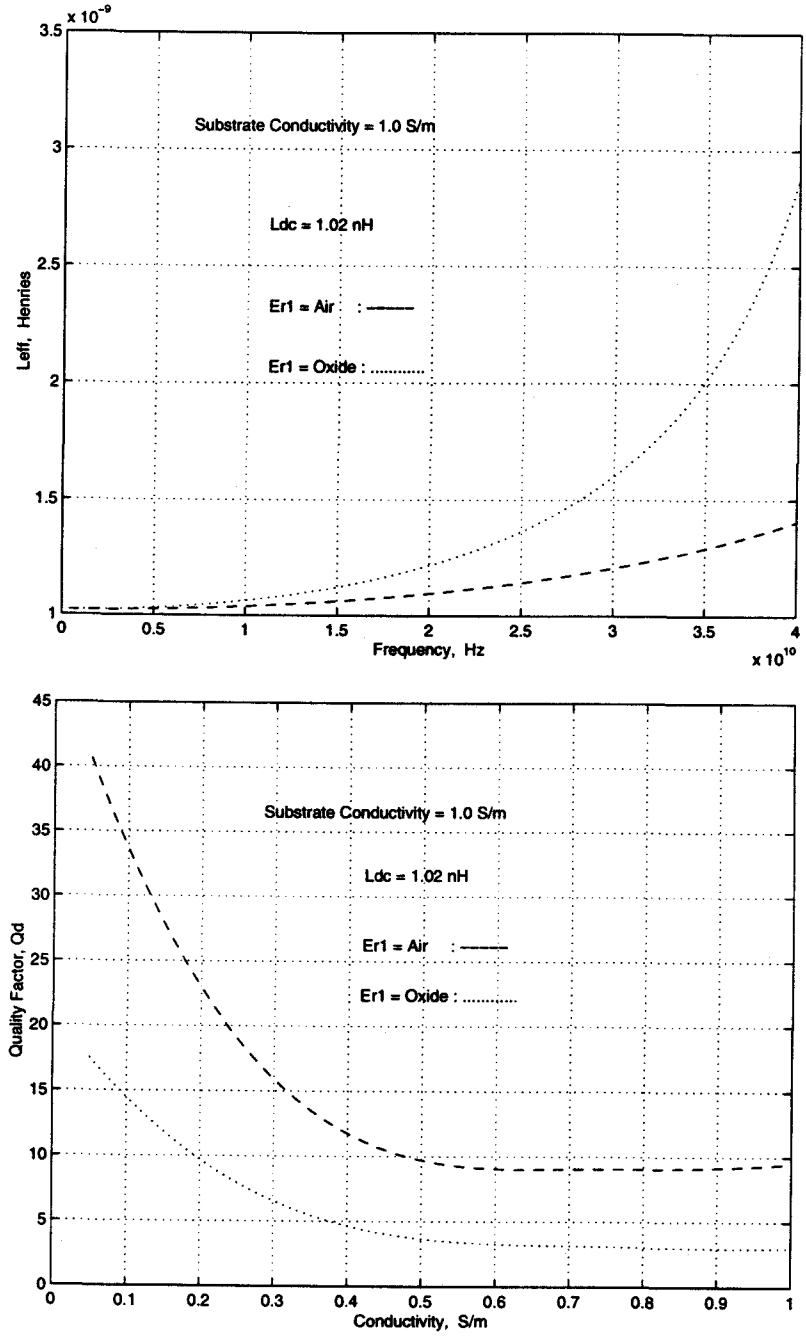

Figure 2.7. (a) Effective spiral inductance vs frequency for the air bridge and the oxide lines. (b) Quality factor corresponding to dielectric loss only for a two turn air bridge spiral and the spiral deposited on a oxide layer.

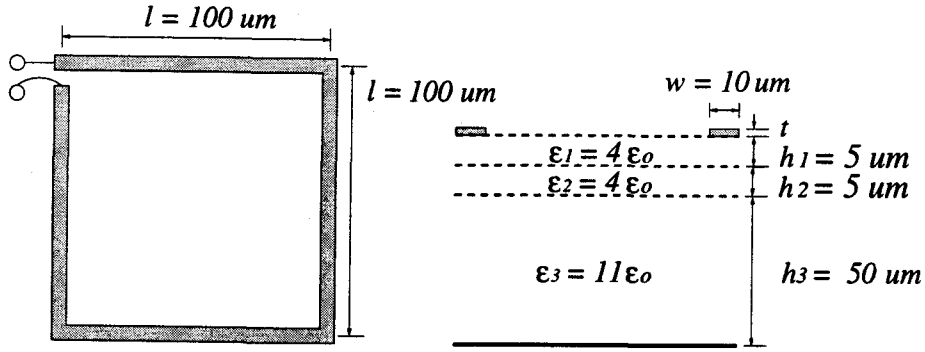

Figure 2.8. A two level one turn rectangular spiral.

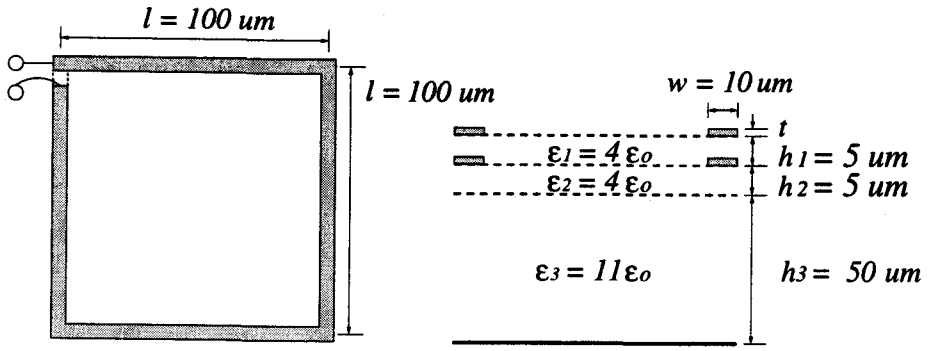

Figure 2.9. A two level two turn rectangular spiral.

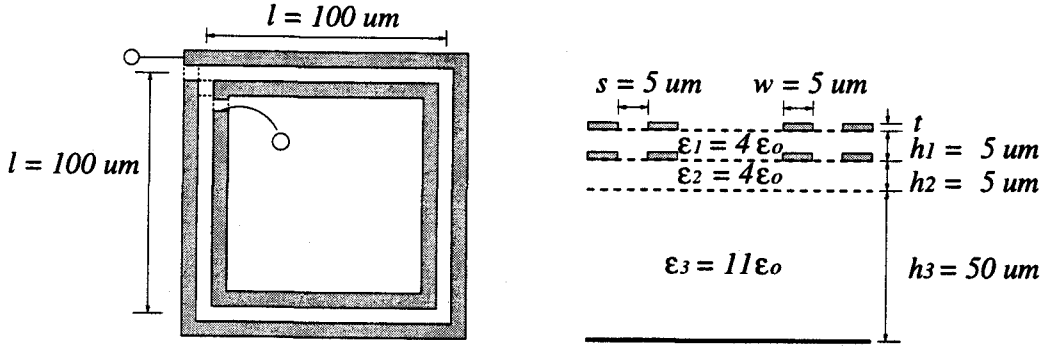

Figure 2.10. A two level four turn rectangular spiral.

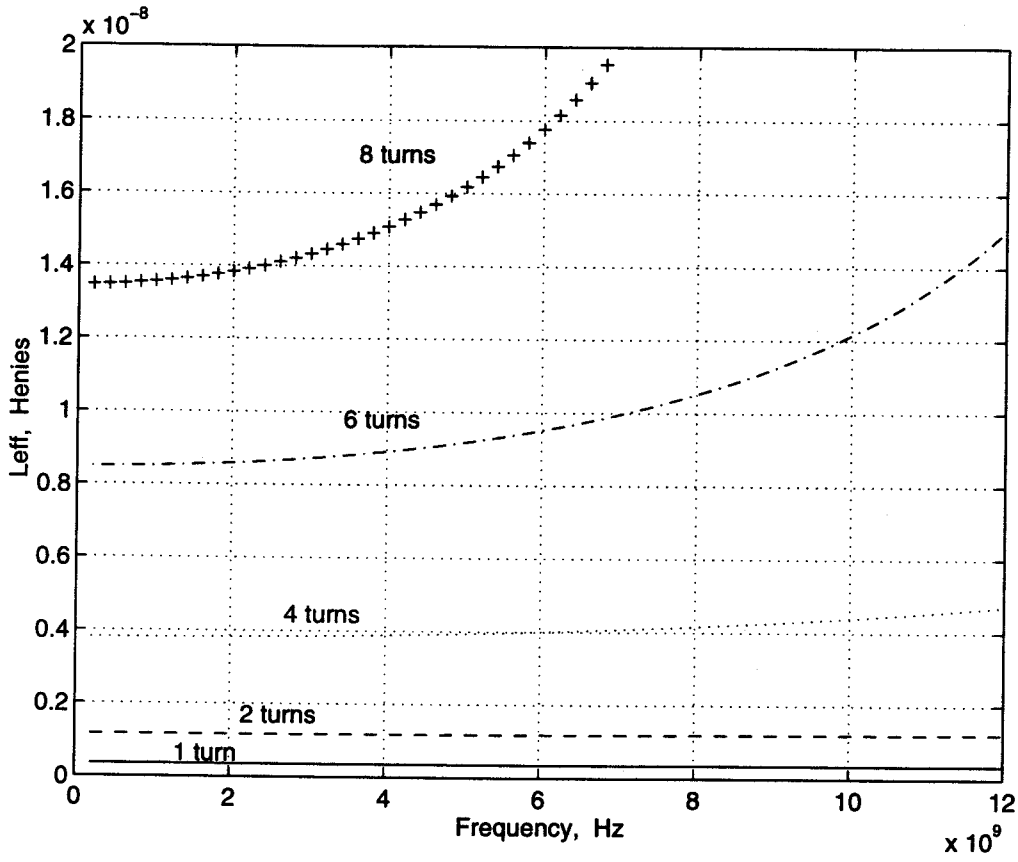

Figure 2.11. Effective two level spiral inductance as a function of frequency and number of turns.

3. ASYMMETRIC COUPLED LINE

The concepts of impedance matching network, guided wave systems, and even- and odd-modes of excitation corresponding to the voltages and the currents on the two coupled lines were introduced. The theory of asymmetric uniform coupled transmission lines in an inhomogeneous medium and a homogeneous medium are reviewed in terms of the properties of normal mode parameters.

3.1. INTRODUCTION

Uniform coupled line circuits are used for many applications including filters, couplers, and impedance matching networks. These circuits are usually designed by utilizing the impedance, admittance, chain, and other parameters characterizing the coupled line four-port network. These parameters may be obtained in terms of the coupled line impedances or admittances, and phase velocities for even- and odd-modes of excitation for the case of coupled TEM lines(homogeneous medium) [33,34] or coupled identical lines in an inhomogeneous medium [35]. Recalling that even- and odd-modes of excitation correspond to the cases where the voltages and the currents on the two lines are equal in magnitude and are in phase for the even-mode and out of phase for the odd-mode, it is seen that such modes cannot propagate independently for the case of asymmetric coupled lines [36]. For asymmetric coupled line cases these modes can be defined only for special cases [36–38] where the line parameters obey certain restrictive relationships.

3.2. COUPLED TRANSMISSION LINES

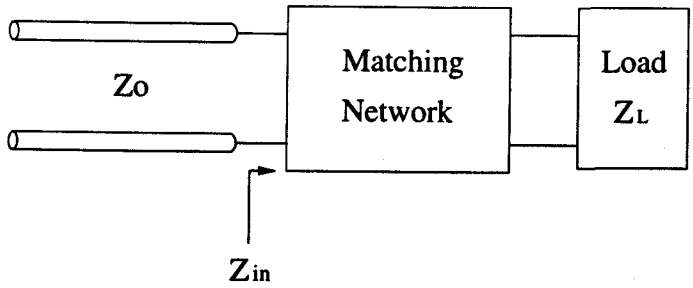

Figure 3.1. Impedance matching network

On designing distributed circuits , such as transmission lines, one of the important considerations is to minimize the power loss in the feed line when the load is matched to the transmission line(assuming the generator is matched). We define this procedure as **impedance matching**.

The basic idea of impedance matching is illustrated in Figure 3.1, which shows an impedance matching network placed between a transmission line and a load impedance. The matching network is ideally lossless, and is usually designed so that the input impedance, *Zin* seen looking into the matching network is characteristic impedance of transmission line, *Zo*. That is *Zin=Zo*. Then the reflections are eliminated on the transmission line to the left of the matching network, although there will be multiple reflections between the matching network and the load. Impedance matching is also important for the following reasons:

- Maximum power is delivered when the load is matched to the line, and the power loss in the feed line is minimized.
- Impedance matching sensitive receiver components(antenna, low-noise amplifier etc.) improves signal to noise ratio of the system.

- Impedance matching in a power distribution network(such as an antenna array feed network) will reduce amplitude and phase errors.

The guided microwave systems in Figure 3.2 can be used for matching network. Microwaves occupy a portion of the EM spectrum extending from 300 MHz to 30 GHz. The conventional guided microwave systems shown in Figure 3.2 (a),(b),(c),(d) were usually used up to 1965. As the printed circuit board techniques were developed MIC shown in Figure 3.2 (e),(f),(g),(h) and MMIC have been most commonly used for the structure of planar transmission lines. Especially the microstrip in Figure 3.2 (f) is one of the most popular types of planar transmission lines because it can be fabricated using photolithographic processes and is easily integrated with other passive and active microwave devices. A conductor of width w is printed on a thin, grounded dielectric substrate of thickness d and relative permittivity ϵ_r.

When two unshielded transmission lines are close together, power can be coupled between the lines due to the interaction of the EM fields of each line. Such lines are referred to as **coupled transmission lines**, and usually consist of 3 conductors in close proximity. Note that we can designate "ground" for the 3rd conductor. Figure 3.3 shows several examples of coupled transmission lines. In general, these coupled transmission lines can support two distinct propagation modes, even- and odd-mode. This feature can be used to implement directional couplers, hybrids, and filters. The even-mode of propagation has the same voltages and currents on the two strips, while the odd-mode of propagation has opposite voltages and currents on the two strips shown in Figure 3.4.

For even-mode, the E-field has even symmetry about the center line, and no current flows between the two strip conductors. This leads to the equivalent circuit

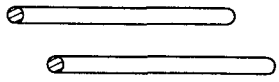

(a) Open two-wire line

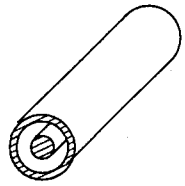

(b) Coaxial line

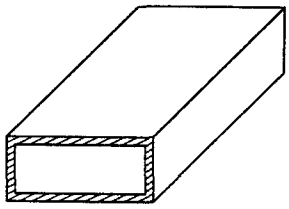

(c) Rectangular waveguide

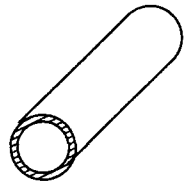

(d) Circular waveguide

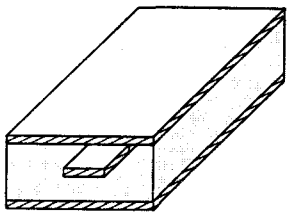

(e) Stripline

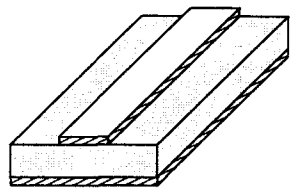

(f) Microstrip

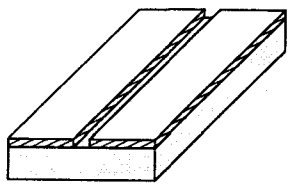

(g) Slotline

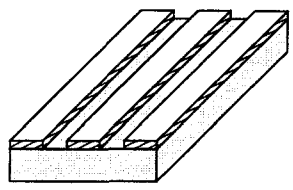

(h) Coplanar waveguide

Figure 3.2. The guided microwave systems

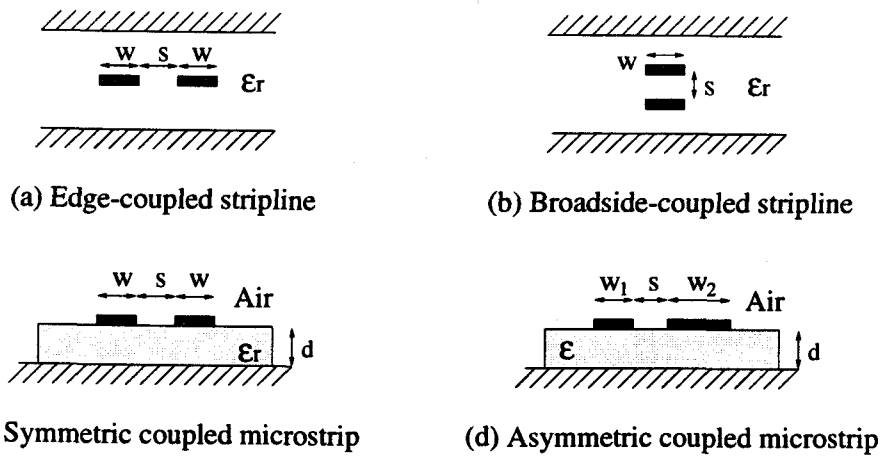

Figure 3.3. Various coupled transmission line geometries

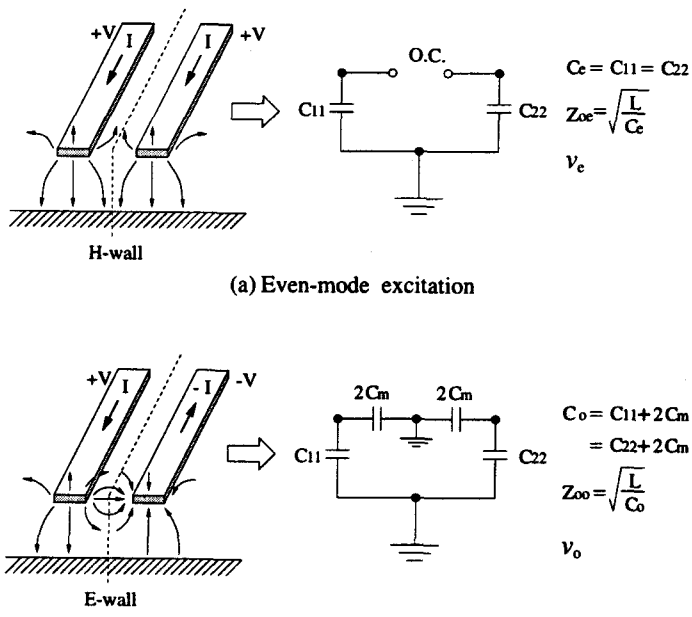

Figure 3.4. Even- and odd-mode of propagation for a coupled line, and the resulting equivalent capacitance networks

shown, where C_m is effectively open-circuited. Then the resulting capacitance of either line to ground for the even-mode is

$$C_e = C_{11} = C_{22}$$

assuming that the two strip conductors are identical in size and location. Then, the characteristic impedance of even-mode is

$$Ze = \sqrt{\frac{L}{C_e}} = \frac{\sqrt{LC_e}}{C_e} = \frac{1}{vC_e}$$

where v is the velocities of propagation of the line.

For even-mode, the electric field lines have an odd symmetry about the center line, and a voltage null exists between the two strip conductors. We can imagine this as a ground plane through the middle of C_m, which leads to the equivalent circuit as shown. In this case, the effective capacitance between either strip conductor and ground is

$$C_o = C_{11} + 2C_m = C_{22} + 2C_m$$

and the characteristic impedance for the odd-mode is

$$Z_o = \frac{1}{vC_o}.$$

3.3. ASYMMETRIC COUPLED LINE ANALYSIS

The even and odd modes of excitations as mentioned above cannot propagate independently for the case of asymmetric coupled lines. The parameters of a general asymmetric asynchronous coupled line four-port are obtained in terms of the line properties for two independent modes of excitations. These modes correspond to a linear combination of voltages and currents on the two lines which are related in

magnitude and phase through terms involving line constants. The four-port circuit parameters are obtained by writing the solutions for voltages and currents on the two lines in terms of the two independent modes and deriving the relationships between port voltages and currents in a suitable form leading to impedance, admittance, chain, or any other parameters.

The behavior of asymmetric coupled line shown in Figure 3.5 is described in general by the following the solution of coupled transmission line equations:

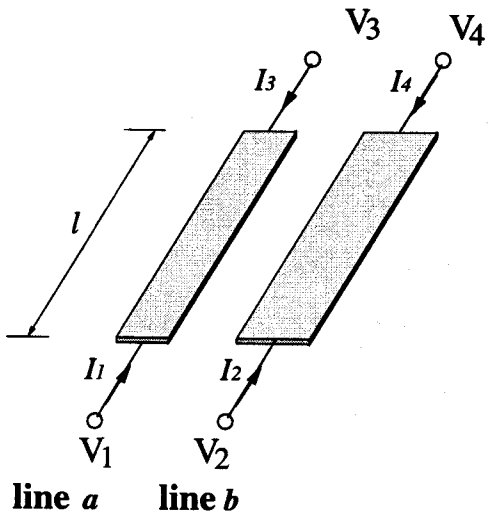

c-mode and π-mode Excitation

Z_{c_1}, Z_{c_2},

Z_{π_1}, Z_{π_2},

v_c, v_π,

β_c, β_π $(\beta = \frac{\omega}{v})$

θ_c, θ_π $(\theta = \beta l)$,

Figure 3.5. Asymmetric coupled transmission line

Coupled transmission line equations are given by,

$$\frac{\partial v]}{\partial z} = -[z]i] \tag{3.1}$$

$$\frac{\partial i]}{\partial z} = -[y]v] \tag{3.2}$$

where, vector $v]$ and $i]$ represents voltages and currents on the two lines, line a and line b in terms of two independent mode, c-mode and π-mode [6].

$\beta_{c,\pi}$ are the phase constants for the two modes, $R_{c,\pi}$ are the ratio of the voltages on the lines for the two normal modes, Z_{c1}, $Z_{\pi 1}$, Z_{c2}, $Z_{\pi 2}$ are the mode impedances of the two lines, and Y_{c1}, $Y_{\pi 1}$, Y_{c2}, $Y_{\pi 2}$ are the corresponding admittances.
where

$$[z] = [R] + j\omega[L],$$

$$[y] = [G] + j\omega[C]$$

and [R],[L],[G],[C] per unit length are line constant matrices.

In terms of impedance parameters, the expression of voltage equations for 4-port can be expressed as follows;

$$[V] = [Z][I],$$

$$\begin{bmatrix} V_1 \\ V_2 \\ V_3 \\ V_4 \end{bmatrix} = \begin{bmatrix} Z_{11} & Z_{12} & Z_{13} & Z_{14} \\ Z_{21} & Z_{22} & Z_{23} & Z_{24} \\ Z_{31} & Z_{32} & Z_{33} & Z_{34} \\ Z_{41} & Z_{42} & Z_{43} & Z_{44} \end{bmatrix} \begin{bmatrix} I_1 \\ I_2 \\ I_3 \\ I_4 \end{bmatrix} = \begin{bmatrix} Z_{11} & Z_{12} & Z_{13} & Z_{14} \\ Z_{12} & Z_{22} & Z_{14} & Z_{24} \\ Z_{13} & Z_{14} & Z_{11} & Z_{12} \\ Z_{14} & Z_{24} & Z_{12} & Z_{22} \end{bmatrix} \begin{bmatrix} I_1 \\ I_2 \\ I_3 \\ I_4 \end{bmatrix} \tag{3.3}$$

where [Z] is the characteristic impedance matrix. And it can be summarized

$$[Z] = \begin{bmatrix} [Z_A] & [Z_B] \\ [Z_B] & [Z_A] \end{bmatrix}$$

where

$$[Z_A] = \begin{bmatrix} [Z_{11}] & [Z_{12}] \\ [Z_{12}] & [Z_{22}] \end{bmatrix}, \qquad [Z_B] = \begin{bmatrix} [Z_{13}] & [Z_{14}] \\ [Z_{14}] & [Z_{24}] \end{bmatrix}.$$

If it is etched on an inhomogeneous medium, the elements of the characteristic impedance 4x4 matrix are given by

$$Z_{11} = Z_{33} = \frac{Z_{c1} coth\gamma_c l}{1 - \frac{R_c}{R_\pi}} + \frac{Z_{\pi 1} coth\gamma_\pi l}{1 - \frac{R_\pi}{R_c}} \tag{3.4}$$

$$Z_{12} = Z_{21} = Z_{34} = Z_{43} = \frac{Z_{c1} R_c coth\gamma_c l}{1 - \frac{R_c}{R_\pi}} + \frac{Z_{\pi 1} R_\pi coth\gamma_\pi l}{1 - \frac{R_\pi}{R_c}} \tag{3.5}$$

$$Z_{22} = Z_{44} = \frac{Z_{c1} {R_c}^2 coth\gamma_c l}{1 - \frac{R_c}{R_\pi}} + \frac{Z_{\pi 1} {R_\pi}^2 coth\gamma_\pi l}{1 - \frac{R_\pi}{R_c}} \tag{3.6}$$

$$Z_{13} = Z_{31} = \frac{Z_{c1} csch\gamma_c l}{1 - \frac{R_c}{R_\pi}} + \frac{Z_{\pi 1} csch\gamma_\pi l}{1 - \frac{R_\pi}{R_c}} \tag{3.7}$$

$$Z_{14} = Z_{23} = Z_{32} = Z_{41} = \frac{Z_{c1} R_c csch\gamma_c l}{1 - \frac{R_c}{R_\pi}} + \frac{Z_{\pi 1} R_\pi csch\gamma_\pi l}{1 - \frac{R_\pi}{R_c}} \tag{3.8}$$

$$Z_{24} = Z_{42} = \frac{Z_{c1} {R_c}^2 csch\gamma_c l}{1 - \frac{R_c}{R_\pi}} + \frac{Z_{\pi 1} {R_\pi}^2 csch\gamma_\pi l}{1 - \frac{R_\pi}{R_c}} \tag{3.9}$$

And in a homogeneous medium such as a strip line, the parameters are bounded as follows; the velocity, the propagation constant, and the electrical length of each mode has same value,

$$v_c = v_\pi = v,$$

$$\gamma_c = \gamma_\pi = j\beta,$$

$$\theta_c = \theta_\pi = \theta.$$

The voltage ratio of each mode has such relationships.

$$R_c = -R_\pi = \sqrt{\frac{Z_2}{Z_1}} = k.$$

And the characteristic impedance 4x4 matrix can be simpler as given by.

$$[Z] = \begin{bmatrix} [Z_A] & [Z_B] \\ [Z_B] & [Z_A] \end{bmatrix}$$

where,

$$Z_{11} = Z_{33} = \frac{-j}{2}[Z^a_{oe} + Z^a_{oo}]cot\theta \tag{3.10}$$

$$Z_{12} = Z_{21} = Z_{34} = Z_{43} = \frac{-j}{2}[Z^a_{eo} - Z^a_{oo}]cot\theta = \frac{-j}{2}[Z^b_{oe} - Z^b_{oo}]cot\theta \tag{3.11}$$

$$Z_{22} = Z_{44} = \frac{-j}{2}[Z^b_{oe} + Z^b_{oo}]cot\theta \tag{3.12}$$

$$Z_{13} = Z_{31} = \frac{-j}{2}[Z^a_{oe} + Z^a_{oo}]csc\theta \tag{3.13}$$

$$Z_{14} = Z_{23} = Z_{32} = Z_{41} = \frac{-j}{2}[Z^a_{eo} - Z^a_{oo}]csc\theta = \frac{-j}{2}[Z^b_{oe} - Z^b_{oo}]csc\theta \tag{3.14}$$

$$Z_{22} = Z_{44} = \frac{-j}{2}[Z^b_{oe} + Z^b_{oo}]csc\theta \tag{3.15}$$

If we consider an open-circuit asymmetric single section consisting of lossless lines as shown in Figure 3.6, the voltage matrix can be reduced to 2-port as,

$$\begin{bmatrix} V_1 \\ V_4 \end{bmatrix} = \begin{bmatrix} Z_{11} & Z_{14} \\ Z_{14} & Z_{44} \end{bmatrix} \begin{bmatrix} I_1 \\ I_4 \end{bmatrix}$$

because of $I_2 = I_3 = 0$.

In an inhomogeneous medium, the characteristic impedance 4x4 matrix is

$$\begin{bmatrix} Z_{11} & Z_{14} \\ Z_{14} & Z_{44} \end{bmatrix} = \begin{bmatrix} \frac{Z_{c1}coth\gamma_c l}{1-\frac{R_c}{R_\pi}} + \frac{Z_{\pi 1}coth\gamma_\pi l}{1-\frac{R_\pi}{R_c}} & \frac{Z_{c1}R_c csch\gamma_c l}{1-\frac{R_c}{R_\pi}} + \frac{Z_{\pi 1}R_\pi csch\gamma_\pi l}{1-\frac{R_\pi}{R_c}} \\ \frac{Z_{c1}R_c csch\gamma_c l}{1-\frac{R_c}{R_\pi}} + \frac{Z_{\pi 1}R_\pi csch\gamma_\pi l}{1-\frac{R_\pi}{R_c}} & \frac{Z_{c1}{R_c}^2 coth\gamma_c l}{1-\frac{R_c}{R_\pi}} + \frac{Z_{\pi 1}{R_\pi}^2 coth\gamma_\pi l}{1-\frac{R_\pi}{R_c}} \end{bmatrix}.$$

In a homogeneous medium, it can be simpler as

$$\begin{bmatrix} Z_{11} & Z_{14} \\ Z_{14} & Z_{44} \end{bmatrix} = \begin{bmatrix} \frac{-j}{2}(Z^a_{oe} + Z^a_{oo})cot\theta & \frac{-j}{2}(Z^a_{eo} - Z^a_{oo})csc\theta \\ \frac{-j}{2}(Z^a_{eo} - Z^a_{oo})csc\theta & \frac{-j}{2}(Z^b_{oe} + Z^b_{oo})csc\theta \end{bmatrix}.$$

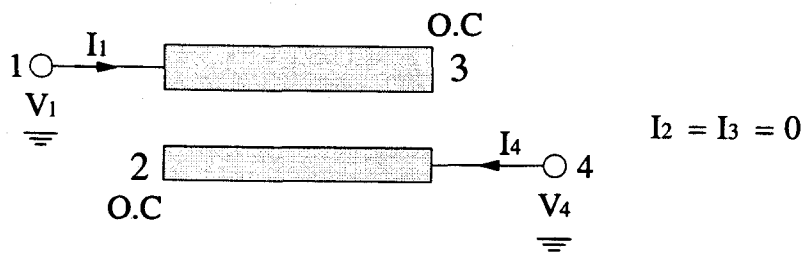

Figure 3.6. An Open-circuit Asymmetric Section

3.4. SUMMARY

The theory of asymmetric uniform coupled transmission lines in an inhomogeneous and a homogeneous medium were reviewed in terms of the properties of normal mode parameters. As an example, the Z-parameters of an open-circuit asymmetric single section consisting of lossless lines which will be used in designing the band-pass filters in the next chapters were also reviewed.

4. ASYMMETRIC COUPLED LINE FILTER DESIGN

4.1. INTRODUCTION

Symmetrical and asymmetrical two-port coupled line structures consisting of a pair of lines in an inhomogeneous medium [6] have various applications as filters and impedance matching network. One of the two-port of the prototypes [7], the open circuited interdigital filters, shown in Figure 4.1, is a wide band filter with DC isolated input and output ports. The filter has been used for application as DC blocks [48–50] because of its improved performance at higher frequency as compared to a lumped capacitor. These DC blocks were introduced by La Combe and Cohen [48], who, for their analysis, used an approximate equivalent circuit, based on the even- and odd-mode propagation in coupled microstrip. A more general approach was presented by Rizzoli [49], who derived the conditions for both flat and first order Chebyshev frequency response and obtained design formulas for DC blocks with a pair of lines. The analysis and design procedures utilizing the expressions for scattering parameters of two-port network, open-circuited interdigital multiple coupled microstrip line structures for applications as wide band DC blocks and filters are presented in [51].

The design procedure for a symmetric coupled line bandpass filter were introduced in Matthaei [46] and Pozar [47] and the design procedure for the asymmetric coupled line has been reported in [50,68,69].

In this chapter, the design procedure utilizing the image impedances and image constant of the asymmetric coupled line single section and its equivalent circuit of the two port incorporating an admittance inverter for general symmetric

as well as asymmetric transformer/filters with a desired impedance transformation for single section, 3-section, 4-section, and multi-section are presented.

4.2. DESIGN OF ASYMMETRIC SINGLE SECTION TRANSFORMER AND FILTER

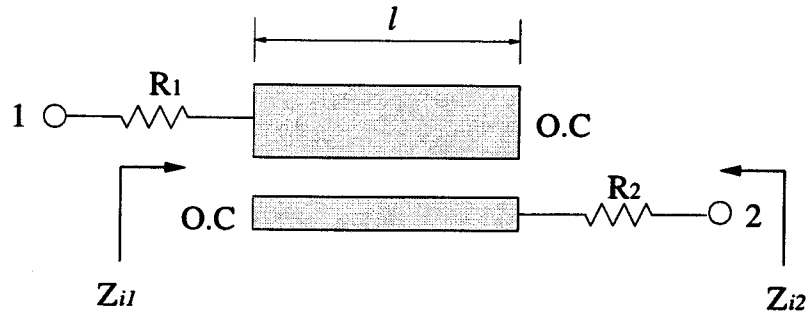

Figure 4.1. A 2-port asymmetric coupled line section having a band-pass response

Symmetrical and non-symmetrical two-port coupled microstrip line structures consisting of a pair of lines in an inhomogeneous medium [6] have various applications as filters and impedance matching network. In this section the basic properties of an open-circuited coupled line structures, shown in Figure 4.1, for applications as wide band DC blocks and filters are examined [51].

The scattering parameters of the two port terminated in R_1 and R_2 as shown in Figure 4.1 are found from the four port immittance matrix [6] to be:

$$[S] = \begin{bmatrix} S_{11} & S_{12} \\ S_{21} & S_{22} \end{bmatrix}$$

where

$$S_{11} = \frac{(Z_{11} - R_1)(Z_{22} + R_2) - Z_{12}^2}{(Z_{11} + R_1)(Z_{22} + R_2) - Z_{12}^2}$$
$$= \frac{K - \frac{j}{2}(A - B)cot\theta}{(K + 2R_1R_2) - \frac{j}{2}(A + B)cot\theta},$$

$$S_{12} = S_{21} = \frac{2\sqrt{R_1 R_2} Z_{12}}{(Z_{11} + R_1)(Z_{22} + R_2) - Z_{12}^2}$$
$$= \frac{-j\sqrt{R_1 R_2}(Z_{oe}^a - Z_{oo}^a)csc\theta}{(K + 2R_1 R_2) - \frac{j}{2}(A + B)cot\theta},$$

$$S_{22} = \frac{(Z_{11} + R_1)(Z_{22} - R_2) - Z_{12}^2}{(Z_{11} + R_1)(Z_{22} + R_2) - Z_{12}^2}$$
$$= \frac{K + \frac{j}{2}(A - B)cot\theta}{(K + 2R_1 R_2) - \frac{j}{2}(A + B)cot\theta},$$

where,

$$Z_{11} = \frac{-j}{2}(Z_{oe}^a + Z_{oo}^a)cot\theta,$$

$$Z_{12} = \frac{-j}{2}(Z_{oe}^a - Z_{oo}^a)csc\theta$$
$$= \frac{-j}{2}(Z_{oe}^b - Z_{oo}^b)csc\theta,$$

$$Z_{22} = \frac{-j}{2}(Z_{oe}^b + Z_{oo}^b)cot\theta,$$

$$K = \frac{1}{4}(Z_{oe}^a - Z_{oo}^a)^2 - \frac{1}{2}(Z_{oe}^a Z_{oo}^b + Z_{oo}^a Z_{oe}^b)cot^2\theta - R_1 R_2,$$

$$A = R_2(Z_{oe}^a + Z_{oo}^a),$$

$$B = R_1(Z_{oe}^b + Z_{oo}^b),$$

and Z_{oe}^a, Z_{oo}^a are the even and odd mode impedance of line a and Z_{oe}^b, Z_{oo}^b are the even and odd mode impedance of line b.

And scattering parameters of a symmetric coupled line are represented by,

$$[S] = \begin{bmatrix} S_{11} & S_{12} \\ S_{21} & S_{22} \end{bmatrix} = \begin{bmatrix} S_{11} & S_{12} \\ S_{12} & S_{11} \end{bmatrix}$$

where,

$$S_{11} = S_{22} = \frac{K'}{(K' + 2R^2) - jR(Z_e + Z_o)cot\theta} \ ,$$

$$S_{12} = S_{21} = \frac{-jR(Z_e - Zo)csc\theta}{(K' + 2R^2) - jR(Z_e + Z_o)cot\theta} \ ,$$

$$K' = \frac{1}{4}(Z_e - Z_o)^2 - Z_e Z_o cot^2\theta - R^2.$$

The matching conditions for the non-symmetric case can be obtained by setting $S_{11} = S_{22} = 0$ (at $l = \frac{\lambda}{4}$ or $\theta = \frac{\pi}{2}$) of the asymmetric and symmetric coupled line for Butterworth response [51].

$$R_1 = \frac{Z^a_{oe} - Z^a_{oo}}{2}\sqrt{\frac{Z^a_{oe} + Z^a_{oo}}{Z^b_{oe} + Z^b_{oo}}} \ ,$$

$$R_2 = \frac{Z^a_{oe} - Z^a_{oo}}{2}\sqrt{\frac{Z^b_{oe} + Z^b_{oo}}{Z^a_{oe} + Z^a_{oo}}} \ ,$$

$$= \frac{Z^b_{oe} + Z^b_{oo}}{Z^a_{oe} + Z^a_{oo}} R_1 \ ,$$

$$R_1 = R_2 = R = \frac{Z_e - Z_o}{2}.$$

The matching conditions of asymmetric and symmetric coupled line for Chebyshev response also can be obtained by setting $S_{11} = S_{22} = 0$ at $l = \frac{\lambda}{4}$ or $\theta = \frac{\pi}{2}$.

$$R_1 R_2 < \frac{1}{4}(Z^a_{oe} - Z^a_{oo})^2 = \frac{1}{4}(Z^a_{oe} - Z^a_{oo})(Z^b_{oe} - Z^b_{oo}) \ ,$$

$$R < \frac{Z_e - Z_o}{2}.$$

For the single section Butterworth response the normalized cut off frequency, $\theta_c = \beta_c\, l = \omega_c \sqrt{\mu_o \epsilon}\, l$, where $|S_{11}| = \Gamma_c$ is obtained as,

$$\theta_c = tan^{-1} \left[\frac{-1 + \sqrt{1 + \chi^2(\frac{1}{\Gamma_c^2} - 1)}}{2} \right]^{\frac{1}{2}}, \tag{4.1}$$

where,

$$\chi = \frac{2(Z_{oe}^a Z_{oo}^b + Z_{oo}^a Z_{oe}^b)}{(Z_{oe}^a - Z_{oo}^a)^2}. \tag{4.2}$$

The smaller the χ is, the larger is the fractional bandwidth[$=2(1 - \frac{2\theta_c}{\pi})$].

For Chebyshev response, θ_c is obtained by letting maximum ripple $|S_{11}| = \Gamma_t$ at $\theta = \frac{\pi}{2}$.

$$\theta_c = tan^{-1} \left[\frac{1 - \Gamma_t}{8(R_1 R_2)^2 \mid \Gamma_t^2 - \Gamma_c^2 \mid} \cdot \left\{ D + \sqrt{D^2 - 4C(1 - \Gamma_c^2) \mid \Gamma_t^2 - \Gamma_c^2 \mid (R_1 R_2)^2} \right\} \right]^{\frac{1}{2}}, \tag{4.3}$$

where,

$$C = Z_{oe}^a Z_{oo}^b + Z_{oo}^a Z_{oe}^b,$$

$$D = 2CR_1R_2(\Gamma_t - \Gamma_c^2) - \frac{1 - \Gamma_t}{4} \left\{ (A - B)^2 - \Gamma_c^2 (A + B)^2 \right\}.$$

The design procedure for a single section filter(DC block) is illustrated with an example of both symmetrical and non-symmetrical open-circuited coupled line.

Examples:

For a specified $R = 50\ \Omega$ and a predicted bandwidth of 80 % taking $|S_{11}| = \Gamma_c = \frac{1}{3}$ for a symmetrical coupled line two-port structure, one can determine Z_e, Z_o,

and χ for a Butterworth response, so that $Z_e = 131.5\ \Omega$, $Z_o = 31.5\ \Omega$, and $\chi = 1.66$ as shown in Figure 4.2. And for an asymmetrical coupled line two-port structure, one can determine Z^a_{oe}, Z^a_{oo}, Z^b_{oe}, Z^b_{oo} for a Butterworth response, so that $Z^a_{oe} = 87.62\ \Omega$, $Z^a_{oo} = 10.16\ \Omega$, $Z^b_{oe} = 120.21\ \Omega$, and $Z^b_{oo} = 42.75\ \Omega$ as shown in Figure 4.3

With maximum ripple, $|\Gamma_t| = \frac{1}{6}$ at $\theta = \frac{\pi}{2}$ for Chebyshev response, we need $R = 50\ \Omega$ for a symmetrical coupled line and $R_1 = 30\ \Omega$, $R_2 = 50\ \Omega$ for an asymmetrical coupled line so that $Z_e = 149.8\ \Omega$, $Z_o = 31.5\ \Omega$ and $Z^a_{oe} = 101.81\ \Omega$, $Z^a_{oo} = 10.16\ \Omega$, $Z^b_{oe} = 134.4\ \Omega$, and $Z^b_{oo} = 42.75\ \Omega$ as shown in Figure 4.2 and Figure 4.3.

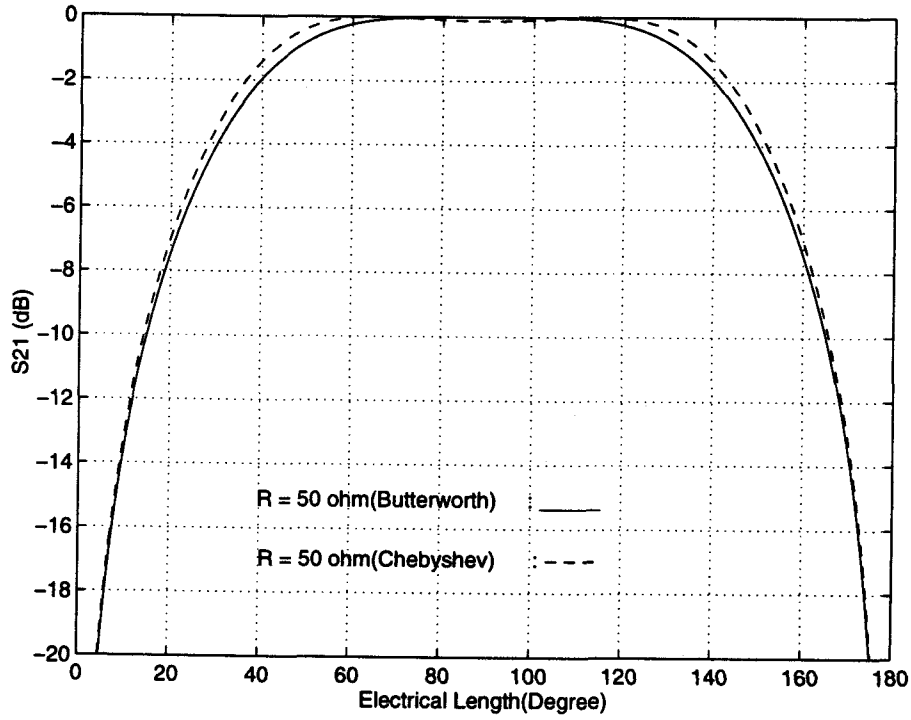

Figure 4.2. Transmission coefficient $|S21|$ vs normalized frequency, θ for a symmetrical coupled line.

The bandwidth of DC blocks depends on the coupling, C_m between the two lines and the structure becomes either impractical or unrealizable by conventional MIC technology for larger bandwidths. Since, for a large bandwidth, the lines have

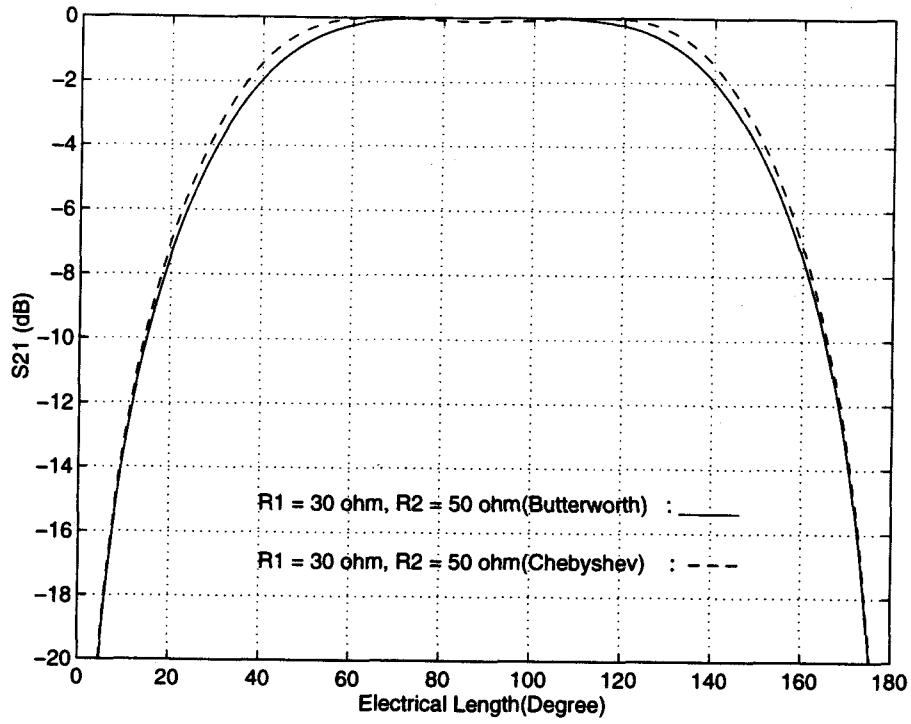

Figure 4.3. Transmission coefficient $|S21|$ vs normalized frequency, θ for an asymmetrical coupled line.

to be very tightly coupled, it is more convenient to use more than two lines. The bandwidth for a given coupling, and hence the line widths and spacing can be increased significantly by utilizing more than two lines.

4.3. DESIGN OF ASYMMETRIC CASCADED MULTI-SECTION TRANSFORMER AND FILTER

4.3.1. Design Procedure

For general multisection filters, the design procedure can be formulated by using the admittance inverter corresponding to the single section equivalent circuit of a coupled asymmetric line section [46,47]. The image impedances and image constant of the asymmetric coupled line singie section and its equivalent circuit of

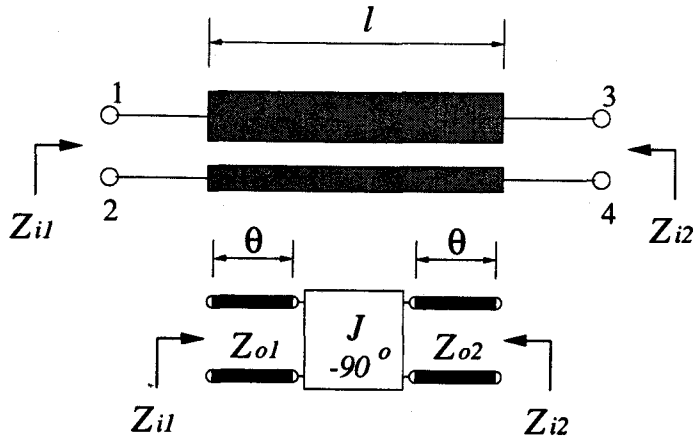

Figure 4.4. (a) An asymmetric coupled line single section. (b) The equivalent circuit of an admittance inverter.

the two port incorporating an admittance inverter as shown in Figure 4.4 are as follows;

The image impedances and image constant of the asymmetric coupled line single section are given by,

$$Z_{i1} = \sqrt{\frac{Z_{11}}{Z_{44}}(Z_{11}Z_{44} - Z_{14}^2)} = \frac{Z_e^a - Z_o^a}{2}\sqrt{\frac{Z_e^a + Z_o^a}{Z_e^b + Z_o^b}}, \tag{4.4}$$

$$Z_{i2} = \sqrt{\frac{Z_{44}}{Z_{11}}(Z_{11}Z_{44} - Z_{14}^2)} = \frac{Z_e^a - Z_o^a}{2}\sqrt{\frac{Z_e^b + Z_o^b}{Z_e^a + Z_o^a}}, \tag{4.5}$$

$$cos\beta = \frac{\sqrt{(Z_e^a + Z_o^a)(Z_e^b + Z_o^b)}}{Z_e^a - Z_o^a}cos\theta. \tag{4.6}$$

The image impedances and image constant of the equivalent circuit are given as,

$$Z_{i1} = Z_{o1}\sqrt{\frac{Z_{o1}Z_{o2}J^2sin^2\theta - cos^2\theta}{sin^2\theta - Z_{o1}Z_{o2}J^2cos^2\theta}}, \tag{4.7}$$

$$Z_{i2} = Z_{o2}\sqrt{\frac{Z_{o1}Z_{o2}J^2sin^2\theta - cos^2\theta}{sin^2\theta - Z_{o1}Z_{o2}J^2cos^2\theta}} = \frac{Z_{o2}}{Z_{o1}}Z_{i1}, \tag{4.8}$$

$$cos\beta = \sqrt{2 + Z_{o1}Z_{o2}J^2 + \frac{1}{Z_{o1}Z_{o2}J^2}}sin\theta cos\theta. \tag{4.9}$$

Then, equating the image impedance equations (4.4), (4.5) and (4.7), (4.8) and the image constant equations (4,6) and (4.9) with the same parameters of the coupled line two port in a homogeneous medium at the center frequency, $\theta = \frac{\pi}{2}$ ($l = \frac{\lambda}{4}$), we get the following mode impedance equations of each line a and line b. This can be applied to design band-pass filters with asymmetric coupled line.

Finally the mode impedances of each line can be derived in terms of the voltage ratio k, input impedance Z_{o1}, and characteristic admittance J as follows;

$$Z^a_{oe} = kZ^2_{o1}J\left[k + \sqrt{2 + (kZ_{o1}J)^2 + \frac{1}{(kZ_{o1}J)^2}}\right] \tag{4.10}$$

$$Z^a_{oo} = kZ^2_{o1}J\left[-k + \sqrt{2 + (kZ_{o1}J)^2 + \frac{1}{(kZ_{o1}J)^2}}\right] \tag{4.11}$$

$$Z^b_{oe} = \frac{1}{2}[(k^2+1)Z^a_{oe} + (k^2-1)Z^a_{oo}] \tag{4.12}$$

$$Z^b_{oo} = \frac{1}{2}[(k^2-1)Z^a_{oe} + (k^2+1)Z^a_{oo}] \tag{4.13}$$

where, the voltage ratio

$$k = \sqrt{\frac{Z_{o2}}{Z_{o1}}} = \sqrt{\frac{Z_{i2}}{Z_{i1}}} = \sqrt{\frac{Z^b_{oe} + Z^b_{oo}}{Z^a_{oe} + Z^a_{oo}}}.$$

4.3.2. Asymmetric Coupled Line Filter of 3-sections

The design parameters for a band-pass filter with 3 coupled line sections ($N = 3$) with four terminating impedances($N+1$), Z_{o1}, Z_{o2}, Z_{o3}, $Z_{o4} = Z_{o1}$ and different six widths($2N$), w_1, w_2, w_3, w_4, w_5, w_6 as shown in Figure 4.5 are then found to be:

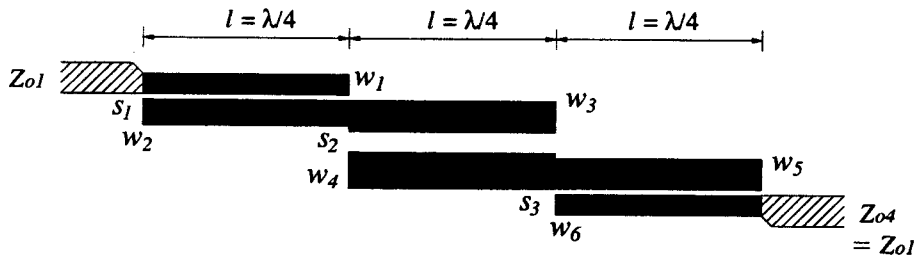

(a) Layout of an N+1 section asymmetric coupled line band-pass filter

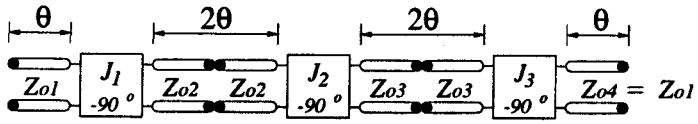

(b) Using admittance inverter for each coupled line section

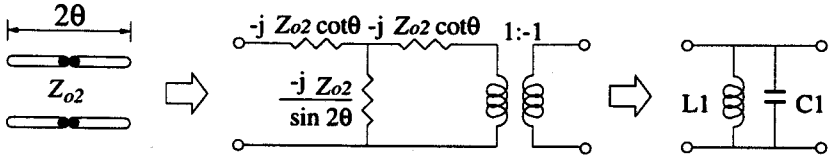

(c) Equivalent circuit for transmission lines of length 2θ

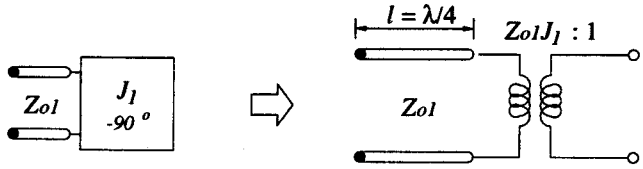

(d) Equivalent circuit of the admittance inverter

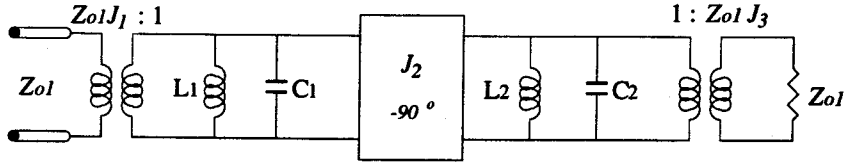

(e) Using results of (c) and (d)

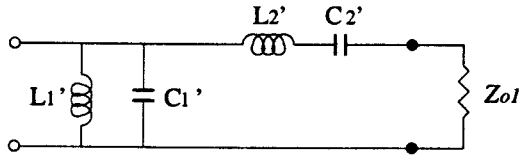

(f) Lumped-element equivalent circuit for a band-pass filter

Figure 4.5. Development of an equivalent circuit for derivation of design equations for a 3-section coupled line band-pass filter

$$Z_{o1}J_1 = \sqrt{\frac{\pi\Delta}{2g_1}} \cdot \sqrt{\frac{Z_{o1}}{Z_{o2}}} = \sqrt{\frac{\pi\Delta}{2g_1}} \cdot \frac{1}{k_1}, \tag{4.14}$$

$$Z_{o2}J_2 = \frac{\pi\Delta}{2\sqrt{g_1 g_2}} \cdot \sqrt{\frac{Z_{o2}}{Z_{o3}}} = \frac{\pi\Delta}{2\sqrt{g_1 g_2}} \cdot \frac{1}{k_2}, \tag{4.15}$$

$$Z_{o3}J_3 = \sqrt{\frac{\pi\Delta}{2g_2 g_3}} \cdot \sqrt{\frac{Z_{o3}}{Z_{o1}}} = \sqrt{\frac{\pi\Delta}{2g_2 g_3}} \cdot \frac{1}{k_3}, \tag{4.16}$$

where the fractional bandwidth is represented by

$$\Delta = \frac{\omega_2 - \omega_1}{\omega_0},$$

$$k_1 = \sqrt{\frac{Z_{o2}}{Z_{o1}}},$$

$$k_2 = \sqrt{\frac{Z_{o3}}{Z_{o2}}},$$

$$k_3 = \sqrt{\frac{Z_{o4}}{Z_{o3}}} = \sqrt{\frac{Z_{o1}}{Z_{o3}}},$$

and g_N represents the element values for Butterworth and Chebyshev low-pass filter prototype.

The design parameters given by equations (4.14)-(4.16) can be plugged into the design equations (4.10)-(4.13) for each section to get the values of the 3-section asymmetric coupled line parameters. For the each section, the mode impedances of each line a, line b can be derived in terms of the voltage ratio k_N(N represents the number of section), characteristic impedances Z_{o1}, Z_{o2}, Z_{o3}, and characteristic admittance J_N of Y inverter of each section.

For the 1^{st} section, we can get those as follows;

$$Z_{oe}^a = k_1 Z_{o1}^2 J_1 \left[k_1 + \sqrt{2 + (k_1 Z_{o1} J_1)^2 + \frac{1}{(k_1 Z_{o1} J_1)^2}} \right] \tag{4.17}$$

$$Z_{oo}^{a} = k_1 Z_{o1}^2 J_1 \left[-k_1 + \sqrt{2 + (k_1 Z_{o1} J_1)^2 + \frac{1}{(k_1 Z_{o1} J_1)^2}} \right] \tag{4.18}$$

$$Z_{oe}^{b} = \frac{1}{2}[(k_1^2 + 1)Z_{oe}^{a} + (k_1^2 - 1)Z_{oo}^{a}] \tag{4.19}$$

$$Z_{oo}^{b} = \frac{1}{2}[(k_1^2 - 1)Z_{oe}^{a} + (k_1^2 + 1)Z_{oo}^{a}] \tag{4.20}$$

where,

$$k_1 = \sqrt{\frac{Z_{o2}}{Z_{o1}}} = \sqrt{\frac{Z_{oe}^{b} + Z_{oo}^{b}}{Z_{oe}^{a} + Z_{oo}^{a}}}.$$

We can also apply these equations to 2^{nd} and 3^{rd} section.

If we also consider very diverse types of coupled line sections, such as 3-section band-pass filter of two asymmetric coupled line sections and one symmetric coupled line section, we can still use those design equations (4-14) - (4-20) for that case.

The next Figure 4.6 shows the development of an equivalent circuit for derivation of design equations for 3-section coupled line band-pass filter with different two terminating impedances $Z_{o1} = Z_{o4}$, $Z_{o2} = Z_{o3}$ and different three widths $w_1 = w_6$, $w_2 = w_3$, $w_4 = w_5$ as another example.

The design parameters are given by,

$$Z_{o1} J_1 = \sqrt{\frac{\pi\Delta}{2g_1}} \cdot \sqrt{\frac{Z_{o1}}{Z_{o2}}} = \sqrt{\frac{\pi\Delta}{2g_1}} \frac{1}{k_1}, \tag{4.21}$$

$$Z_{o2} J_2 = \frac{\pi\Delta}{2\sqrt{g_1 g_2}}, \tag{4.22}$$

$$Z_{o2} J_3 = \sqrt{\frac{\pi\Delta}{2g_2 g_3}} \cdot \sqrt{\frac{Z_{o2}}{Z_{o1}}} = \sqrt{\frac{\pi\Delta}{2g_2 g_3}} k_1, \tag{4.23}$$

where the fractional bandwidth is represented by

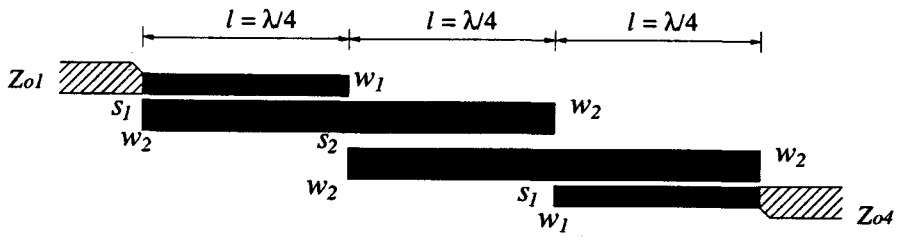

(a) Layout of an N+1 section asymmetric coupled line band-pass filter

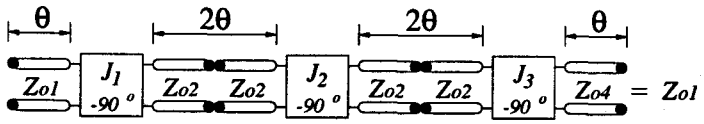

(b) Using admittance inverter for each coupled line section

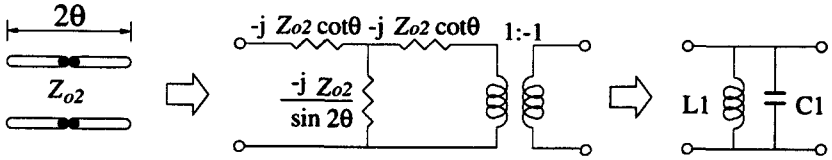

(c) Equivalent circuit for transmission lines of length 2θ

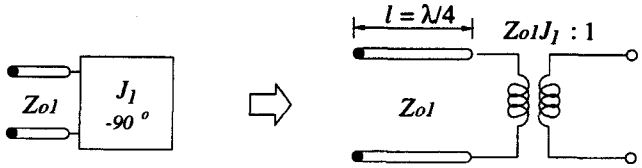

(d) Equivalent circuit of the admittance inverter

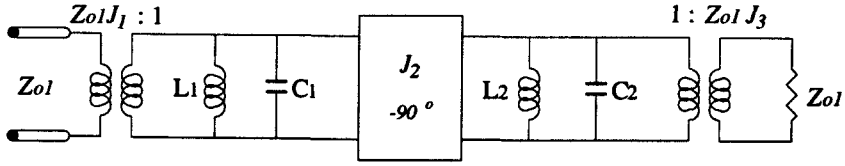

(e) Using results of (c) and (d)

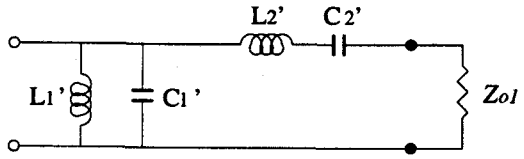

(f) Lumped-element equivalent circuit for a band-pass filter

Figure 4.6. Development of an equivalent circuit for derivation of design equations for a 3-section coupled line band-pass filter with two asymmetric and one symmetric coupled line sections.

$$\Delta = \frac{\omega_2 - \omega_1}{\omega_0},$$

$$k_1 = \sqrt{\frac{Z_{o2}}{Z_{o1}}},$$

$$k_2 = \sqrt{\frac{Z_{o3}}{Z_{o2}}} = 1,$$

and

$$k_3 = \sqrt{\frac{Z_{o4}}{Z_{o3}}} = \sqrt{\frac{Z_{o1}}{Z_{o2}}}.$$

4.3.3. Asymmetric Coupled Line Filter of 4-sections

The design parameters for a band-pass filter with 4 coupled line sections ($N = 4$) with five terminating impedances($N+1$), Z_{o1}, Z_{o2}, Z_{o3}, Z_{o4}, $Z_{o5} = Z_{o1}$ and eight different widths($2N$), w_1, w_2, w_3, w_4, w_5, w_6, w_7, w_8 as shown in Figure 4.7 are then found to be:

$$Z_{o1}J_1 = \sqrt{\frac{\pi\Delta}{2g_1}} \cdot \sqrt{\frac{Z_{o1}}{Z_{o2}}} = \sqrt{\frac{\pi\Delta}{2g_1}} \cdot \frac{1}{k_1}, \tag{4.24}$$

$$Z_{o2}J_2 = \frac{\pi\Delta}{2\sqrt{g_1 g_2}} \cdot \sqrt{\frac{Z_{o2}}{Z_{o3}}} = \frac{\pi\Delta}{2\sqrt{g_1 g_2}} \cdot \frac{1}{k_2}, \tag{4.25}$$

$$Z_{o3}J_3 = \frac{\pi\Delta}{2\sqrt{g_2 g_3}} \cdot \sqrt{\frac{Z_{o3}}{Z_{o4}}} = \frac{\pi\Delta}{2\sqrt{g_2 g_3}} \cdot \frac{1}{k_3}, \tag{4.26}$$

$$Z_{o4}J_4 = \sqrt{\frac{\pi\Delta}{2g_3 g_4}} \cdot \sqrt{\frac{Z_{o4}}{Z_{o1}}} = \sqrt{\frac{\pi\Delta}{2g_1}} \cdot \frac{1}{k_4}, \tag{4.27}$$

where the fractional bandwidth is represented by

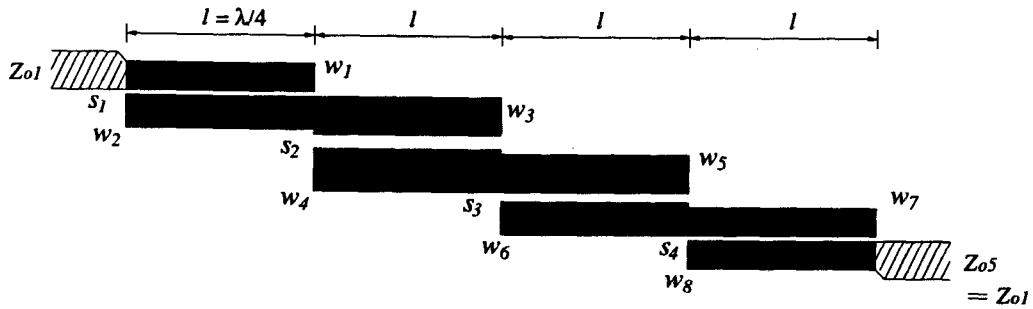

(a) Layout of an 4-section asymmetric coupled line band-pass filter

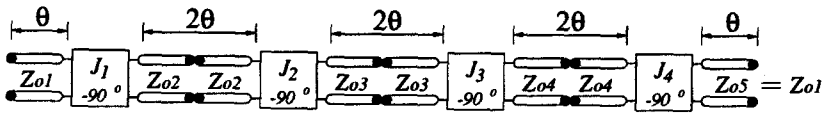

(b) Using admittance inverter for each coupled line section

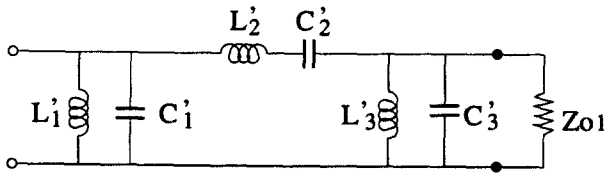

(c) Lumped-element equivalent circuit for a band-pass filter

Figure 4.7. Development of an equivalent circuit for derivation of design equations for a 4-section coupled line band-pass filter

$$\triangle = \frac{\omega_2 - \omega_1}{\omega_0},$$

and

$$k_1 = \sqrt{\frac{Z_{o2}}{Z_{o1}}},$$

$$k_2 = \sqrt{\frac{Z_{o3}}{Z_{o2}}},$$

$$k_3 = \sqrt{\frac{Z_{o4}}{Z_{o3}}},$$

$$k_4 = \sqrt{\frac{Z_{o5}}{Z_{o4}}} = \sqrt{\frac{Z_{o1}}{Z_{o4}}},$$

and g_N represents the element values for Butterworth and Chebyshev low-pass filter prototype in Table 5.1 and Table 5.2.

The design parameters given by equations (4.24)-(4.27) can be applied to the design equations (4.17)-(4.20) of 3-section coupled line filter in a same way. So we can have the equations of Z^a_{oe}, Z^a_{oo}, Z^b_{oe}, and Z^b_{oo} of each section.

4.3.4. Asymmetric Coupled Line Filter of Multi-sections

The general design equations for the multi-section asymmetric coupled line filter also can be derived by the same way of derivation of design equations for 3-section or 4-section asymmetric coupled line filter as earlier presented.

The design parameters for a asymmetric coupled line band-pass filter with multi-sections(N) with $N+1$ terminating impedances, Z_{o1}, Z_{o2}, Z_{o3}, ..., Z_{oN}, Z_{oN+1} = Z_{o1} and different $2N$ widths w_1, w_2, w_3, ..., w_{2N-1}, w_{2N} are found to be:

$$Z_{o1}J_1 = \sqrt{\frac{\pi\triangle}{2g_1}} \cdot \sqrt{\frac{Z_{o1}}{Z_{o2}}} = \sqrt{\frac{\pi\triangle}{2g_1}} \cdot \frac{1}{k_1}, \tag{4.28}$$

$$Z_{o2}J_2 = \frac{\pi\triangle}{2\sqrt{g_1 g_2}} \cdot \sqrt{\frac{Z_{o2}}{Z_{o3}}} = \frac{\pi\triangle}{2\sqrt{g_1 g_2}} \cdot \frac{1}{k_2}, \tag{4.29}$$

$$Z_{o3}J_3 = \frac{\pi\triangle}{2\sqrt{g_2 g_3}} \cdot \sqrt{\frac{Z_{o3}}{Z_{o4}}} = \frac{\pi\triangle}{2\sqrt{g_2 g_3}} \cdot \frac{1}{k_3}, \tag{4.30}$$

$$\vdots$$

$$Z_{oN-1}J_{N-1} = \frac{\pi\triangle}{2g_{N-2}g_{N-1}} \cdot \sqrt{\frac{Z_{oN-1}}{Z_{oN}}} = \frac{\pi\triangle}{2\sqrt{g_{N-2}g_{N-1}}} \cdot \frac{1}{k_{N-1}}, \tag{4.31}$$

$$Z_{oN}J_N = \sqrt{\frac{\pi\triangle}{2g_{N-1}g_N}} \cdot \sqrt{\frac{Z_{oN}}{Z_{oN+1}}} = \sqrt{\frac{\pi\triangle}{2g_{N-1}g_N}} \cdot \frac{1}{k_N}, \tag{4.32}$$

where the fractional bandwidth is represented by

$$\triangle = \frac{\omega_2 - \omega_1}{\omega_0}.$$

And we can get line mode impedances,Z^a_{oe}, Z^a_{oo}, Z^b_{oe}, Z^b_{oo} of each section from the following general equations;

$$Z^a_{oe} = k_N Z^2_{oN} J_N \left[k_N + \sqrt{2 + (k_N Z_{oN} J_N)^2 + \frac{1}{(k_N Z_{oN} J_N)^2}} \right], \tag{4.33}$$

$$Z^a_{oo} = k_N Z^2_{oN} J_N \left[-k_N + \sqrt{2 + (k_N Z_{oN} J_N)^2 + \frac{1}{(k_N Z_{oN} J_N)^2}} \right], \tag{4.34}$$

$$Z^b_{oe} = \frac{1}{2}[(k_N^2 + 1)Z^a_{oe} + (k_N^2 - 1)Z^a_{oo}], \tag{4.35}$$

$$Z^b_{oo} = \frac{1}{2}[(k_N^2 - 1)Z^a_{oe} + (k_N^2 + 1)Z^a_{oo}], \tag{4.36}$$

where N is the number of the section. That is,

$$k_N = \sqrt{\frac{Z_{oN+1}}{Z_{oN}}}.$$

4.4. SUMMARY

The basic properties of an open-circuited coupled line structures, for applications as wide band DC blocks and filters were examined and some examples were introduced. The design procedure utilizing the asymmetric coupled line, equivalent two port circuit incorporating an admittance inverter was presented. Design of general symmetric as well as asymmetric transformer/filters with a desired impedance transformation and band width for single section and multi-section filters were presented.

5. SINGLE LEVEL DESIGN AND EXPERIMENT

5.1. INTRODUCTION

This chapter presents a methodology for designing asymmetric coupled line band-pass filter circuits on a single level dielectric medium such as alumina or FR-4. The circuit with 3-sections was fabricated on FR-4 and measured and a circuit with 4-sections was introduced as another example. For physical realization the normal mode parameters, $\beta_{c,\pi}$, $R_{c,\pi}$ and the relationships between characteristic impedances and capacitances in an inhomogeneous medium and a homogeneous medium, respectively derived and the design procedure were introduced. For validation of the design methodology and the sensitivity analysis of the 3-section band-pass filter, a *SPICE* model [52–54] on *LIBRA* and a full-wave *EM* simulator, *MOMENTUM* were used.

5.2. DESIGN METHODOLOGY OF SINGLE LEVEL FILTERS

The immittance matrix elements for the coupled line four-port have been derived in terms of the normal mode parameters of the coupled system [6,7]. These parameters are the propagation constants, $\beta_{c,\pi}$, the mode voltage ratios $R_{c,\pi}$, on the two lines, and the partial mode impedances and admittances of the two lines for the normal modes of the coupled system. For the case of lossless coupled lines, characterized by their self- and mutual inductances per unit length and capacitances per unit length as given by L_1, L_2, L_m and C_1, C_2, C_m where L_i and $C_i (i = 1,2)$ are self-inductance and capacitance per unit length of line i in presence of line $j (j = 1,2: \ j \neq i)$, and L_m and C_m are mutual inductance and capacitance per unit

length, respectively, for the quasi-TEM case, these normal mode parameters in an inhomogeneous medium are given by

$$\beta_{c,\pi} = \frac{\omega}{\sqrt{2}}\left[L_1C_1 + L_2C_2 - 2L_mC_m \right.$$
$$\left. \pm\sqrt{(L_2C_2 - L_1C_1)^2 + 4(L_mC_1 - L_2C_m)(L_mC_2 - L_1C_m)}\right]^{\frac{1}{2}} \tag{5.1}$$

$$R_{c,\pi} = \frac{V_2}{V_1} =$$
$$\frac{L_2C_2 - L_1C_1 \pm \sqrt{(L_2C_2 - L_1C_1)^2 + 4(L_mC_1 - L_2C_m)(L_mC_2 - L_1C_m)}}{2(L_mC_2 - L_1C_m)} \tag{5.2}$$

$$Z_{c1} = \frac{\omega}{\beta_c}\left(L_1 - \frac{L_m}{R_\pi}\right) = \frac{\beta_c}{\omega}\left(\frac{1}{C_1 - R_cC_m}\right) = \frac{1}{Y_{c1}} \tag{5.3}$$

$$Z_{\pi 1} = \frac{\omega}{\beta_\pi}\left(L_1 - \frac{L_m}{R_c}\right) = \frac{\beta_\pi}{\omega}\left(\frac{1}{C_1 - R_\pi C_m}\right) = \frac{1}{Y_{\pi 1}} \tag{5.4}$$

$$Z_{c2} = -R_cR_\pi Z_{c1} = \frac{1}{Y_{c2}} \tag{5.5}$$

$$Z_{\pi 2} = -R_cR_\pi Z_{\pi 1} = \frac{1}{Y_{\pi 2}} \tag{5.6}$$

where $\beta_{c,\pi}$ are the phase constants for the two modes, $R_{c,\pi}$ are the ratio of the voltages on the lines for the two normal modes, Z_{c1}, $Z_{\pi 1}$, Z_{c2}, $Z_{\pi 2}$ are the mode impedances of the two lines, and Y_{c1}, $Y_{\pi 1}$, Y_{c2}, $Y_{\pi 2}$ are the corresponding admittances.

In a homogeneous medium, we have the following normal mode parameters;

$$\beta = \beta_c = \beta_\pi = \frac{\omega}{\sqrt{2}}\sqrt{L_1C_1 + L_2C_2 - 2L_mC_m} \tag{5.7}$$

$$k = R_c = -R_\pi = \sqrt{\frac{L_mC_1 - L_2C_m}{L_mC_2 - L_1C_m}} = \sqrt[4]{\frac{L_2C_1}{L_1C_2}} = \sqrt{\frac{C_1}{C_2}}$$
$$= \sqrt{\frac{Z_{o2}}{Z_{o1}}} = \sqrt{\frac{Z_{i2}}{Z_{i1}}} = \sqrt{\frac{Z^b_{oe} + Z^b_{oo}}{Z^a_{oe} + Z^a_{oo}}}. \tag{5.8}$$

From these conditions we can get the following relationships between Z^a_{oe},Z^a_{oo},Z^b_{oe},Z^b_{oo} and C_1,C_2,C_m.

$$Z^a_{oe} = \frac{\beta}{\omega}\left[\frac{C_1 + k^2 C_m}{C_1^2 - k^2 C_m^2}\right] = \frac{1}{v}\left[\frac{C_2 + C_m}{C_1 C_2 - C_m^2}\right] \tag{5.9}$$

$$Z^a_{oo} = \frac{\beta}{\omega}\left[\frac{C_1 - k^2 C_m}{C_1^2 - k^2 C_m^2}\right] = \frac{1}{v}\left[\frac{C_2 - C_m}{C_1 C_2 - C_m^2}\right] \tag{5.10}$$

$$Z^b_{oe} = k^2\frac{\beta}{\omega}\left[\frac{C_1 + C_m}{C_1^2 - k^2 C_m^2}\right] = \frac{1}{v}\left[\frac{C_1 + C_m}{C_1 C_2 - C_m^2}\right] \tag{5.11}$$

$$Z^b_{oo} = k^2\frac{\beta}{\omega}\left[\frac{C_1 - C_m}{C_1^2 - k^2 C_m^2}\right] = \frac{1}{v}\left[\frac{C_1 - C_m}{C_1 C_2 - C_m^2}\right] \tag{5.12}$$

or,

$$C_1 = \frac{1}{v}\left[\frac{Z^b_{oe} + Z^b_{oo}}{Z^a_{oe}Z^b_{oo} + Z^a_{oo}Z^b_{oe}}\right] \tag{5.13}$$

$$C_2 = \frac{1}{v}\left[\frac{Z^a_{oe} + Z^a_{oo}}{Z^a_{oe}Z^b_{oo} + Z^a_{oo}Z^b_{oe}}\right] \tag{5.14}$$

$$C_m = \frac{1}{v}\left[\frac{Z^a_{oe} - Z^a_{oo}}{Z^a_{oe}Z^b_{oo} + Z^a_{oo}Z^b_{oe}}\right] = \frac{1}{v}\left[\frac{Z^b_{oe} - Z^b_{oo}}{Z^a_{oe}Z^b_{oo} + Z^a_{oo}Z^b_{oe}}\right] \tag{5.15}$$

$$\frac{C_1}{C_2} = k^2 = \frac{Z^b_{oe} + Z^b_{oo}}{Z^a_{oe} + Z^a_{oo}} \tag{5.16}$$

$$\frac{C_m}{C_1} = \frac{Z^a_{oe} - Z^a_{oo}}{Z^b_{oe} + Z^b_{oo}} = \frac{Z^b_{oe} - Z^b_{oo}}{Z^b_{oe} + Z^b_{oo}} \tag{5.17}$$

$$\frac{C_m}{C_2} = \frac{Z^b_{oe} - Z^b_{oo}}{Z^a_{oe} + Z^a_{oo}} = \frac{Z^a_{oe} - Z^a_{oo}}{Z^a_{oe} + Z^a_{oo}} \tag{5.18}$$

where v is the propagation velocity in a homogeneous dielectric medium.

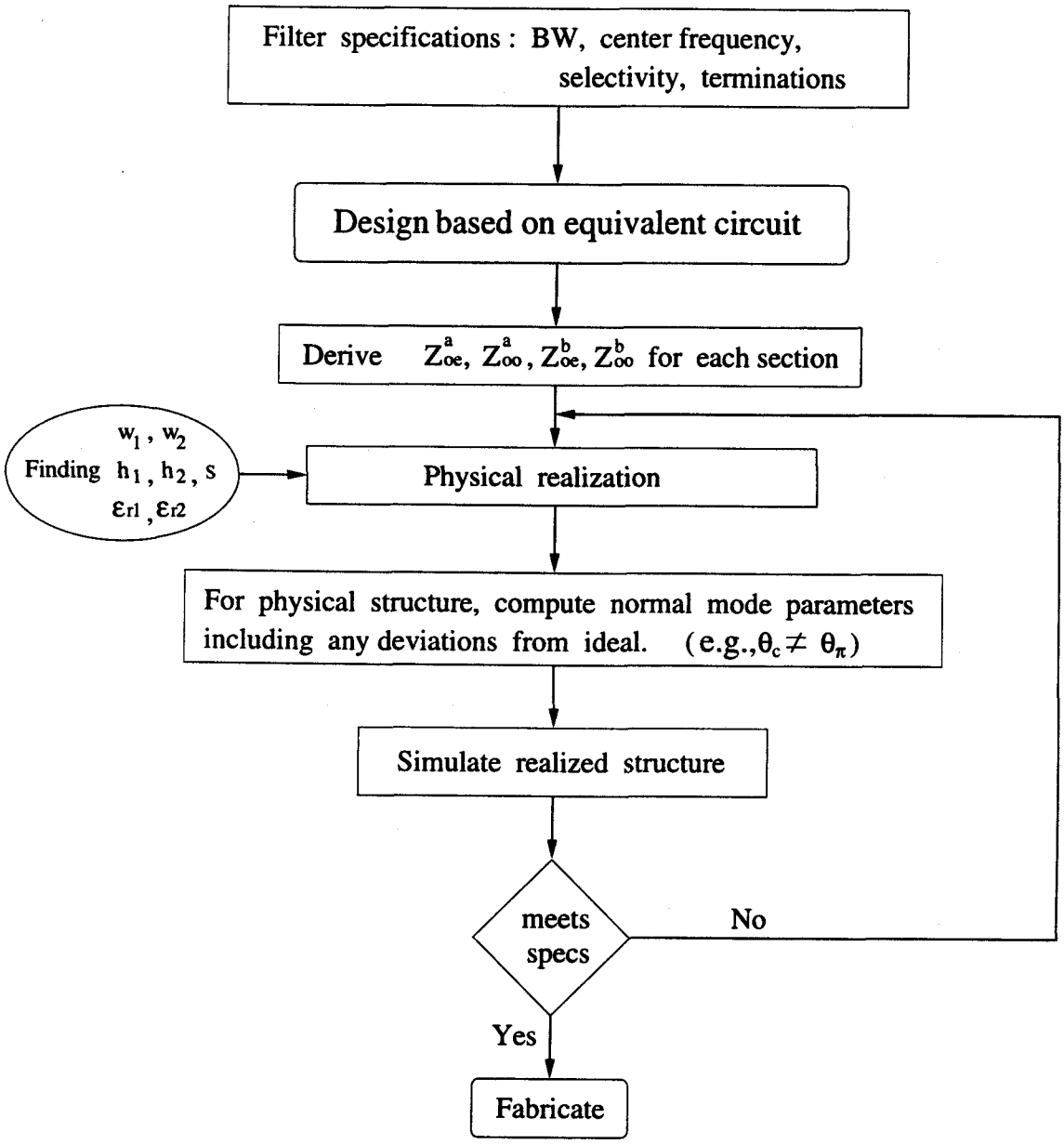

Figure 5.1. The design procedure for coupled line filters.

The design procedure developed for the single level filter is summarized in Figure 5.1. The design procedure [64,68,69] consists of three steps:

step 1. Design based on an equivalent circuit and expression for normal mode parameters [6] for each coupled line section.

step 2. Finding physical dimensions (widths, spaces, thickness, dielectric constant) to realized the desired normal mode parameters as computed in step 1.

step 3. Optimizations and fabrication of the realized structure obtained in step 2.

For step 1, we start with filter specifications(number of coupled sections, bandwidth, center frequency, selectivity, terminating impedances Z_{oN}) and then find g_N, element values for Butterworth or Chebyshev low-pass filter prototypes [46,47] as shown in Table 5.1 and Table 5.2.

From these specifications, we can derive the admittance inverter parameters for each asymmetric coupled section as following;

$$Z_{o1}J_1 = \sqrt{\frac{\pi\triangle}{2g_1}} \cdot \sqrt{\frac{Z_{o1}}{Z_{o2}}} = \sqrt{\frac{\pi\triangle}{2g_1}} \cdot \frac{1}{k_1}, \tag{5.19}$$

$$Z_{o2}J_2 = \frac{\pi\triangle}{2\sqrt{g_1 g_2}} \cdot \sqrt{\frac{Z_{o2}}{Z_{o3}}} = \frac{\pi\triangle}{2\sqrt{g_1 g_2}} \cdot \frac{1}{k_2}, \tag{5.20}$$

$$Z_{o3}J_3 = \frac{\pi\triangle}{2\sqrt{g_2 g_3}} \cdot \sqrt{\frac{Z_{o3}}{Z_{o4}}} = \frac{\pi\triangle}{2\sqrt{g_2 g_3}} \cdot \frac{1}{k_3}, \tag{5.21}$$

$$\vdots$$

$$Z_{oN-1}J_{N-1} = \frac{\pi\triangle}{2g_{N-2}g_{N-1}} \cdot \sqrt{\frac{Z_{oN-1}}{Z_{oN}}} = \frac{\pi\triangle}{2\sqrt{g_{N-2}g_{N-1}}} \cdot \frac{1}{k_{N-1}}, \tag{5.22}$$

$$Z_{oN}J_N = \sqrt{\frac{\pi\triangle}{2g_{N-1}g_N}} \cdot \sqrt{\frac{Z_{oN}}{Z_{oN+1}}} = \sqrt{\frac{\pi\triangle}{2g_{N-1}g_N}} \cdot \frac{1}{k_N}, \tag{5.23}$$

where N is the number of sections, the fractional bandwidth is

$$\triangle = \frac{\omega_2 - \omega_1}{\omega_0},$$

and the voltage ratio is represented by,

$$k_N = \sqrt{\frac{Z_{oN+1}}{Z_{oN}}}.$$

Then the normal mode parameters for homogeneous medium, the line mode impedances Z^a_{oe}, Z^a_{oo}, Z^b_{oe}, Z^b_{oo}, and the voltage ratio $k_N = \sqrt{\frac{Z_{o2}}{Z_{o1}}}$ are obtained from the equivalent circuit of admittance inverters.

For step 2, normal mode parameters obtained from step 1 are utilized to come up with physical dimensions which are later plugged into an *SPICE* model on *LIBRA* shown in Figure 5.2 and an *EM* simulator *MOMENTUM* to verify the design.

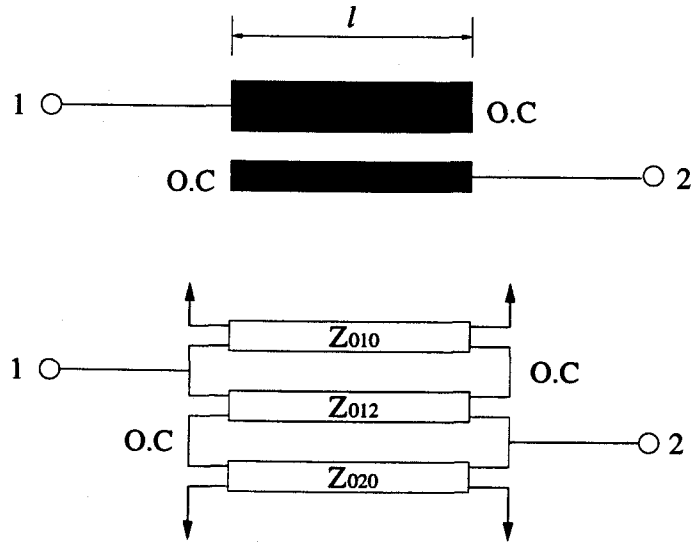

Figure 5.2. An open circuited asymmetric coupled line of a single section and an equivalent *SPICE* circuit model.

In order to obtain physical dimensions for each coupled section, w_1, w_2, s, h, ϵ_r we can use a *LINPAR* program taking up a segmentation and boundary element

method comparing the 2x2 capacitance $[C]$ matrix calculated from the normal mode parameters, which were derived from equations (5.13)-(5.15) and 2x2 capacitance $[C]$ matrix which will be determined from the $LINPAR$ for each section. Approximate values of physical dimensions based on capacitance values can be used for an initial guess for the iterative evaluation of physical dimensions.

For step 3, S-parameters are determined for each coupled line section, and then these S-parameters are used in simulation programs which have theoretical responses. To get S-parameters for this circuit we need to change the $[Z]$ matrix(open-circuited 2-port) to $[ABCD]$ matrix for each section then to $[S]$ matrix again(Appendix A). Here $[ABCD]$ matrices for each coupled line section are combined together to be changed to 2x2 $[S]$ matrix for the complete circuit for all the coupled line sections. The other possible simulation methods for a theoretical response are a $SPICE$ model on $LIBRA$ [52–54] and the EM simulator $MOMENTUM$.

The $SPICE$ model on $LIBRA$ can consider the effects of open-ends in some examples. But the EM simulator $MOMENTUM$, a full-wave simulator, using the method of moments can also calculate the insertion loss and the return loss considering those effects of discontinuities and open-ends accurately.

Finally the filter performance obtained from physical dimensions is compared with the desired filter specifications.

5.3. DESIGN EXAMPLE I

5.3.1. 3-section Butterworth asymmetric coupled line filter

A Butterworth band-pass filter with three coupled line sections which dielectric constant ϵ_r is 4.6 and fractional bandwidth $\Delta = 10\ \%(0.2\ GHz)$ at center frequency $f_o = 2\ GHz$ is designed.

A general configuration for a coupled line band-pass filter made up of three coupled line sections which have lengths $l = \lambda/4 = 17.48\ mm$ is shown in Figure 5.3.

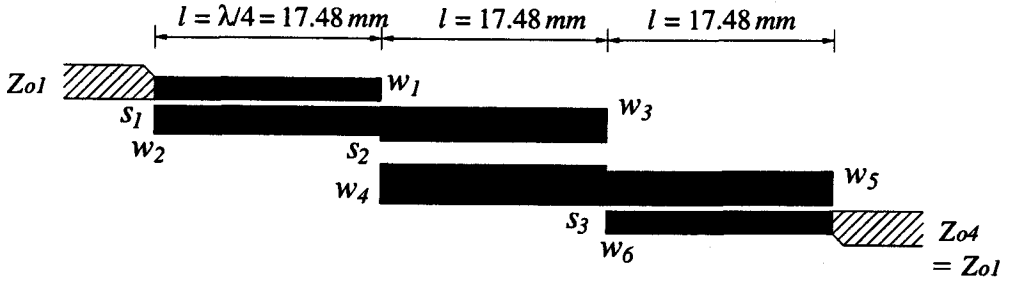

(a) Layout of an 3- section asymmetric coupled line band-pass filter which has section length $l = 17.48\ mm$ at 2 GHz.

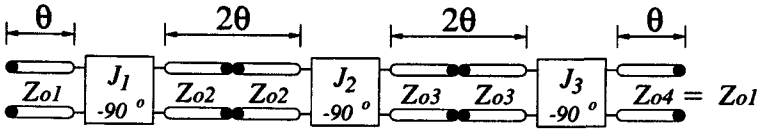

(b) An equivalent circuit using admittance inverter for each coupled line section which $Z_{o1} = 50$, $Z_{o2} = 45$, $Z_{o3} = 40$, $Z_{o4} = 50\ Ohm$.

Figure 5.3. A layout and an equivalent circuit of Y inverters for a 3-section coupled line band-pass filter.

The Butterworth filter is assumed to have selected terminating impedances for each section $Z_{o1} = 50\ \Omega$, $Z_{o2} = 45\ \Omega$, and $Z_{o3} = 40\ \Omega$ $Z_{o4} = Z_{o1} = 50\ \Omega$ according to different widths, w_1, w_2, w_3, w_4, w_5, w_6. The design parameters for a band-pass filter with 3 coupled line sections (N = 3) are given by,

$$Z_{o1}J_1 = \sqrt{\frac{\pi\Delta}{2g_1}}\sqrt{\frac{Z_{o1}}{Z_{o2}}} = 0.3513, \tag{5.24}$$

$$Z_{o2}J_2 = \frac{\pi\Delta}{2\sqrt{g_1 g_2}}\sqrt{\frac{Z_{o2}}{Z_{o3}}} = 0.1178, \tag{5.25}$$

$$Z_{o3}J_3 = \sqrt{\frac{\pi\Delta}{2g_2 g_3}}\sqrt{\frac{Z_{o3}}{Z_{o1}}} = 0.2981, \tag{5.26}$$

and g_N represents the element values for Butterworth and Chebyshev low-pass filter prototype as shown in Table 5.1 and Table 5.2. And we can notice that $g_1 = g_2 g_3$ from the tables.

N	g_1	g_2	g_3	g_4	g_5
1	2.0000	1.0000			
2	1.4142	1.4142	1.0000		
3	1.0000	2.0000	1.0000	1.0000	
4	0.7654	1.8478	1.8478	0.7654	1.0000

Table 5.1. Element values for Butterworth low-pass filter prototypes ($g_o = 1$, $\omega_c = 1$, $N = 1$ to 4)

	0.5 dB Ripple				
N	g_1	g_2	g_3	g_4	g_5
1	0.6986	1.0000			
2	1.4029	0.7071	1.9841		
3	1.5963	1.0967	1.5963	1.0000	
4	1.6703	1.1926	2.3661	0.8419	1.9841

Table 5.2. Element values for Chebyshev low-pass filter prototypes (0.5 dB ripple, $g_o = 1$, $\omega_c = 1$, $N = 1$ to 4)

From the equations (5.24)-(5.26), (5.13)-(5.15), and (4.33)-(4.36) we can get 2x2 capacitance $[C]$ matrix for each section. Once we have the line mode impedances,Z^a_{oe}, Z^a_{oo}, Z^b_{oe}, Z^b_{oo} of each section, and the capacitance $[C]$ matrix for each section, then we get the electrical and physical dimensions corresponding to a

3-section Butterworth by *LINPAR* which are given in the Table 5.3. And expected ideal filter responses, the magnitude response and the phase response of S_{21} are shown in Figure 5.4 and Figure 5.5.

Section No.	*1*	*2*	*3*	*Ends*
Z^a_{eo} *(Ohm)*	*71.36*	*50.27*	*59.35*	
Z^a_{oo} *(Ohm)*	*39.75*	*40.84*	*29.54*	$Z_{01} = Z_{04}$
Z^b_{eo} *(Ohm)*	*65.81*	*45.21*	*70.46*	*= 50 (Ohm)*
Z^b_{oo} *(Ohm)*	*34.19*	*35.78*	*40.65*	
C_1 *(nF)*	*0.1414*	*0.1588*	*0.1768*	
C_m *(nF)*	*-0.0447*	*-0.0185*	*-0.0474*	
C_2 *(nF)*	*0.1571*	*0.1787*	*0.1414*	
w_1 *(mm)*	*0.96*	*1.51*	*1.522*	
w_2 *(mm)*	*1.22*	*1.86*	*0.932*	*w = 1.06*
s *(mm)*	*0.3*	*0.96*	*0.273*	
$h_1 = h_2$ *(mm)*	*1.4478*			

Table 5.3. Normal parameters, capacitance matrices, and physical dimensions for the 3-section asymmetric coupled line Butterworth band-pass filter.

5.3.2. Optimizations from a *SPICE* Model on *LIBRA*

The responses of a 3 coupled line section filter also can be obtained by a simulation of *SPICE* model on *LIBRA* [52–54]. This *SPICE* model for a 3 coupled line section filter consists of 9 transmission lines(*TLIN*4-element) totally, where each section has 3 transmission lines. The Figure 5.6 shows the *SPICE* model equivalent circuit on *LIBRA* for 3 coupled line section band-pass filter.

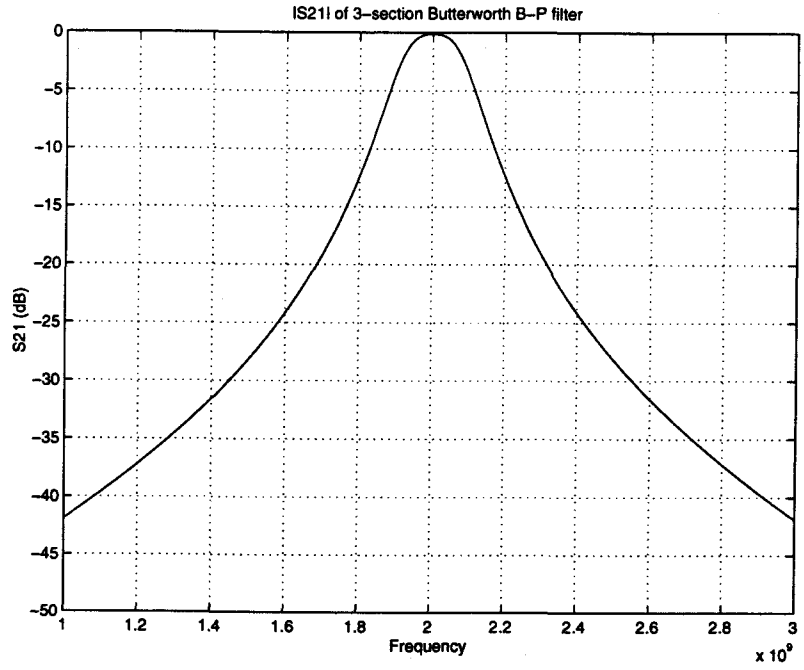

Figure 5.4. Magnitude of S_{21} for a 3-section asymmetric coupled line Butterworth band-pass filter

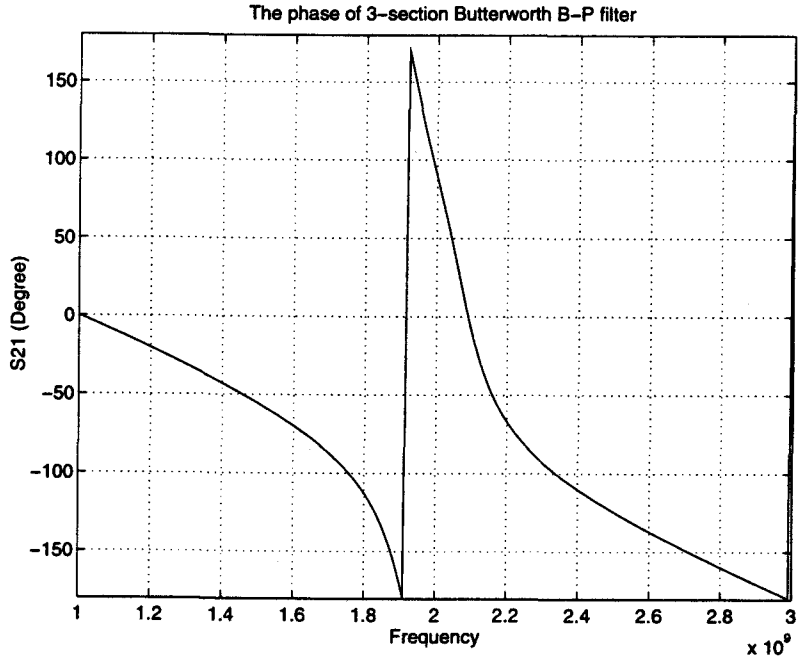

Figure 5.5. Phase of S_{21} for a 3-section asymmetric coupled line Butterworth band-pass filter

The response in Figure 5.7 is almost identical with that of the Figure 5.4.

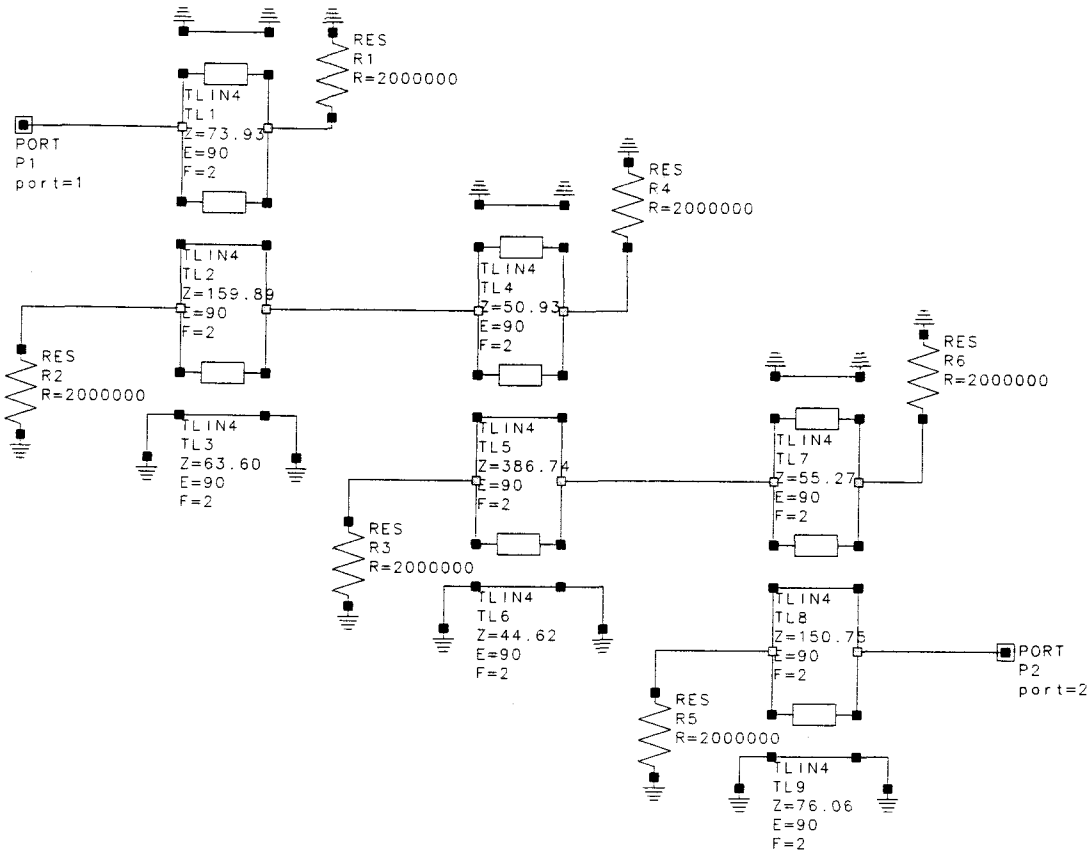

Figure 5.6. A SPICE model of the equivalent circuit of the single layer 3-section filter

5.3.3. Optimizations on *MOMENTUM* and Comparison

Another possible theoretical response can be obtained on a full-wave *EM* simulator, *MOMENTUM*(HP-EEsof product) taking up "the method of moments". This calculates the insertion loss and the return loss accurately considering those effects of discontinuities and open-ends.

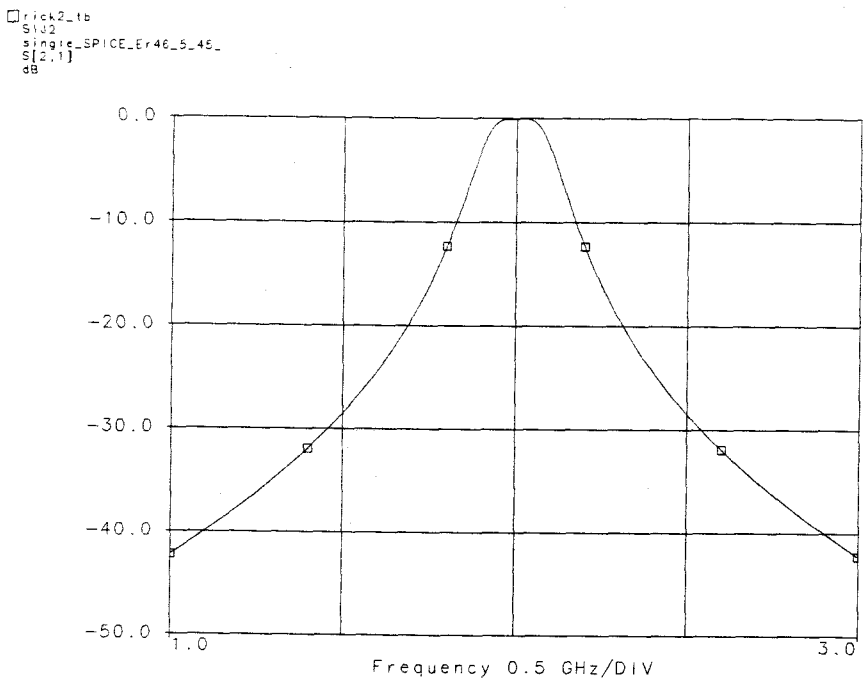

Figure 5.7. The response $|S_{21}|$ of the SPICE model of the equivalent circuit of the single layer 3-section filter.

The Figure 5.8 show the physical layout and the mesh configuration on a single level which correspond to the physical dimensions in Table 5.3 for a strip line of 3-sections.

Simulated this model on the *MOMENTUM*, we had a response of frequency shifted and less narrow band width than expected shown in Figure 5.9. The center frequency was 1.956 GHz and the band width, 0.16 GHz (80 % of 0.2 GHz). The length of each section l was reduced from 17.48 mm to 17.1 mm to shift the center frequency from 1.956 GHz to 2 GHz shown in Figure 5.10.

There could be many ways of increasing the band width of this 3-section band-pass filter on a single level by increasing the coupling coefficient, $k_c = \frac{C_m}{\sqrt{C_1 C_2}}$; First we can decrease the widths of conductors on upper level and/or lower level.

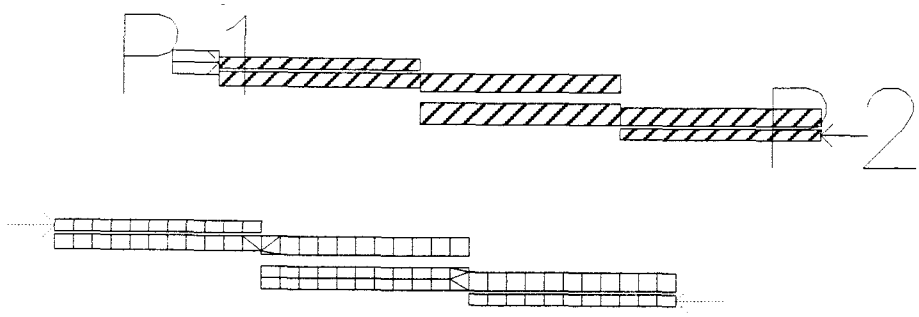

Figure 5.8. A physical layout and a mesh configuration on a single level generated by *MOMENTUM* for a 3-section band-pass filter.

Second we can decrease the spaces between coupled lines for each section. Finally we can increase the thickness of the dielectric substrates.

The most favorable way of increasing the band width of this circuit is increasing the thickness of the dielectric substrate. The reason for this will be explained in the following section, 5.3.4 Sensitivity.

Finally the optimized response having a more wide band width 0.2 GHz at -3 dB as shown in Figure 5.11 was obtained by increasing the thicknesses of the dielectric substrate, $h_1 = h_2 = 1.5926\ mm$ from 1.4478 mm by 10 %(0.1448 mm) up.

An asymmetric coupled line 3-section band-pass filter was fabricated in a strip line for an inexpensive FR-4 material, which dielectric constant(ϵ_r) is 4.6, having a nominal $tan\ \delta = 0.02$. It was measured by HP-8752C(Network Analyzer) and showing -3.1 dB loss at 2.2 GHz in Figure 5.12. And Figure 5.13 was produced by *MOMENTUM* for the same physical dimensions which was fabricated. Comparing Figure 5.12 and Figure 5.13, the responses show very close losses,-3.1 dB and -2.9 dB due to a tangent loss except 0.2 GHz frequency shift from the center frequency.

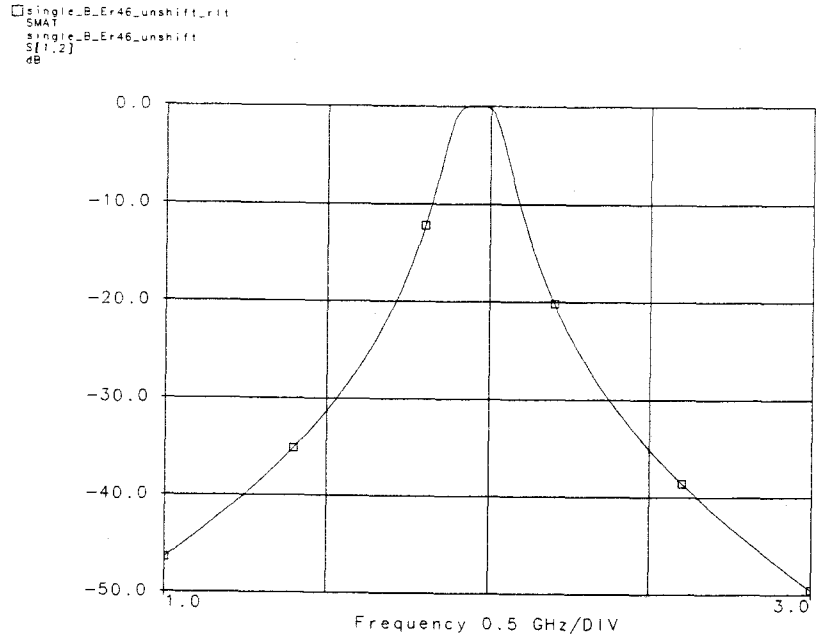

Figure 5.9. The response $|S_{21}|$ of a single level 3-section filter by *MOMENTUM* showing $f_o = 1.956\ GHz$ and band width $= 0.16\ GHz$.

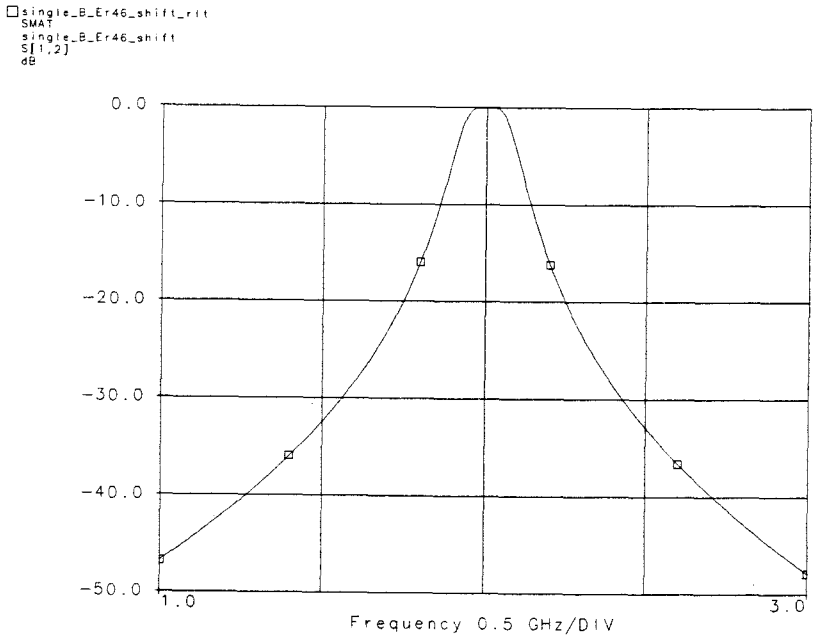

Figure 5.10. The shifted response $|S_{21}|$ of a single level 3-section filter by *MOMENTUM* showing the band width $= 0.16\ GHz$.

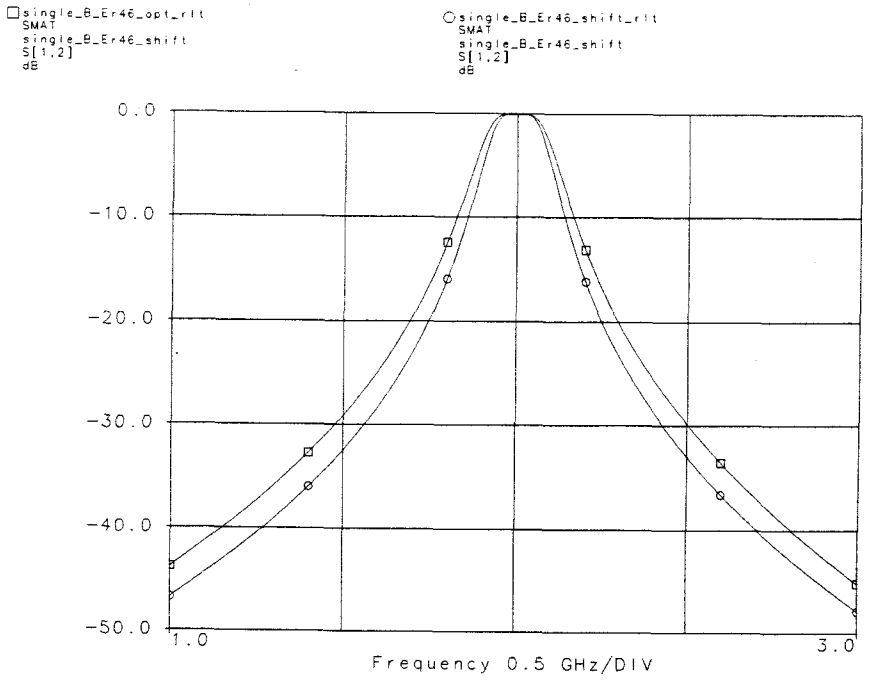

Figure 5.11. The shifted and optimized responses $|S_{21}|$ of a single level 3-section filter by *MOMENTUM* showing the band width is 0.16 GHz and 0.2 GHz.

In conclusion we can say that a full-wave EM simulator "*MOMENTUM*" validates the design methodology proposed here.

We can see more responses according to varying the tangent loss of the dielectric substrate. Figure 5.14 shows the responses of -1.5 dB loss, -2.9 dB loss, and -4.2 dB loss in the cases of the tangent loss 0.01, 0.02, and 0.03 respectively.

5.4. SENSITIVITY ANALYSIS

Characteristics of strip lines are primarily functions of conductor width w, space between conductors s, thickness of the dielectric substrate h, and dielectric constant of the substrate ϵ_r. These are also influenced by factors such as conductor thickness t, frequency of operation(dispersion), and size of enclosure. Substrate

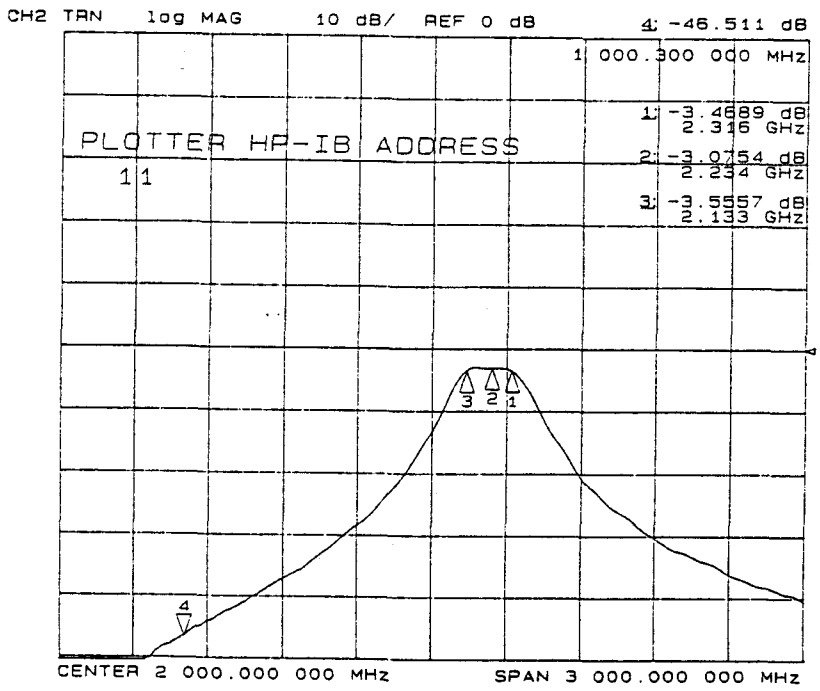

Figure 5.12. The measured response of 3-section coupled line filter.

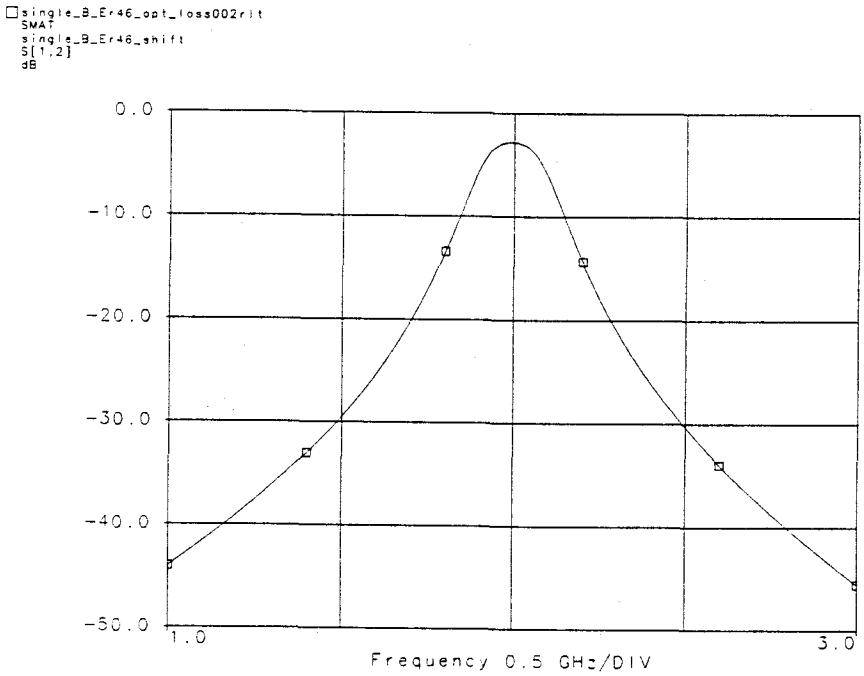

Figure 5.13. The theoretical response -2.9 dB loss in the case of $tan\ \delta = 0.02$ (by *MOMENTUM*).

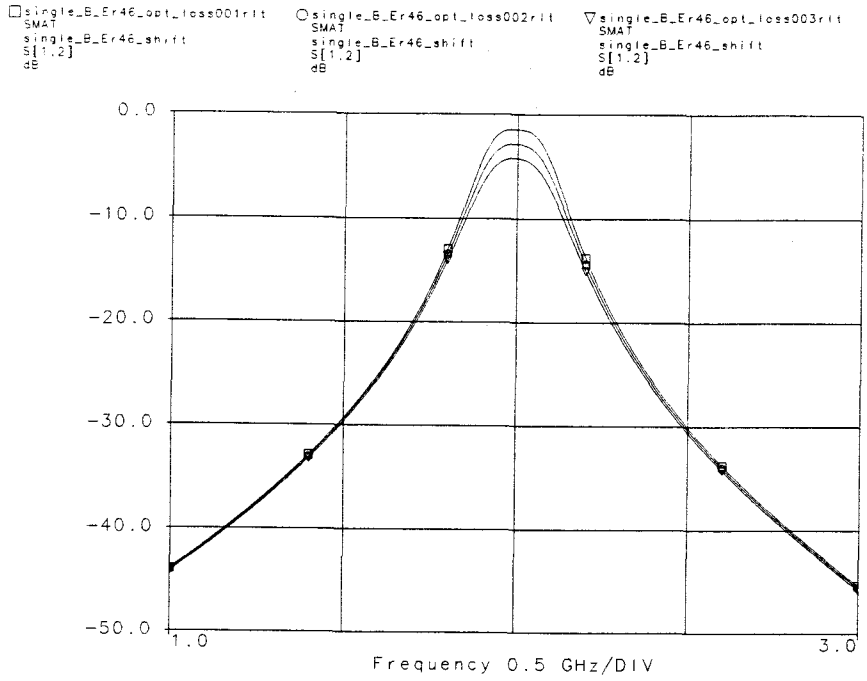

Figure 5.14. The theoretical responses, -1.5 dB, -2.9 dB, and -4.2 dB loss in the case of $tan\ \delta = 0.01$, 0.02, and 0.03(by $MOMENTUM$).

properties, like surface finish, metallization thickness, and the fabrication process, determine the accuracy of fabrication of the conductor width. In addition to the error in fabrication of the conductor width, the thickness and the dielectric constant of the substrate have some manufacturing tolerances. Since it is very difficult to incorporate arrangements for post-fabrication adjustments in MICs, it is necessary to take into account the effect of tolerances at the design stage itself.

The effect of tolerances on the performance of the circuits can be analyzed using the sensitivity analysis [59,60]. This approach is the easiest method of predicting the worst case behavior corresponding to a given set of tolerances. It does not require the actual statistical distribution of tolerances. Only their maximum absolute values are needed. Sensitivity analysis is useful in situations where deviations in parameters can be considered incremental. This implies that the circuit charac-

teristics should be slowly varying functions in the domain of parameter variation around the exact parameter values.

Here the sensitivity factors for the 3-section band-pass filter on a single level were constrainded to the following five factors and the tolerances of the factors were taken up $\pm$ 5 %: width of the line a of each section w_1, w_3, w_5, width of the line b of each section w_2, w_4, w_6, space between line a and line b s, thickness of the dielectric substrate h, and dielectric constant ϵ_r.

As shown in Figure 5.15 and Figure 5.16 the responses of 5 % increased widths of line a, line b of each section have a less narrow band width, while the responses of 5 % reduced widths of line a, line b of each section have a more wide band width.

The responses are showing that the tolerance of the widths of the line a and line b of each section do not make them sensitive.

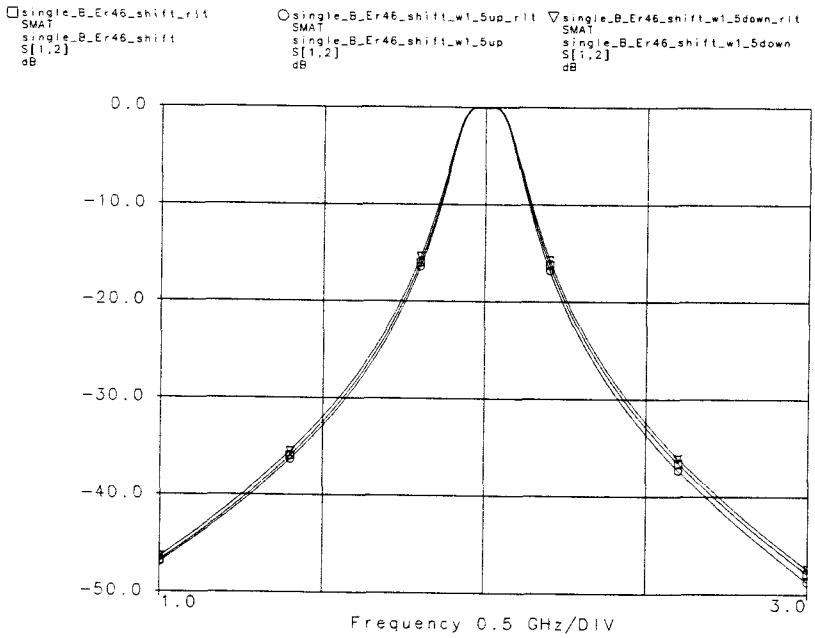

Figure 5.15. Responses for three cases of an optimized, a 5 % increased of w_1,w_3,w_5, and a 5 % decreased of w_1,w_3,w_5.

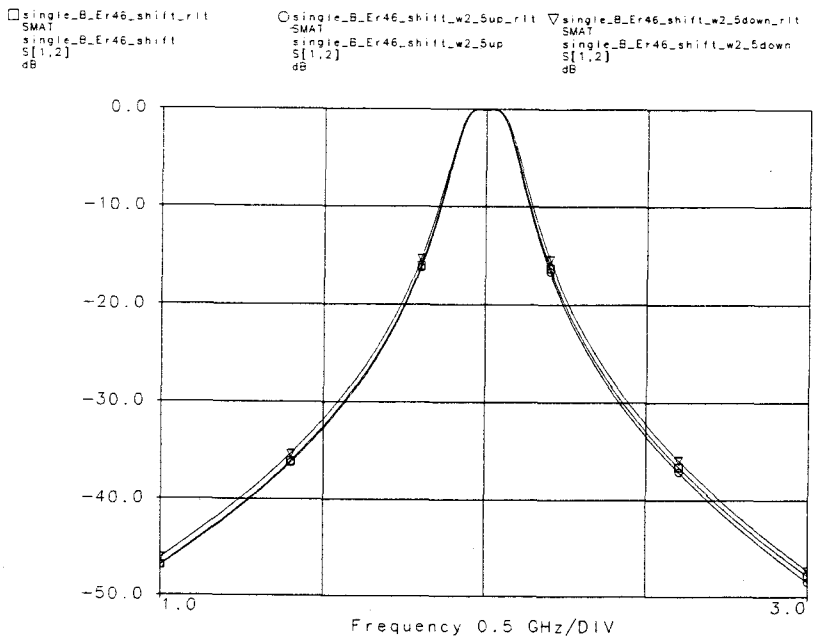

Figure 5.16. Responses for three cases of an optimized, a 5 % increased of w_2,w_4,w_6, and a 5 % decreased of w_2,w_4,w_6.

Figure 5.17 shows that the response of the 5 % increased space between line a, line b of each section has a band width of 0.15 GHz(6.3 % reduced from 0.16 GHz), while the response of the 5 % reduced space between coupled lines of each section has a band width of 0.17 GHz(6.3 % increased from 0.16 GHz) at the center frequency $2GHz$.

Comparing response of Figure 5.17 with those of the Figure 5.15 and Figure 5.16 we can notice that the tolerance of the space between two lines of each section makes the response much more sensitive.

Figure 5.18 also shows that the response of the 5 % increased thicknesses of the substrate, h_1 and h_2 has a band width of 0.18 GHz (12.6 % increased from

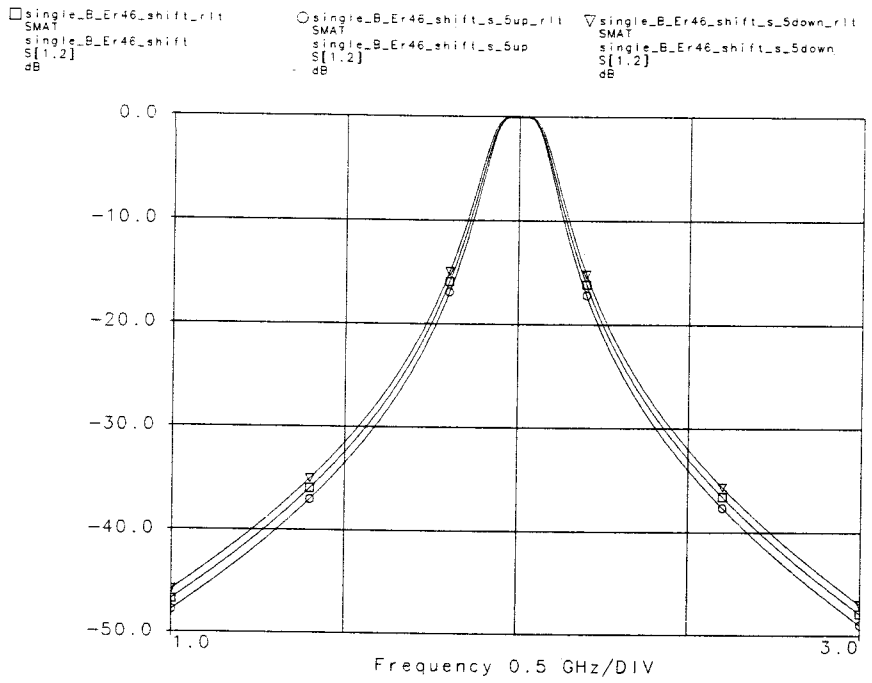

Figure 5.17. Responses for three cases of an optimized, a 5 % increased of s_1,s_2,s_3, and a 5 % decreased of s_1,s_2,s_3.

0.16 GHz), while the response of the 5 % decreased thickness has a band width of 0.14GHz(12.6 % reduced from 0.16 GHz).

This means that the tolerance of the thickness of substrate makes the circuit most sensitive and in the procedure of the optimizations increasing the thickness, h of the substrate guarantees the increase of the band width we expect.

Figure 5.19 shows that response of the 10 % and 20 % increased thicknesses of the substrate has a band width of 0.2 GHz(25 % increased from 0.16 GHz) and 0.24 GHz(50 % increased from 0.16 GHz).

$\pm$ 5 % of tolerances($\pm$ 0.23) for the dielectric constant, $\epsilon_r = 4.6$ make the responses be shifted sensitively as shown in Figure 5.20. Increasing 5 % of the dielectric constant makes the center frequency $f_o = 2\ GHz$ to 1.95 GHz shifted, while decreasing 5 % of it makes it 2.05 GHz shifted.

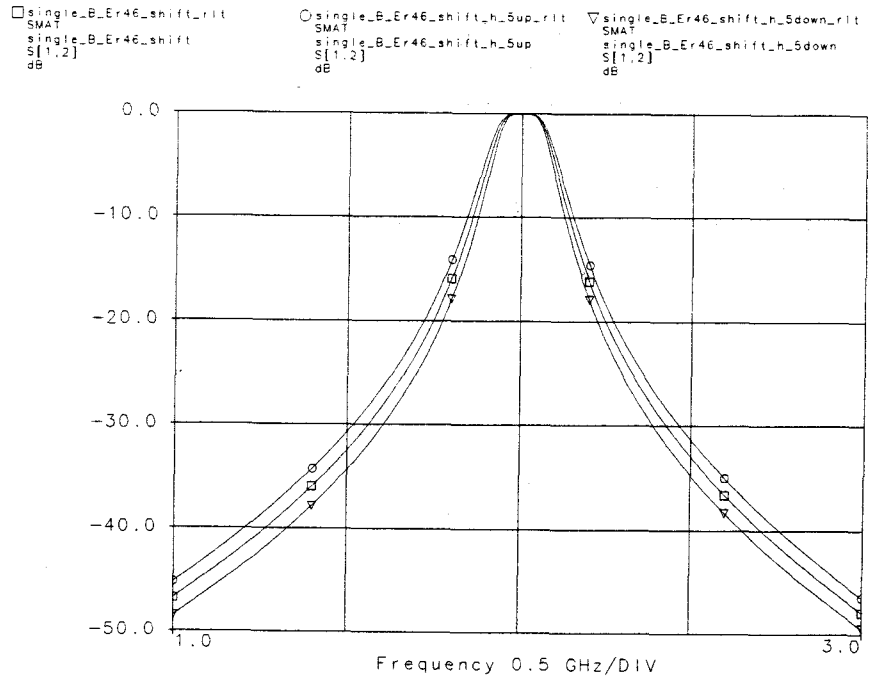

Figure 5.18. Responses for three cases of an optimized, a 5 % increased of h_1,h_2 and a 5 % decreased of h_1,h_2.

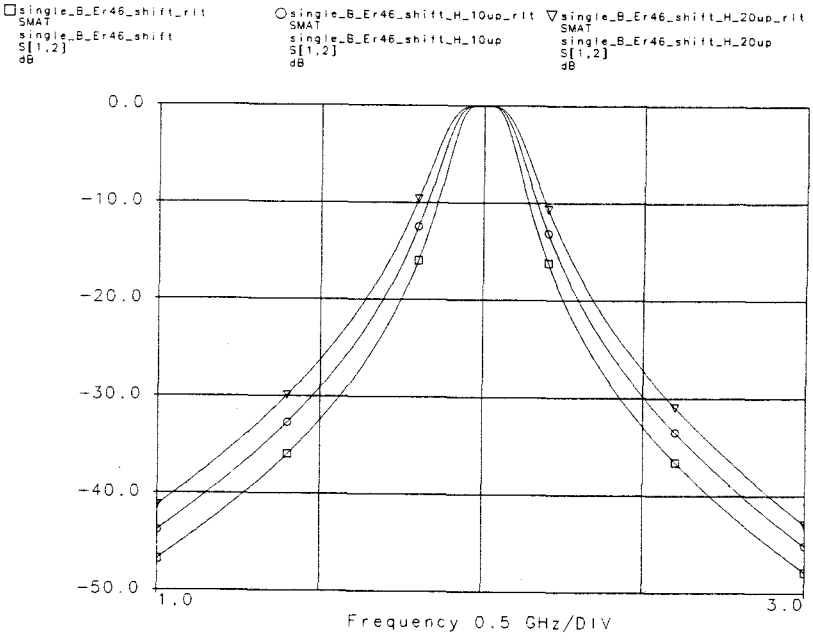

Figure 5.19. Responses for three cases of an optimized, 10 %, and 20 % increased of h_1,h_2.

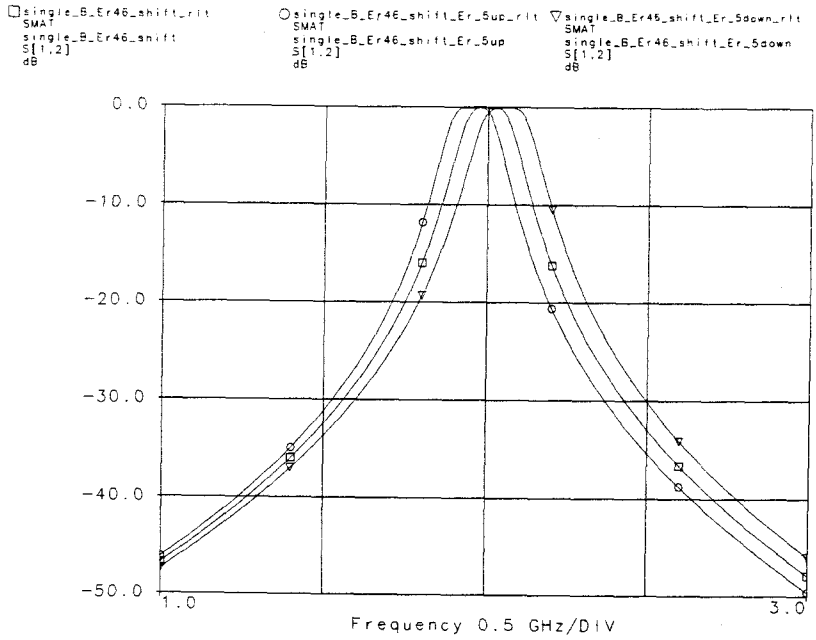

Figure 5.20. Responses for three cases of an optimized, a ϵ_r = 4.6 + 5 %, and a ϵ_r = 4.6 - 5 %.

5.5. DESIGN EXAMPLE II

A Chebyshev asymmetric coupled line band-pass filter with four sections which dielectric constant ϵ_r is 4.6, fractional bandwidth Δ = 10 %(0.2 GHz) and -0.5 dB ripple at center frequency $f_o = 2\ GHz$ is designed.

A general configuration for a coupled line band-pass filter made up of four coupled line sections which have lengths $l = \lambda/4 = 17.48\ mm$ is shown in Figure 5.21.

The Chebyshev filter is assumed to have selected terminating impedances for each section $Z_{o1} = 50\ \Omega$, $Z_{o2} = 45\ \Omega$, and $Z_{o3} = 40\ \Omega$ $Z_{o4} = 35\ \Omega$, $Z_{o5} = Z_{o1} = 50\ \Omega$ according to different widths, w_1, w_2, w_3, w_4, w_5, w_6, w_7, w_8. The design parameters for a band-pass filter with 4 coupled line sections ($N = 4$) are given by,

$$Z_{o1} J_1 = \sqrt{\frac{\pi \Delta}{2 g_1}} \sqrt{\frac{Z_{o1}}{Z_{o2}}} = 0.3307, \tag{5.27}$$

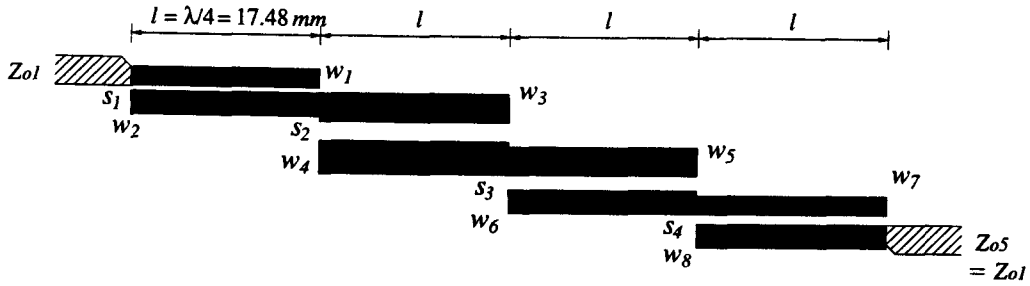

(a) Layout of an 4- section asymmetric coupled line band-pass filter which has section length $l = 17.48\,mm$ at 2 GHz.

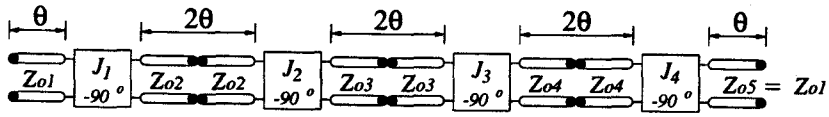

(b) An equivalent circuit using admittance inverter for each coupled line section which $Z_{o1} = 50$, $Z_{o2} = 45$, $Z_{o3} = 40$, $Z_{o4} = 35$, $Z_{o5} = 50\,Ohm$.

Figure 5.21. A layout and an equivalent circuit of Y inverters for a 4-section coupled line band-pass filter.

$$Z_{o2}J_2 = \frac{\pi\triangle}{2\sqrt{g_1 g_2}}\sqrt{\frac{Z_{o2}}{Z_{o3}}} = 0.1259, \tag{5.28}$$

$$Z_{o3}J_3 = \frac{\pi\triangle}{2\sqrt{g_2 g_3}}\sqrt{\frac{Z_{o3}}{Z_{o4}}} = 0.1269, \tag{5.29}$$

$$Z_{o4}J_4 = \sqrt{\frac{\pi\triangle}{2g_3 g_4}}\sqrt{\frac{Z_{o4}}{Z_{o1}}} = 0.2625. \tag{5.30}$$

and g_N represents the element values for Butterworth and Chebyshev low-pass filter prototype as shown in Table 5.1, Table 5.2 and we can notice that $g_1 = g_2 g_3$ in those tables.

From the equations (5.27)-(5.30), (5.13)-(5.15), and (4.33)-(4.36) we can get the 2x2 capacitance $[C]$ matrix for each section like 3-section coupled line Butterworth band-pass filter. Once we have the line mode impedances, Z^a_{oe}, Z^a_{oo}, Z^b_{oe}, Z^b_{oo} of

Section No.	*1*	*2*	*3*	*4*
Z_{eo}^{a} *(Ohm)*	*69.80*	*50.67*	*45.01*	*51.57*
Z_{oo}^{a} *(Ohm)*	*40.04*	*40.60*	*36.12*	*25.32*
Z_{eo}^{b} *(Ohm)*	*64.31*	*45.60*	*39.94*	*68.05*
Z_{oo}^{b} *(Ohm)*	*34.55*	*35.53*	*31.05*	*41.80*
C_1 *(nF)*	*0.1417*	*0.1588*	*0.1787*	*0.2025*
C_m *(nF)*	*-0.0427*	*-0.0197*	*-0.0224*	*-0.0484*
C_2 *(nF)*	*0.1575*	*0.1787*	*0.2042*	*0.1417*
w_1 *(mm)*	*0.99*	*1.502*	*1.835*	*1.96*
w_2 *(mm)*	*1.25*	*1.843*	*2.282*	*0.925*
s *(mm)*	*0.328*	*0.912*	*0.808*	*0.264*
$h_1 = h_2 = h_3$ *(mm)*	*1.4478*			

Table 5.4. Normal parameters, capacitance matrices, and physical dimensions for the 4-section asymmetric coupled line Chebyshev band-pass filter. Having same ends, $w = 1.06\ mm$ as *Table* $5-3$.

each section, and the capacitance $[C]$ matrix for each section then we get the electrical and physical dimensions corresponding to a 4-section Chebyshev by $LINPAR$ program given in the Table 5.4.

The expected ideal filter responses, the magnitude response and the phase response of S_{21} are shown in Figure 5.22 and Figure 5.23.

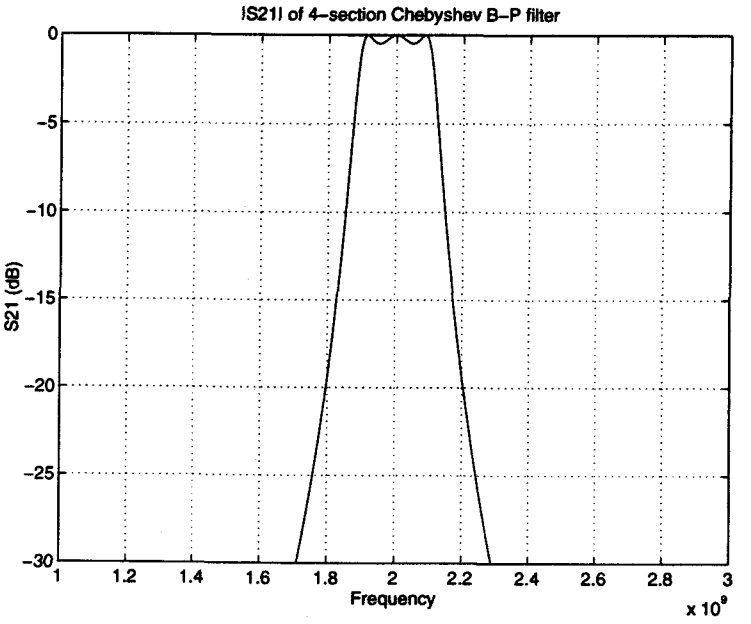

Figure 5.22. Magnitude of S_{21} Chebyshev response for a 4-section asymmetric coupled line Chebyshev band-pass filter

5.6. SUMMARY

In conclusion, procedures of physical realization of asymmetric coupled line band-pass filter circuits on a single level were presented and as an example an asymmetric coupled line Butterworth band-pass filter with 3-sections was fabricated in a strip line for a FR-4 material, simulated, and measured. For these the characteristics of the normal mode parameters, the propagation constants, $\beta_{c,\pi}$, the mode voltage

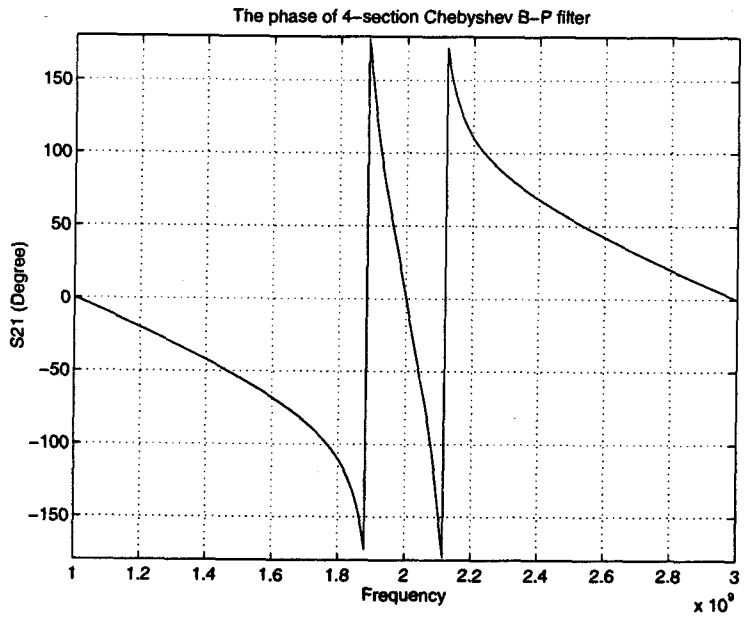

Figure 5.23. Phase of S_{21} Chebyshev response for a 4-section asymmetric coupled line Chebyshev band-pass filter

ratios $R_{c,\pi}$, on the two lines, and the partial mode impedances and admittances, the relationships between characteristics line mode impedances and capacitances of the two lines of the coupled system in an inhomogeneous and a homogeneous medium were examined.

For the optimizations and validations of the filter a *SPICE* model on *LIBRA* and a full-wave *EM* simulator, *MOMENTUM* were used. A sensitivity of the filter also was examined for the effect of tolerances on the performance of the filter. Another procedure of physical realization of 4-section asymmetric coupled line Chebyshev band-pass filter was presented.

6. MULTILEVEL FILTER DESIGN

This chapter presents a methodology for designing asymmetric coupled line filter circuits in multilevel and the sensitivity analysis of the fabricated 3-section band-pass filter. Methods for arriving at filter dimensions are described for the embedded(homogeneous dielectric) configurations. The method developed here is verified by comparison with results obtained from a full-wave electromagnetic simulation.

6.1. INTRODUCTION

Recent advances in high density low cost RF and microwave three dimensional integration technologies using LTCC(Low Temperature Cofired Ceramics), laminate and multilayer integrated circuits have increased interest in the design of embedded passive components such as inductors, capacitors and filters. As an example Figure 6.1 shows a two level coupled topology for application as band-pass filter in wireless systems and other applications. The design of coupled line filters using symmetrical coupled lines has been well established and well suited for single layer metallization structures in the form of coupled microstrip and strip lines. In a layered structure, similar design techniques for asymmetric coupled line filters offers the design flexibility and enables one to design the filters when the physical realization of symmetrical coupled line filter in a layered or physically asymmetric environment becomes tedious or impossible. In addition, asymmetric coupled line filters can naturally be used for impedance matching over a desired band of frequencies.

In this chapter, the basic methodology for single level asymmetric coupled line filters which was developed in Chapter 4 and Chapter 5 is applied to design typical two level filter for RF applications. The equivalent two level circuit for the single level circuit, procedures of realizations, the equivalent *SPICE* circuit model simulations on *LIBRA*, procedures of optimization, sensitivity analysis, and validation on a *EM* simulator, *MOMENTUM* are presented.

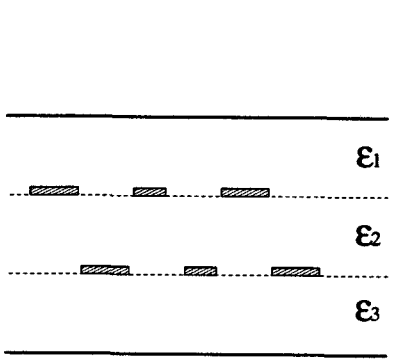

(a) A schematic of a two level multiconductor structure

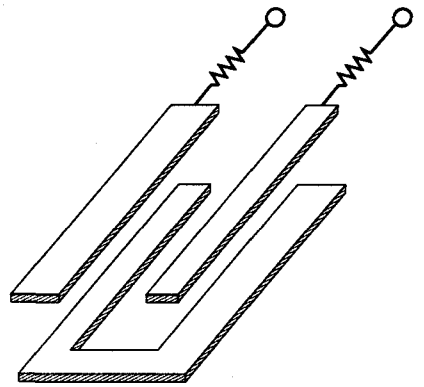

(b) A two level coupled topology of two sections

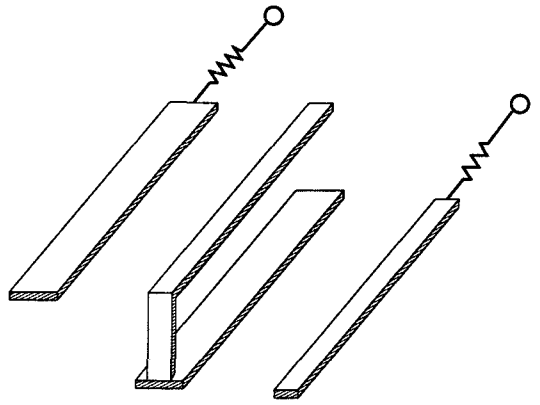

(c) Another two level coupled topology of two sections

Figure 6.1. A single section of a two level coupled topology.

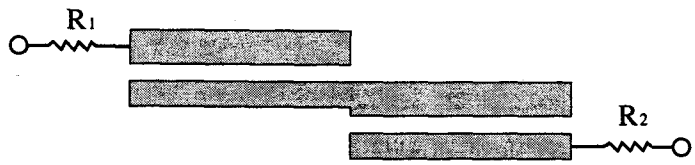

Figure 6.2. An asymmetric coupled line filter with two sections.

6.2. DESIGN METHODOLOGY OF MULTILAYER FILTERS

In general the filters can be designed by using the network functions associated with the general broadside and edge-coupled strip structures with the required boundary conditions at the strip ports [61]- [69]. The design procedure can be facilitated by first realizing the unfolded structure on a single level for a specified frequency response and then designing the physical structure. The unfolded structure is in general represented by asymmetric coupled line filter as shown in Figure 6.2 for prototype a two section structure.

There could be more examples of unfolded 3-section coupled line and 4-section coupled line on a single level which can be folded to multi-level filters such as folded coupled line filters or meander coupled line filters as shown in Figure 6.3 and Figure 6.4.

The design procedure for the multilevel filters also consists of three steps:

step 1. Initial design of the coupled line filter and finding physical dimensions on a single level.

step 2. Decision of the topology for the multilevel filter (including the number of multilevel) and finding physical dimensions (widths, spaces, thickness, dielectric constant) of the equivalent multilevel filter to the single level filter decided from step 1.

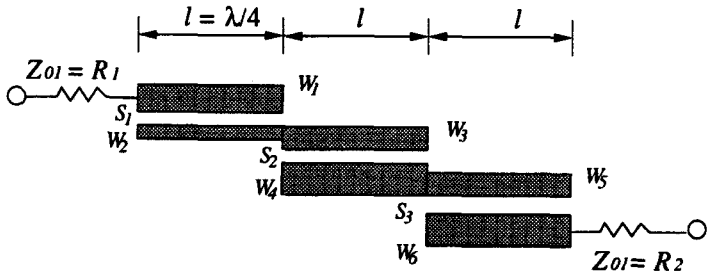

(a) 3-section coupled line filter on a single level

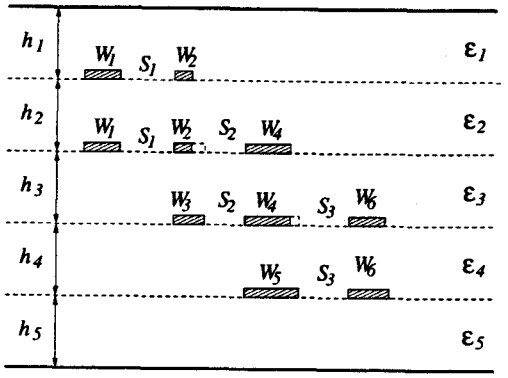

(b) Side view of 3-section coupled line

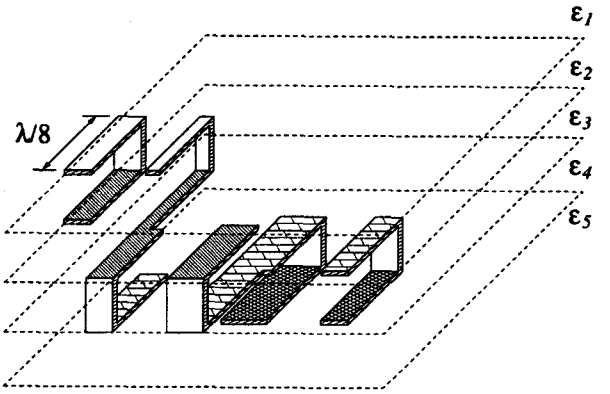

(c) 4 level folded coupled lines

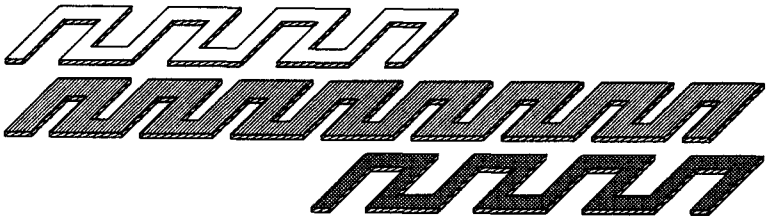

(d) 3 level meander coupled lines

Figure 6.3. A multilevel topology of 3-section coupled line

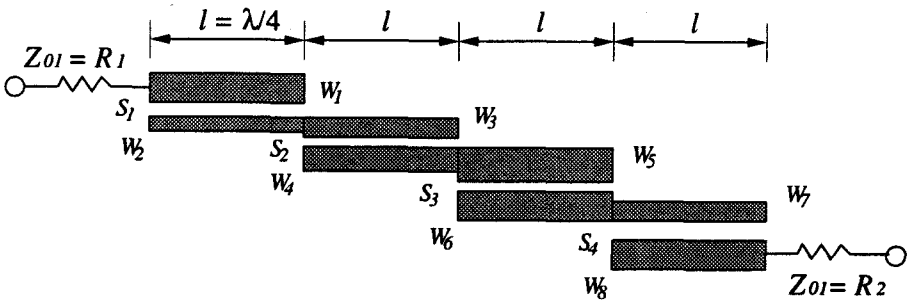

(a) 4-section coupled line filter on a single level

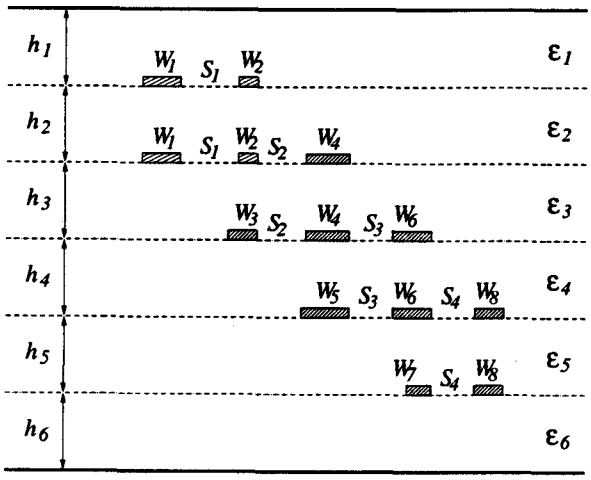

(b) Side view of 4-section coupled line

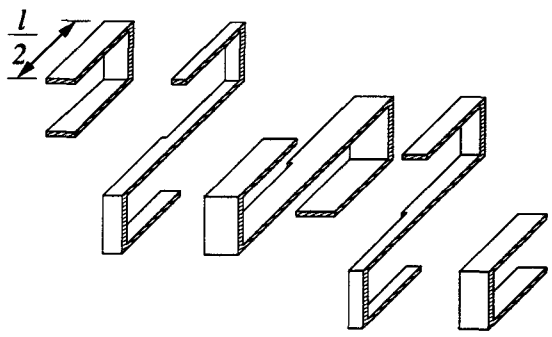

(c) 5 level folded coupled lines

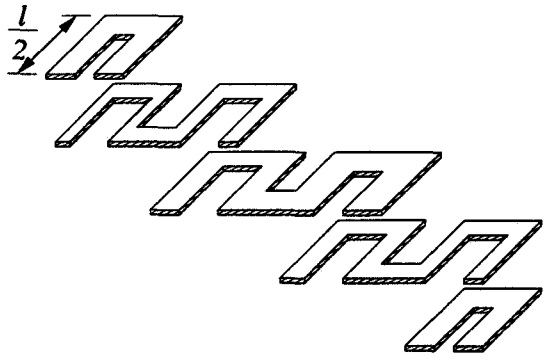

(d) 5 level meander coupled lines

Figure 6.4. A multilevel topology of 4-section coupled line

step 3. Optimizations and fabrication of the physical structure obtained in step 2 to validate the design methodology for the multilevel filter.

The design procedure for single level filters, Figure 5.1 also can be used here for the designing of the multilayer filter.

For step 1, we start with filter specifications(number of coupled sections, bandwidth, center frequency, selectivity, terminating impedances Z_{oi}) and the physical dimensions of the filter on a single level for each coupled line section obtained from Chapter 5.

For step 2, we have to decide which type of topology for the multilevel filter we want. Then the physical dimensions on a single level must be changed to those on multilevel. The physical dimensions are the widths of the conductors on the upper level and/or lower level, spaces between the conductors of each section, the thickness of the dielectric substrate, and the dielectric constant. The variable elements would be the spaces or offsets between the conductors on the different level, and the thickness of the dielectric substrate, and the dielectric constant. Actually the dimensions of widths of the conductors of each section should not be changed at the first step of converting from a single level to a multilevel.

For examples, if we choose the topology of Figure 6.3 (c) 4 level folded coupled line filter the 1^{st} section of the 3-section coupled line filter on a single level can be folded to two halfs, which length of one half section corresponding to $l/2 = \lambda\ /8$, then the other half folded section will be located in the next lower level. This procedure can be applied to 2^{nd} and 3^{rd} sections repeatedly. If we choose the topology of Figure 6.4 (d) 5 level meander coupled line filter the 1^{st} line with w_1 of the 1^{st} section of the 4-section coupled line filter on a single level can be meandered to two halfs, which length of each half section corresponds to $l/2 = \lambda\ /8$ on the 1^{st} level. The 2^{nd} line which corresponds to $l = \lambda\ /2$ and has two different widths, w_2 and w_3

can be meandered and located on the 2^{nd} level. This same procedures also can be applied to 3^{rd}, 4^{th}, and 5^{th} level.

One thing we have to remember in the procedure of physical realizations is that the width of the connection lines between the half folded or the half meadered lines must be the average of the other two lines. to avoid unexpected effects.

For step 3 of design procedure, we need to use a *SPICE* model on *LIBRA* or a *EM* simulator *MOMENTUM* which were used in Chapter 5. For use of a *SPICE* model on *LIBRA* we need to have an equivalent lumped element circuit to the multilevel filter at first. Then this must be converted to the equivalent *SPICE* model circuit on *LIBRA*. For the simulation and optimization on the *EM* simulator *MOMENTUM* we need to make the physical structure we decided in the "layout" window. Then it generates another window, "test" and we can set up the requirements such as thickness of the dielectric substrate, dielectric constant, etc. Now we have a meshed physical structure can be simulated and optimized. Once we get the optimized circuit we fabricate the multilevel filter, measure and compare the responses.

6.3. SIMULATIONS AND OPTIMIZATIONS FROM A *SPICE* MODEL ON *LIBRA*

For a multilevel filter design in a homogeneous medium, we will use the same specifications, normal mode parameters, and physical dimensions of the 3-section asymmetric coupled line band-pass filter on a single level designed in the Chapter 5.

For step 2 we want to choose a topology of two level asymmetric coupled line filter shown in Figure 6.5 which has the same length, $l = \lambda/4$ as that of each section on a single level topology. Then we have to find the physical dimensions, widths w,

spaces s, thickness h, dielectric constant ϵ_r for the two level topology to satisfy the obtained normal mode parameters of a single level for each section.

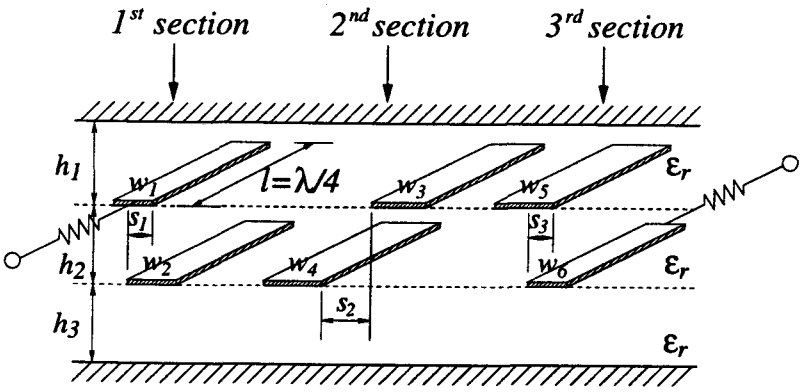

(a) 2 level coupled line band-pass filter excluding connections between each section.

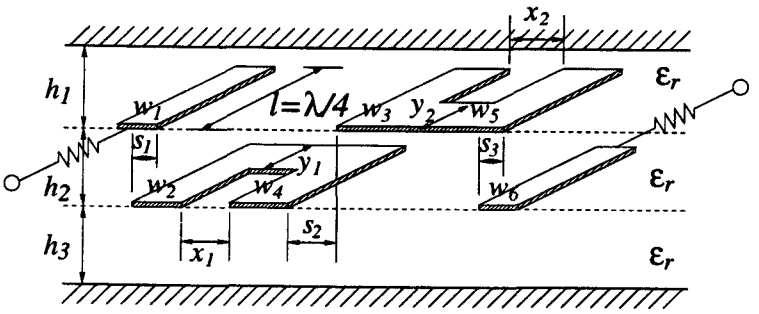

(b) 2 level coupled line band-pass filter with 3 sections including connections.

Figure 6.5. A sideview of folded two level topology of 3 section coupled lines.

A program "*LINPAR*" was used to realize the physical dimensions on a two level topology. Figure 6.5 (a) shows the physical dimensions, w_1, w_2, s_1 of the 1^{st} section, w_3, w_4, s_2 of the 2^{nd} section, w_5, w_6, s_3 of the 3^{rd} section, $l = \lambda\ /4$ on a two level correspond to those of the single level. Figure 6.5 (b) shows the physical dimensions after considering the connections between the folded lines i.e. which

lengths x_1, x_2, and widths y_1 $(= \frac{w_2+w_4}{2})$, y_2 $(= \frac{w_3+w_5}{2})$, the average of the other two lines.

For step 3, Figure 6.6 and Figure 6.7 show the equivalent lumped element circuit and the equivalent $SPICE$ model circuit on $LIBRA$ not including the connecting lines and open-ends of each section, whereas Figure 6.8 shows the equivalent $SPICE$ model circuit on $LIBRA$ including those of each section.

The equivalent lumped element circuit consists of 21 lumped elements of admittance values and the equivalent $SPICE$ circuit also has same number of transmission lines($TLIN4$-element on $LIBRA$).

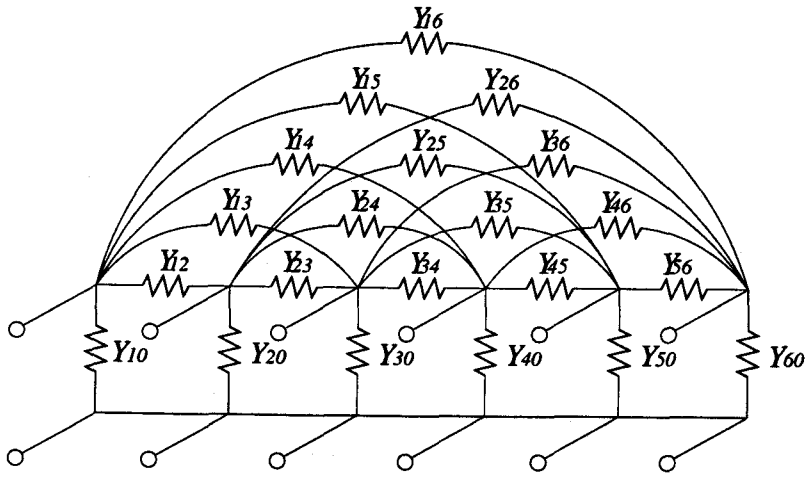

Figure 6.6. The equivalent lumped element circuit representing the characteristic admittances of multiconductor configuration oriented model.

Figure 6.9 shows finally an optimized response of the two level coupled line band-pass filter with 3 sections excluding the effects of the connecting lines and open-ends for each section by the simulation of the equivalent $SPICE$ model circuit on $LIBRA$ in Figure 6.7.

Figure 6.10 shows an optimized response of the two level coupled line band-pass filter with 3 sections including the effects of the connecting lines and open-ends for each section by the simulations and optimizations of the equivalent $SPICE$ model circuit on $LIBRA$ in Figure 6.8.

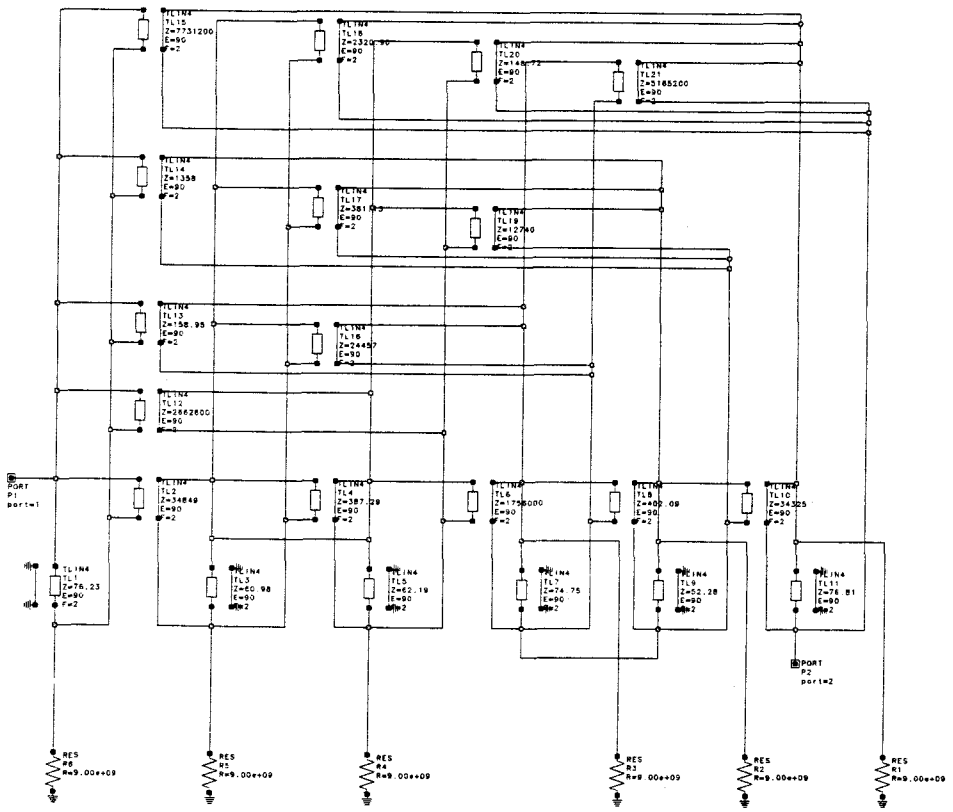

Figure 6.7. The equivalent $SPICE$ model circuit on $LIBRA$ excluding connecting lines and open-ends for each section.

The response of $|S_{21}|$ of Figure 6.7 shows -0.1 dB loss and 0.16 GHz of band width BW at the center frequency 2 GHz, while the response of $|S_{21}|$ of Figure 6.8 shows -0.2 dB and 0.13 GHz of band width BW at the center frequency 1.64 GHz. The latter was 0.36 GHz shifted from 2 GHz after adding 2 $TLIN4$-elements and

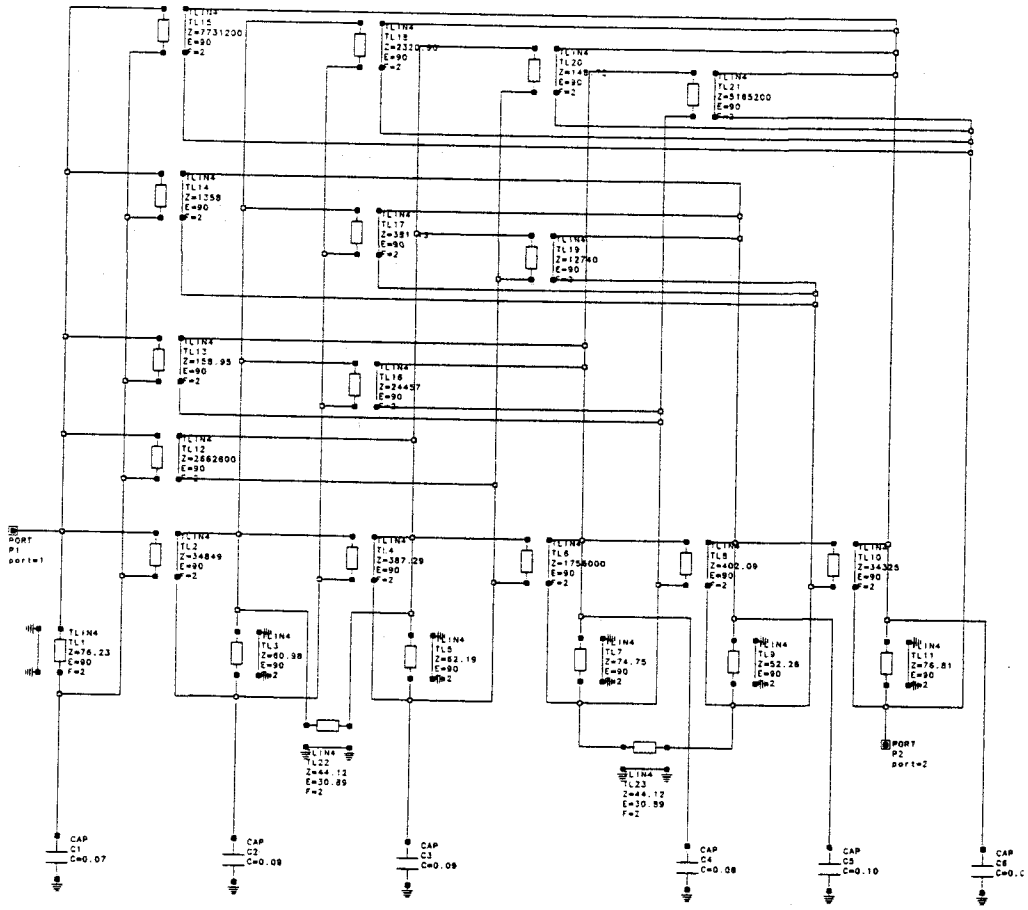

Figure 6.8. The equivalent *SPICE* model circuit on *LIBRA* including connecting lines and open-ends for each section.

6 capacitance values corresponding to the connections between w_2 and w_4, w_3 and w_5 (the two $TLIN4$-elements between bottom 2^{nd} and 3^{rd} $TLIN4$-elements, and 4^{th} and 5^{th} $TLIN4$-elements), and 6 open-ends as shown in Figure 6.8.

From the Figure 6.10 we can notice that the frequency above the pass-band decays more rapidly than that obtained by the equivalent $SPICE$ model circuit in Figure 6.7. This may be caused by discontinuity reactances which were not taken into account in Figure 6.7. And the center frequency shift is likely caused by other open-end, discontinuity capacitances.

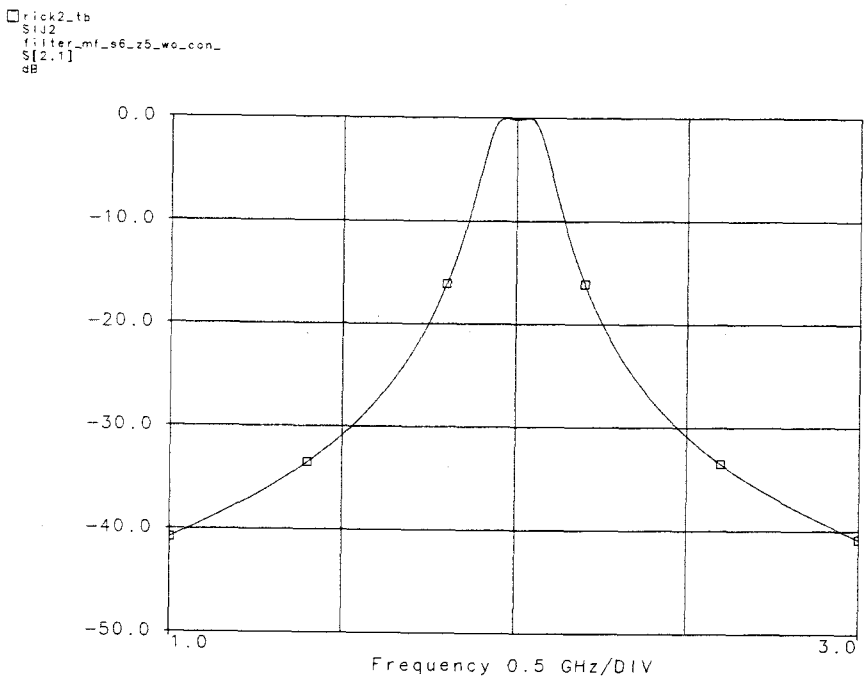

Figure 6.9. The response of the equivalent $SPICE$ model circuit on $LIBRA$ excluding connecting lines and open-ends for each section.

Figure 6.11 shows an optimized physical dimensions for a 3 section asymmetric coupled line band-pass filter on two level by $SPICE$ model.

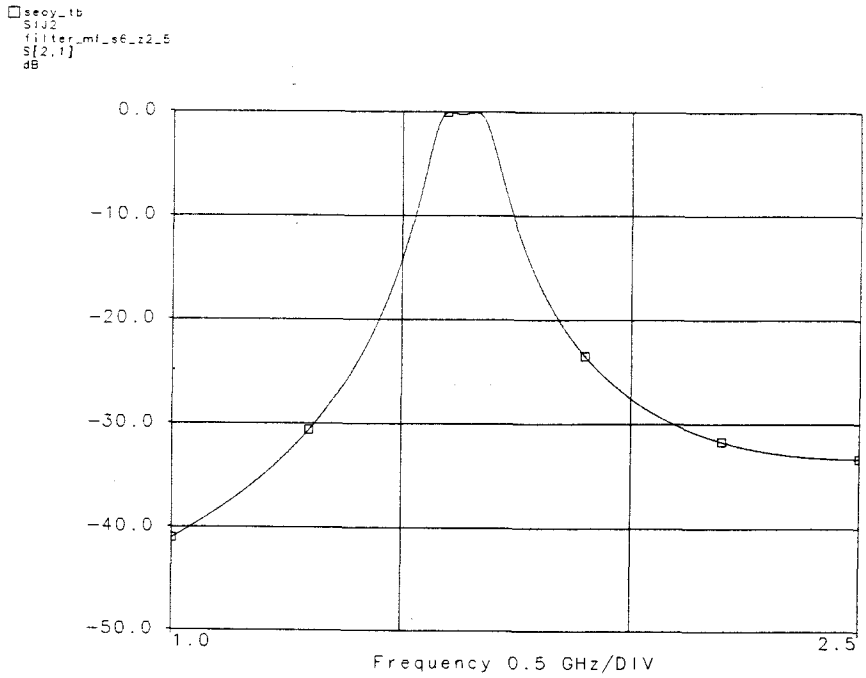

Figure 6.10. The response of the equivalent *SPICE* model circuit on *LIBRA* including connecting lines and open-ends for each section.

6.4. OPTIMIZATIONS ON *MOMENTUM* AND COMPARISON

We can also use a full-wave *EM* simulator, *MOMENTUM*(HP-EEsof product) taking up "the method of moments" for step 3. For more accurate and faster simulations and optimizations by the *EM* simulator *MOMENTUM* we need to decide the physical dimensions in the "layout" window of the *MOMENTUM*. Then it generates another window, "test" and we are asked to set up the thickness of the dielectric substrate, the dielectric constant, and etc. Then we have a meshed physical structure to analyze and optimize. Figure 6.12 generated by those procedures shows the physical layout and the mesh configuration for a 3-section band-pass filter on a two level.

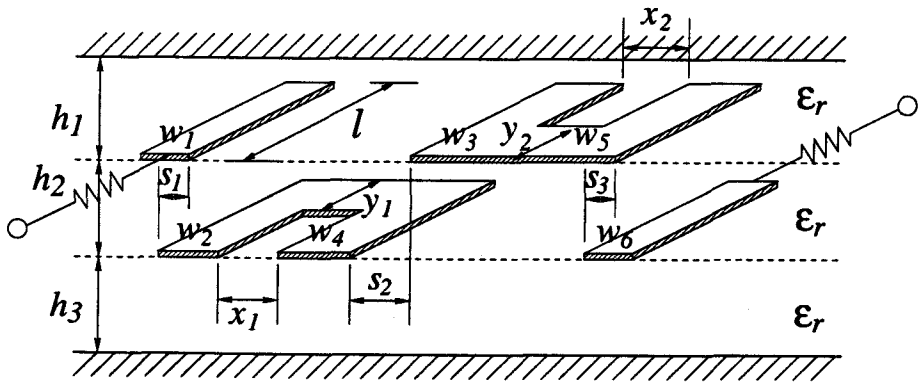

$w_1 = 5\ mm$ $\quad$ $s_1 = 3\ mm$

$w_2 = 6\ mm$ $\quad$ $* \ s_2 = 5\ mm$

$w_3 = 7\ mm$ $\quad$ $s_3 = 3\ mm$

$w_4 = 9\ mm$ $\quad$ $h_1 = h_2 = h_3 = 6\ mm$

$w_5 = 8\ mm$ $\quad$ $* \ x_1 = x_2 = 6\ mm$

$w_6 = 5\ mm$ $\quad$ $y_1 = y_2 = 8\ mm$

$* \ l = 14.3\ mm$ $\quad$ $\varepsilon_r = 4.6$

$f_o = 2\ GHz$

$*$: *Difference from the physical dimensions by* MOMENTUM

Figure 6.11. An optimized physical dimensions of the topology for a 3 section asymmetric coupled line band-pass filter on two level by $SPICE$ model.

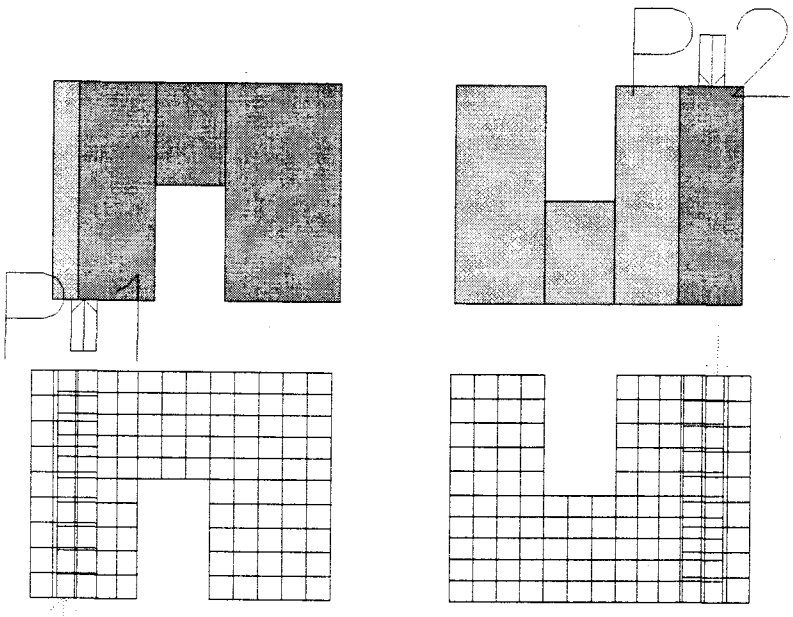

Figure 6.12. A physical layout and a mesh configuration on a two level generated by *MOMENTUM* for a 3-section band-pass filter.

The optimum physical dimensions and the response through the procedures of optimization is shown in Figure 6.13 and Figure 6.14.

The design methodology for the multilevel coupled line filter was validated by computing the response of the physical structure on the *EM* simulator, *MOMENTUM* except less narrow band width, $BW = 0.1\ GHz$ corresponding to 50 % of that of single level($BW = 0.2\ GHz$).

If the 2-level 3-section band-pass filter for the fabrication is realized on $FR-4$ dielectric substrate which $tan\ \delta = 0.02$ it represents -5.7 dB loss at the center frequency and the response is shown in Figure 6.15.

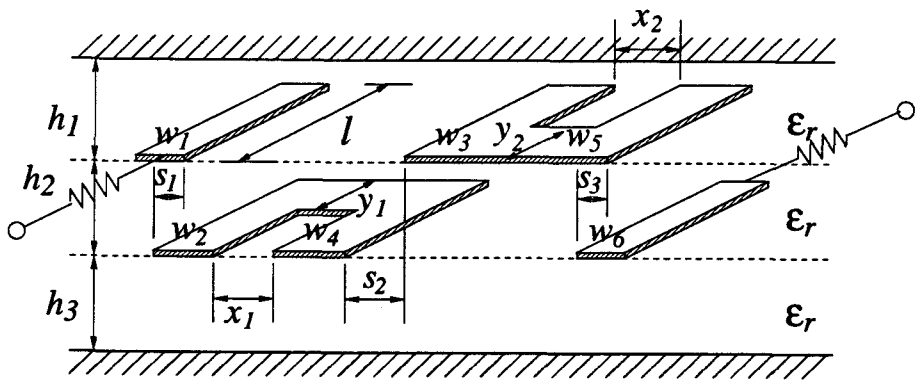

$w_1 = 5\ mm$	$s_1 = 3\ mm$
$w_2 = 6\ mm$	$*s_2 = 9\ mm$
$w_3 = 7\ mm$	$s_3 = 3\ mm$
$w_4 = 9\ mm$	$h_1 = h_2 = h_3 = 6\ mm$
$w_5 = 8\ mm$	$*x_1 = x_2 = 5.4\ mm$
$w_6 = 5\ mm$	$y_1 = y_2 = 8\ mm$
$* \ l = 17\ mm$	$\varepsilon_r = 4.6$
	$f_o = 2\ GHz$

$*$: *Difference from the physical dimensions by* SPICE *model*.

Figure 6.13. A sideview and the physical dimensions of the topology for a 3 section asymmetric coupled line band-pass filter on two level optimized by *MOMENTUM*.

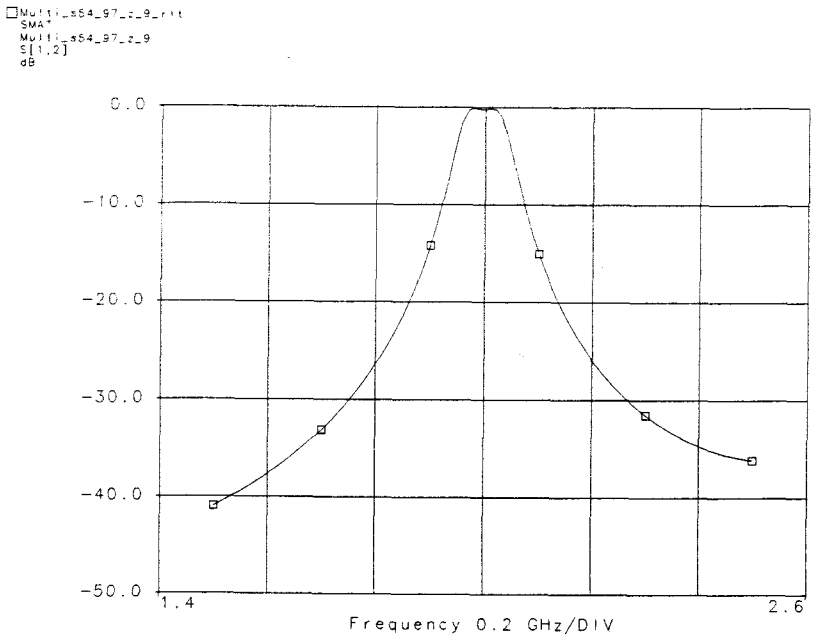

Figure 6.14. The response of a 3-section band-pass filter on two level optimized by *MOMENTUM*.

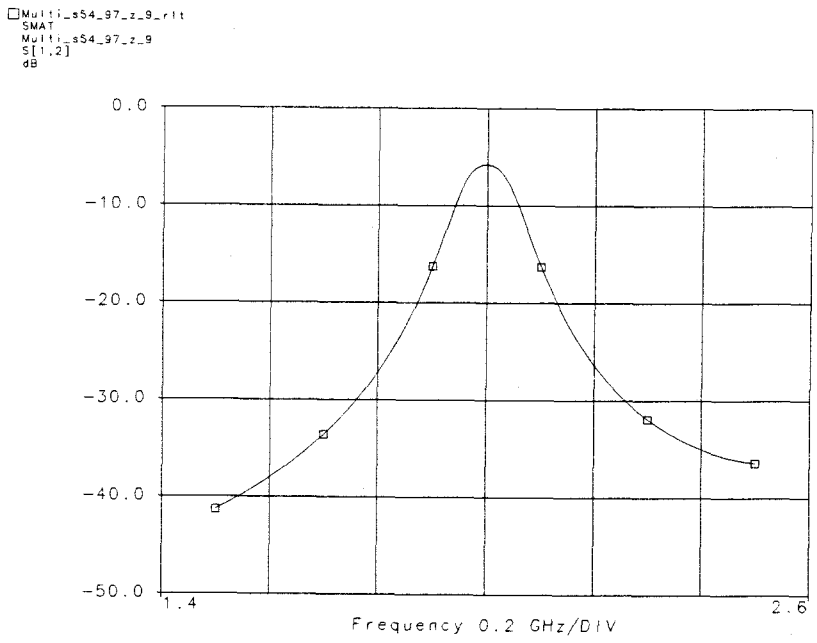

Figure 6.15. The response of a 3-section band-pass filter on two level which $tan\ \delta$ = 0.02 of the dielectric substrate of an optimized.

6.5. SENSITIVITY ANALYSIS

The effect of tolerances on the performance of strip lines on two level also can be analyzed using the sensitivity approach [59,60]. This approach is the easiest method of predicting the worst case behavior corresponding to a given set of tolerances. It does not require the actual statistical distribution of tolerances.

Here the sensitivity factors for the 3-section band-pass filter on a two level were also constrainded to the following five factors and the tolerances of the factors were taken up $\pm$ 5 %: widths of the lines on 1^{st} level w_1, w_3, w_5, widths of the lines on 2^{nd} level w_2, w_4, w_6, spaces s_1 between w_1 and w_2, s_2 between w_3 and w_4, s_3 between w_5 and w_6, thicknesses of the dielectric substrate h_1, h_2, h_3 and dielectric constant ϵ_r.

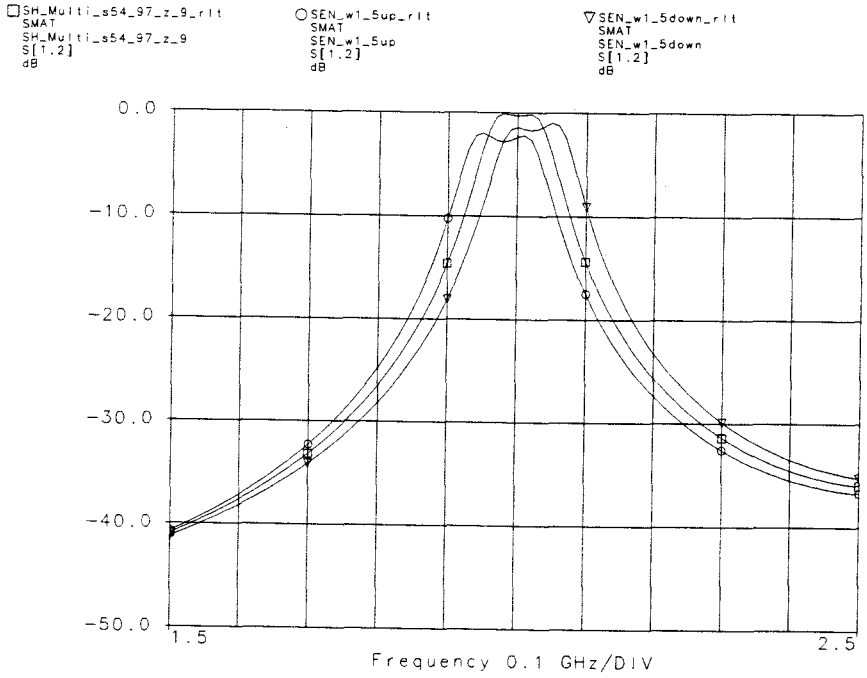

Figure 6.16. Responses for three cases of an optimized, a 5 % increased of w_1,w_3,w_5, and a 5 % decreased of w_1,w_3,w_5.

As shown in Figure 6.16 the response of 5 % increased or 5 % decreased widths of the lines on 1^{st} level have not affected about the band width unlike the response in a single level. The response of 5 % increased widths on 1^{st} level has -2.8 dB loss and a shifted center frequency 1.98 GHz while the response of 5 % decreased widths has -1.8 dB loss and a shifted center frequency 2.02 GHz.

While Figure 6.17 shows a little different pattern from that of the Figure 6.16. The response of 5 % increased widths on 1^{st} level has -1.1 dB loss and a shifted center frequency 1.98 GHz while the response of 5 % decreased widths has -3.1 dB loss and a shifted center frequency 2.02 GHz.

This represents that the tolerance of widths of the lines of two level makes the response more sensitive than those of a single level.

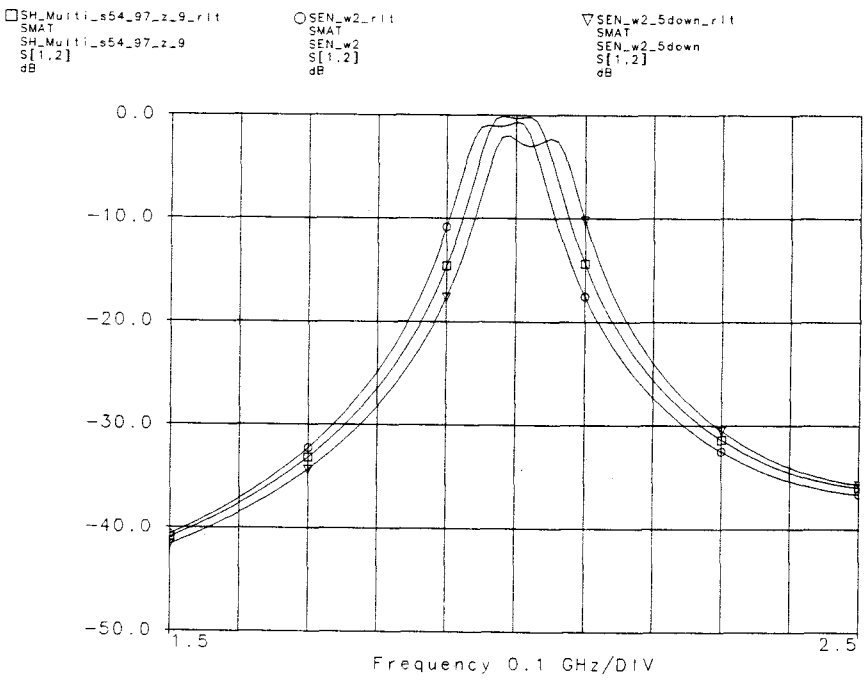

Figure 6.17. Responses for three cases of an optimized, a 5 % increased of w_2,w_4,w_6, and a 5 % decreased of w_2,w_4,w_6.

Figure 6.18 shows almost same pattern to that of the Figure 5.17 in Chapter 5. As shown in Figure 6.18 the response of the 5 % increased spaces s_1, s_2, and s_3 between w_1 and w_2, w_3 and w_4, and w_5 and w_6 has a band width of 0.09 GHz(10 % reduced from 0.1 GHz), while the response of the 5 % reduced spaces has 0.11 GHz(10 % increased from 0.1 GHz) at the center frequency $2GHz$. This gives us important informations that decreasing the spaces s_1, s_2, and s_3 guarantee a more wide band width comparatively with some losses at the center frequency for optimization.

And this represents that the tolerance of the space between two lines on different levels do not make the response sensitive.

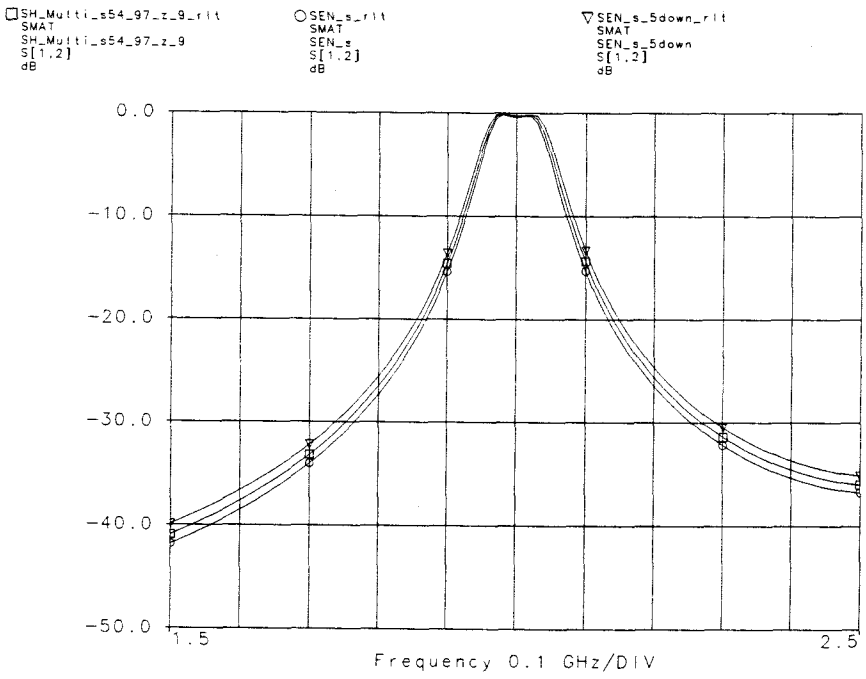

Figure 6.18. Responses for three cases of an optimized, a 5 % increased of s_1,s_2,s_3, and a 5 % decreased of s_1,s_2,s_3.

Figure 6.19 shows that the responses of the 5 % increased or decreased thicknesses of the substrate have similar ones to those of single level in Chapter 5 except

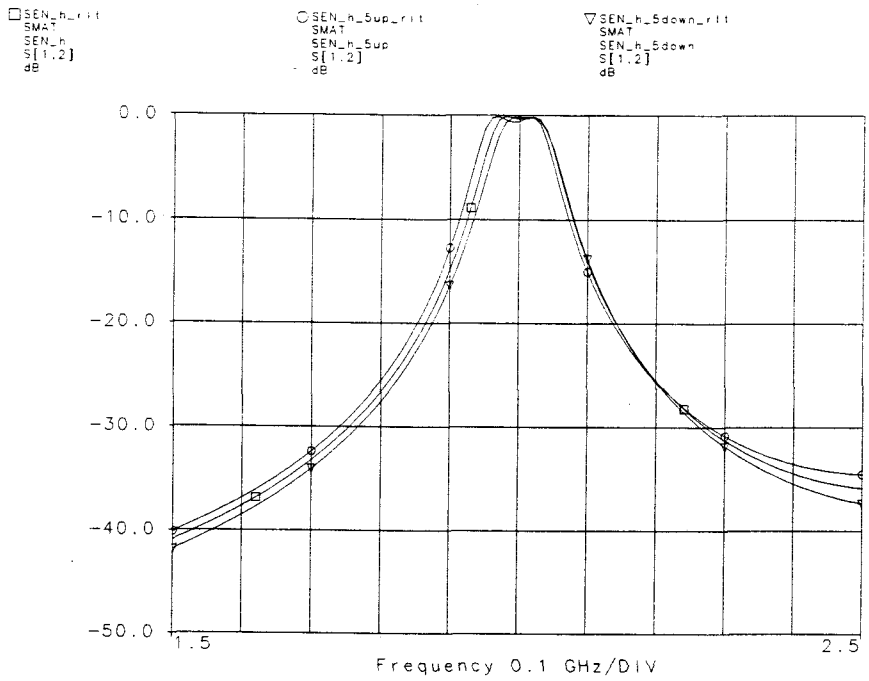

Figure 6.19. Responses for three cases of an optimized, a 5 % increased of h_1,h_2,h_3, and a 5 % decreased of h_1,h_2,h_3.

the center frequency shift. The response of the 5 % increased thicknesses of the substrate, h_1, h_2, and h_3 has a band width of 0.11 GHz (10 % increased from 0.1 GHz) at 1.99 GHz, while the response of the 5 % decreased has a band width of 0.09 GHz(10 % reduced from 0.1 GHz) 2.01 GHz.

From this fact we notice that increasing the thickness of the substrate helps increasing the band width but it accompanies some losses at the center frequency.

This also gives us important informations that decreasing the spaces between two lines on different levels guarantees increasing the band width for optimizations than increasing the thickness of the substrate does as shown in Figure 6.18 and Figure 6.19.

Unlike the responses from Figure 5.19 of Chapter 5, Figure 6.20 shows the responses become very sensitive as increasing the thickness of the substrate 10 %, 20 %, 30 % up. These discrepancies probably come from the fact two level circuit has one more dielectric substrate layer h_3 than one level has.

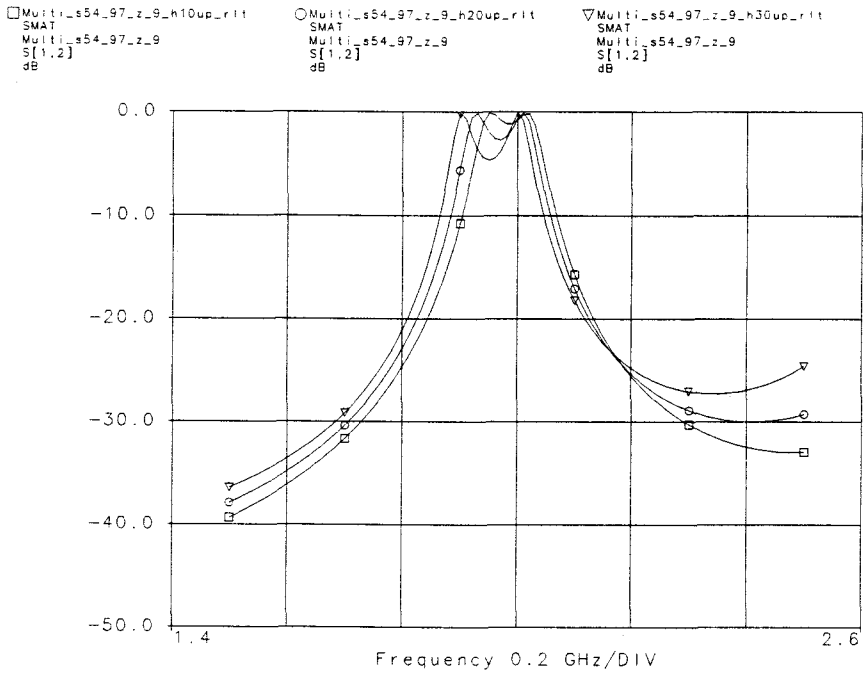

Figure 6.20. Responses for three cases of a 10 %, a 20 %, and a 30 % increased of h_1,h_2,h_3 on two level.

As shown in Figure 6.21 $\pm$ 5 % of tolerances($\pm$ 0.23) for the dielectric constant, $\epsilon_r = 4.6$ make the responses be shifted sensitively. Increasing 5 % of the dielectric constant makes the center frequency $f_o = 2\ GHz$ to 1.95 GHz shifted, while decreasing 5 % of it makes it 2.05 GHz shifted.

It gives us the fact the tolerance of the dielectric constant makes the two level circuit sensitive and the center frequency shifted but it does affect to the response of magnitude unlike the single level in Chapter 5.

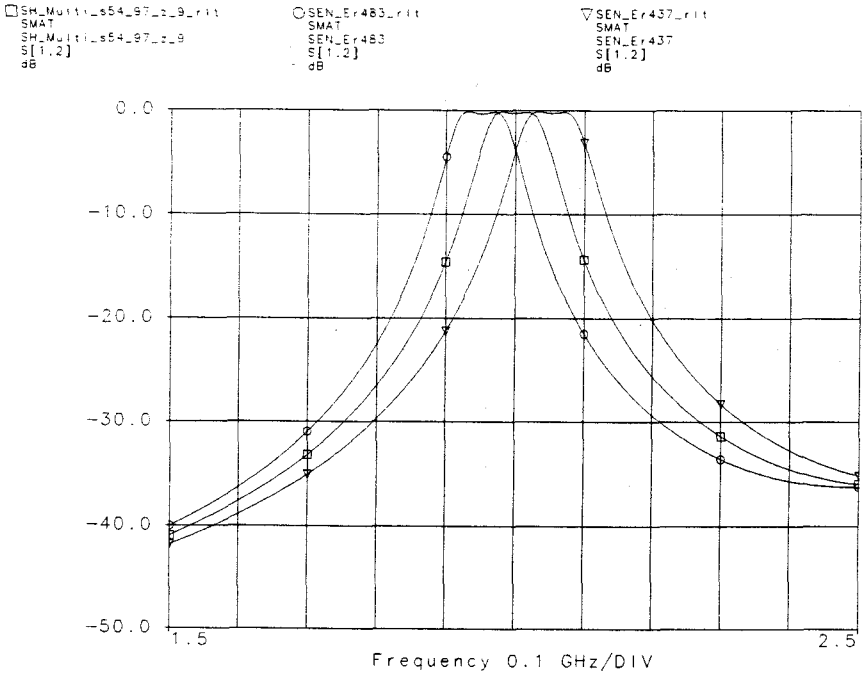

Figure 6.21. Responses for three cases of an optimized, a $\epsilon_r = 4.6 + 5$ %, and a $\epsilon_r = 4.6 - 5$ %.

6.6. SUMMARY

The procedures for the physical realization of asymmetric multilevel coupled line filter circuits were presented and as an example an asymmetric two level coupled line band-pass filter with 3-sections was realized. For the optimizations and validations of the filter a *SPICE* model on *LIBRA* and a full-wave *EM* simulator, *MOMENTUM* were used. Sensitivity of the filter also were examined for the effect of tolerances on the performance of the filter.

7. CONCLUSION AND SUGGESTIONS FOR FUTURE WORK

This dissertation was devoted to the study of designing of coupled line filters in a multilayer in an inhomogeneous and a homogeneous medium. Although multilayer circuit configurations have been used for digital and low frequency systems, RF and microwave circuits are usually fabricated in single layer configurations. The use of multilayer circuit configurations makes microwave circuits more compact and the design more flexible.

The dissertation has presented the basic analysis techniques for spiral inductors which form an important component in RF circuits. The computation of the spiral model parameters is presented including the quality factor. It is shown that both the quality factor and the inductance values can be enhanced by using two and multilevel spirals.

For general asymmetric coupled line filters the use of the admittance inverter corresponding to the single section equivalent circuit of a coupled asymmetric line section enables us to formulate the design procedure for coupled line band-pass filters. This conventional synthesis procedure forms the first step in the realization of single and multilevel band-pass filters. The design when translated into a physical geometry by the quasi-static field solver like $ML2DN$ can be optimized by the use of $SPICE$ compatible equivalent circuits. The final design can always be validated by a rigorous electromagnetic simulations or measurements and demonstrated in this thesis.

This dissertation has also presented theoretical, simulated and experimental results on the proposed methodology for designing of multi-section multilevel coupled line filters in an inhomogeneous medium or a homogeneous medium. For

validation of this proposed design methodology, the equivalent *SPICE* circuit models were simulated on *LIBRA* for a single and two level structures. A full-wave *EM* simulator, *MOMENTUM* was also used to simulate the scattering parameters of the filters in order to validate the design. The effect of tolerances on the performance of the circuits were analyzed using the sensitivity analysis [60] in terms of conductor width w, space between conductors s, thickness of the dielectric substrate h, and dielectric constant of the substrate ϵ_r.

Embedded passives is an emerging area in RF and microwave IC's and modules and with various possible topologies, there are many opportunities in future theoretical and experimental research work. For different topologies with small foot prints, design methodologies need to be formulated. This includes various passives like capacitors, inductors, transformers, and different kind of filters. At higher frequencies, inter-element coupling in these high density circuits must be included in the design cycle. Fabrication and measurements of these components poses new challenges in terms of 3-D metallization alignments and calibration techniques.

BIBLIOGRAPHY

[1] H. Uchida, **"Fundamentals of Coupled Lines and Multiwire Antennas,"** H.Uchida Sandai Press 1967.

[2] P. Kuznetsov and R. Stratonovich, **"The Propagation of Electromagnetic Waves in Multiconductor Transmission Lines,"** Pergamon 1964.

[3] S. Frankel, **"Multiconductor Transmission Line Analysis,"** Artech House 1977.

[4] F.Y. Chang, **"Transient Analysis of Lossless Coupled Transmission Lines in a Homogeneous Dielectric Medium,"** *IEEE Trans. on MTT*, pp. 616-626, Sept. 1970.

[5] Y.K. Chin, **"Analysis and applications of multiple coupled Line structures in an inhomogeneous medium,"** PhD. Dissertation, Electrical and Computer Engineering Department, Oregon State University, Corvallis, OR, 1982.

[6] V.K. Tripathi, **"Asymmetric Coupled Transmission Lines in an Inhomogeneous Medium,"** *IEEE Trans. on MTT.*, Vol. MTT-23, pp. 734-739, Sept. 1975.

[7] V.K. Tripathi, **"On the Analysis of Symmetrical Three-Line Microstrip Circuits,"** *IEEE Trans. on MTT.*, Vol. MTT-25, pp. 726-729, September 1977.

[8] V.K. Tripathi, **"The Scattering Parameters and Directional Coupler Analysis of Characteristically Terminated Three-Line Structures in an Inhomogeneous Medium,"** *IEEE Trans. on MTT.*, Vol. MTT-29, pp. 22-26, January 1981.

[9] A.R. Djordjevic, T.K. Sarkar, R.F. Harrington, **"The Time Domain Response of Multiconductor Transmission Lines,"** *Proc. IEEE*, pp. 743-764, June 1987.

[10] V.K. Tripathi and J.B. Rettig, **"A SPICE model for multiple coupled microstrips and other transmission lines,"** *IEEE Trans. on MTT.*, pp. 1513-1518, December 1985.

[11] V.K. Tripathi and R.J. Bucolo, **"Analysis and Modeling of Multilevel Parallel and Crossing Interconnection Lines,"** *IEEE Trans. Electron on Devices*, pp. 650-658, March 1987.

[12] V.K. Tripathi and H. Lee, **"Spectral-Domain Computation of Characteristic Impedances and Multiport Parameters of Multiple Coupled Microstrip Lines,"** *IEEE Trans. on MTT.*, pp. 215-221, January 1989.

[13] V.K. Tripathi and N. Orhanovic, **"Time Domain Characterization and Analysis of Dispersive Dissipative Interconnects,"** *IEEE Trans. Circuits and Systems*, pp. 938-945, November 1992.

[14] N. Orhanovic, L. Hayden and V.K. Tripathi, **"Analysis and Modeling of Uniformly and Nonuniformly Coupled Lossy Lines for Interconnections and Packaging in hybrid and Monolithic Circuits,"** *SPIE Intl. conf. on Advances in Interconnects and Packaging"*, Vol. 1389, pp. 273-284, November 1990.

[15] V.K. Tripathi and A. Biswas, **"Computer Aided Analysis and Design of Multiple Nonuniformly Coupled Microstrips and Other Transmission Lines,"** *Proc. European Microwave Conference, Budapest*, pp. 525-530, September 1990.

[16] R. T. Kollipara, *et al.*, **"Modeling and Design of Interdigital Structures,"** *IEEE Tran. Electron Devices*, pp. 2575-2577, Nov. 1991.

[17] V.K. Tripathi, **"Reply to Comments on "Spectral-Domain Computation of Characteristic Impedances and Multiport Parameters of Multiple Coupled Microstrip Lines,"** *IEEE Trans. on MTT*, Vol. 40, No. 8, Aug. 1992.

[18] H.S. Chang and V.K. Tripathi, **"Extended matrix Method for the Analysis of Nonlinear Directional Couplers with Saturable Coupling Media,"** *Optical Engineering*, pp. 735-738, April 1993.

[19] N. Orhanovic, P. Wang, and V.K. Tripathi, **"Time Domain Simulation of Uniform and Nonuniform Multiconductor Lossy Lines by the Method of Characteristics,"** *IEEE Trans. Computer-Aided Design of Integrated Circuits*, pp. 900-904, June 1993.

[20] S. Luo, A. Biswas, and V.K. Tripathi, **"Finline Multiport Couplers,"** *IEEE Trans. on MTT.*, pp. 2208-2215, December 1994.

[21] Y.Seo and V.K. Tripathi, **"Spiral Inductors in RFIC's and MMIC's,"** *1995 Asia Pacific Microwave Conference Proc.*, Taejon, Korea, pp. 454-457, October 1995.

[22] Y.Seo, *et al.*, **"Modeling Interconnect Coupling Between Analog, Digital, and RF layout Components for MCM Design**, *IMAPS Intl. J. Mi-*

crocircuits & Electronic Packaging, Vol. 19, No. 4, pp. 441-448, Fourth Quarter, 1996.

[23] R.D. Lutz, *et al.*, **"Spiral Inductor Design Issues in a Multilayered Medium,"** *Proc. ISHM Intl. Sym.*, Oct. 1996.

[24] R.L. Remke and G.A. Burdick, **"Spiral Inductors for Hybrid and Microwave Applications,"** *Proc. 24th Electron Components Conf.*, Washington, D.C., pp. 152-161, May 1974.

[25] E. Pettenpaul *et al.*, **"CAD Models of Lumped Elements on GaAs up to 18 GHz,"** *IEEE Trans. on MTT.*, pp. 294-304, Vol. 36, Feb. 1988.

[26] V.K. Tripathi, C. Holmes, M. Cochrane, and B. Allen, **"A Distributed CAD Model for Microstrip Spiral Inductors,"** *European Microwave Conference Digest*, pp. 723-724, September 1993.

[27] A. Hill and V.K. Tripathi, **"Analysis and Modelling of Coupled Microstrip Bend Discontinuities,"** *IEEE Int. Microwave Sym.*, pp. 1143-1146, June 1989.

[28] R.T. Kollipara and V.K. Tripathi, **"Spectral Domain Analysis of Multiconductor Structures with Rectangular and Trapezoidal Cross Sections,"** *Microwave and Optics Letters*, John Wiley, Jan. 1990.

[29] J.N. Burghartz, M. Soyuer, and K. A. Jenkins, **"Microwave Inductors and Capacitors in Standard Multilevel Interconnect Silicon Technology,"** *IEEE Trans. on MTT.*, Vol. MTT-44, pp. 100-104, Jan. 1996.

[30] H.M. Greenhouse, **"Design of Planar Rectangular Microelectronic Inductors,"** *IEEE Trans. Parts, Hybrids, and Packaging*, Vol. PHP-10, pp. 101-109, June 1974.

[31] A. Hill and V.K. Tripathi, **"An Efficient Algorithm for the 3D Analysis of Passive Microstrip Components and Discontinuities for Microwave and Millimeter Wave Circuits,"** *IEEE Trans. on MTT.*, Vol. 41, pp. 83-91, Jan. 1991.

[32] A.E. Ruehli, **"Equivalent Circuit Models for Three-Dimensional Multiconductor Systems,"** *IEEE Trans. on MTT.*, Vol. MTT-22, pp. 216-221, Mar. 1974.

[33] E.M. Jones and J.T. Balljahn, **"Coupled-Strip-Transmission Line Filters and Directional Couplers,"** *IRE Trans. Microwave theory Tech.*, Vol. MTT-4, pp. 75-81, Apr. 1956.

[34] H. Ozaki and J. Ishii, **Synthesis of a Class of Strip-Line Filters,"** *IRE Trans. Circuit Theory*, Vol. CT-5, pp. 104-109, june 1958.

[35] G.I. Zysman and A.K. Johnson, **"Coupled Transmission Line Networks in an Inhomogeneous Dielectric Medium,"** *IEEE Trans. on MTT.*, Vol. MTT-17, pp. 753-759, Oct. 1969.

[36] R.A. Speciale, **Fundamental Even- and Odd-Mode Waves for Nonsymmetrical Coupled Lines in Non-Homogeneous Media,"** *IEEE MTT Intl. Microwave Sym. Digest Tech.*, pp. 156-158, June 1974.

[37] E.G. Cristal, **Coupled-Transmission Line Directional Couplers with Coupled Lines of Unequal Characteristic Impedance,"** *IEEE Trans. on MTT.*, Vol. MTT-14, pp. 337-346, July 1966.

[38] C.B. Sharpe, **"An Equivalence Priciple for Nonuniform Transmission Line Directional Couplers,"** *IEEE Trans. on MTT.*, Vol. MTT-15, pp. 398-405, July 1967.

[39] H. Amemiya, **"Time Domain Analysis of Multiple Parallel Transmission Lines,"** *RCA Rev.*, vol. 28, pp. 241-276, June 1967.

[40] M.K. Krage and G.I. Haddad, **"Characteristics of Coupled Microstrip Transmission Lines - I : Coupled-Mode Formulation of Inhomogeneous Lines,"** *IEEE Trans. on MTT.*, Vol. MTT-18, pp 217-222, Apr. 1970.

[41] K.D. Marx, **"Propagation Modes, Equivalent Circuits, and Characteristic Terminations for Multiconductor Transmission Lines with Inhomogeneous Dielectrics,"** *IEEE Trans. on MTT.*, Vol. MTT-21, pp. 450-457, July 1973.

[42] D.G. Swanson, **"A novel method for modeling coupling between several microstrip lines in MIC's and MMIC's,"** *IEEE Trans. on MTT.*, Vol. MTT-39, pp. 917-923, June 1991.

[43] S. Cheng and M.L. Edwards, **"TEM equivalent circuits for quasi-TEM couplers,"** *IEEE MTT-S Intl. Microwave Symp. Dig.*, pp. 387-390, 1990.

[44] R. Levy, **"New equivalent circuits for inhomogeneous coupled lines with synthesis applications,"** *IEEE Trans. on MTT.*, Vol. MTT-36, June 1988.

[45] F. Romeo and M. Santomauro, **"Time-domain simulation of n coupled transmission lines,"** *IEEE Trans. on MTT.*, Vol. MTT-35, pp. 131-137, Feb. 1987.

[46] G. Matthaei, L. Young and E. M. T. Jones, **"Microwave Filters, Impedance-Matching Networks, and Coupling Structures,"** Dedham, MA: Artech House.

[47] D.M. Pozar, **"Microwave Engineering,"** MA: Addison-Wesley, 1990.

[48] D. Lacombe, and J. Cohen, **"Octave-band Microstrip DC Blocks,"** *IEEE Trans. on MTT.*, Vol. MTT-20, pp. 550-555, Aug. 1972.

[49] V. Rizzoli, **"Anaysis and Design of Microstrip DC Blocks,"** *Microwave Jour.*, Vol. 20, pp. 109-110, June 1977.

[50] D. Kajfez, *et al.*, **"Asymmetric Microstrip DC Block with Rippled Response,"** IEEE MTT-S Intl. Microwave Sym. Digest, pp. 301-303, 1981.

[51] Y.K. Chin, **"Analysis Applications of Multiple coupled Line Structure in an Inhomogeneous Medium,"** Ph.D. dissertation, Electrical and Computer Engineering Department, Oregon State University, 1982.

[52] A. Tripathi, V. K. Tripathi, **"A Configuration Oriented SPICE Model for Multiconductor Transmission Lines in an Inhomogeneous Medium,"** IEEE MTT-S Intl. Microwave Sym. Digest, pp. 1857-1860, 1996.

[53] K.D. Marx and R.I. Eastin, **"A configuration-oriented SPICE model for multiconductor transmission lines with homogeneous dielectrics,"** *IEEE Trans. on MTT.*, Vol. MTT-38, pp. 1123-1129, Aug. 1990.

[54] C.R. Paul, **"Simple SPICE Model for Coupled Transmission Lines,"** *IEEE Intl. Symp. Electromagnetic Compatibility*, Seattle, Aug. 1988.

[55] D.G. Swanson, **"A novel method for modeling coupling between several microstrip lines in MIC's and MMIC's,"** *IEEE Trans. on MTT.*, Vol. MTT-39, pp. 917-923, June 1991.

[56] S. Cheng and M.L. Edwards, **"TEM equivalent circuits for quasi-TEM couplers,"** *IEEE MTT-S Intl. Microwave Symp. Dig.*, pp. 387-390, 1990.

[57] R. Levy, **"New equivalent circuits for inhomogeneous coupled lines with synthesis applications,"** *IEEE Trans. on MTT.*, Vol. MTT-36, June 1988.

[58] F. Romeo and M. Santomauro, **"Time-domain simulation of n coupled transmission lines,"** *IEEE Trans. on MTT.*, Vol. MTT-35, pp. 131-137, Feb. 1987.

[59] S.D. Shamasundara and K.C. Gupta, **"Sensitivity Analysis of Coupled Microstrip Directional Couplers** *IEEE Trans. on MTT.*, Vol, MTT-26, No. 10, Oct. 1978.

[60] K.C. Gupta, *et al.*, **"Microstrip Lines and Slotlines,"** Artech House, 1996.

[61] V.K. Tripathi and A. Hill, **"Equivalent circuit modeling of losses and dispersion in single and coupled lines for microwave and millimeter wave integrated circuits,"** *IEEE Trans. on MTT.*, Vol, MTT-36, pp. 256-262, Feb. 1988.

[62] G.L. Matthaei and G.C. Chinn, **"Approximate calculation of the high-frequency resistance matrix for multiple coupled lines,"** *IEEE MTT-S Intl. Microwave Symp. Dig.*, pp. 1353-1354, 1992.

[63] A. M. Pavio and A. Kikel, **"A Monolithic or Hybrid Broadband Compensated Balun,"** *IEEE MTT-S Intl. Microwave Sym. Digest*, pp. 483-486, 1990.

[64] C. Tsai and K.C. Gupta, **"A generalized model for coupled lines and its applications to two-layer planar circuits,"** *IEEE Trans. on MTT.*, Vol. MTT-40, pp. 2190-2199, Dec. 1992.

[65] S. Banba and H. Ogawa, **"Multilayer MMIC Directional Coupler Using Thin Dielectric Layers,"** *IEEE Trans. on MTT.*, Vol. 43, pp. 1270-1275, June 1995.

[66] M. Engels and R.H. Jansen, **"Design of Integrated Compensated Baluns,"** *Microwave and Optical Tech. Letters*, Vol. 14, No. 2, pp. 75-81, Feb. 1997.

[67] W. Schwab, *et al.*, **"Multilayer Suspended stripline and Coplanar Line Filter,"** *IEEE Trans. on MTT.*, Vol. 42, pp. 1403-1406, July 1994.

[68] C. Cho and K.C. Gupta, **"Design of Multilayer Coupled Line Filter Circuits,"** *Proc. Wireless Comm. Conf.*, pp. 37-40, Aug. 1996.

[69] C. Cho and K.C. Gupta, **"Design of Multilayer Coupled Line Filter Circuits,"** *IEEE Intl. Microwave Sym.*, Denver, Jun. 1997.

APPENDIX

APPENDIX

Z-parameters for an asymmetric coupled line section with open-circuited port 3 and port 4 in a homogeneous medium are given by,

$$Z_{11} = \frac{-j}{2}(Z^a_{oe} + Z^a_{oo})cot\theta,$$

$$Z_{12} = Z_{21} = \frac{-j}{2}(Z^a_{oe} - Z^a_{oo})csc\theta$$
$$= \frac{-j}{2}(Z^b_{oe} - Z^b_{oo})csc\theta,$$

$$Z_{22} = \frac{-j}{2}(Z^b_{oe} + Z^b_{oo})cot\theta.$$

$ABCD$-parameters can be obtained as follows;

$$A = \frac{Z_{11}}{Z_{21}},$$

$$B = \frac{Z_{11}Z_{22} - Z_{12}Z_{21}}{Z_{21}},$$

$$C = \frac{1}{Z_{21}},$$

$$D = \frac{Z_{22}}{Z_{21}}.$$

Then S-parameters are represented

$$S_{11} = \frac{A + B/Z_{o1} - CZ_{o1} - D}{A + B/Z_{o1} + CZ_{o1} + D},$$

$$S_{12} = \frac{2(AD - BC)}{A + B/Z_{o1} + CZ_{o1} + D},$$

$$S_{21} = \frac{2}{A + B/Z_{o1} + CZ_{o1} + D},$$

$$S_{22} = \frac{-A + B/Z_{o1} - CZ_{o1} + D}{A + B/Z_{o1} + CZ_{o1} + D}.$$